IN-PLANE BEHAVIOUR OF MASONRY INFILLED RC FRAMES WITH INTERFACIAL GAPS SUBJECTED TO QUASI-STATIC LOADING

by

Ryan Steeves

Submitted in partial fulfilment of the requirements
for the degree of Master of Applied Science

at

Dalhousie University
Halifax, Nova Scotia
April 2017

TABLE OF CONTENTS

LIST OF TABLES

LIST OF FIGURES

ABSTRACT

Previous research on masonry infilled frames has shown that the presence of infill-to-frame interfacial gaps and infill openings can affect the in-plane strength and stiffness of the infilled frame system. However, most of these studies used infilled steel frames, and subjected to monotonic loading. The parameters in terms of gap magnitude and location were also limited. For design, the American Standard, MSJC 2013, allows for infilled frames with a gap of less than 9.5 mm located at the frame top beam and infill interface to be considered as participating infills in lateral load resistance, but in this case, a 0.5 reduction factor shall be applied to the design strength and stiffness of the infill. The Canadian standard, CSA S304-14, requires that no gaps be present at the infill to bounding frame interface for the infill to be considered participating in lateral load resistance.

This study was motivated to further investigate the effects of interfacial gaps and infill openings on the in-plane behaviour of masonry infilled frames. To augment the existing database, this study focused on reinforced concrete (RC) frames and adopted cyclic loading scheme. Four scaled masonry infilled RC frame specimens, as well as one bare RC frame specimen, were subject to quasi-static cyclic loading to failure. The four infilled frame specimens had the following interfacial gap scenarios: 1) a gap at the top beam-infill interface of 12 and 25 mm, respectively; 2) a gap at the column-infill interfaces of 12 mm (6 mm gap on each side); and 3) a full separation gap of 12 mm with 12 mm gap at the beam-infill and 12 mm at column-infill interfaces (6 mm gap on each side). Of the infilled specimens, two specimens also had a window opening accounting for 16% of the infill area. Quasi-static loading followed the ATC-24 loading protocol in order to measure cyclic response. Results from a previous study (Hu 2015) completed in the same experimental program were used for comparison purpose.

Experimental results showed that compared to the bare frame specimen, a noticeable increase in strength and stiffness was observed with presence of infill regardless of the presence of gaps or infill openings. When compared to a specimen with no gaps, a reduction in ultimate strength and stiffness was observed with the presences of gaps. As the beam-to-infill gap size increased, the reduction in ultimate strength also increased; however, the initial stiffness remained virtually the same when gap increased from 12 mm to 25 mm. The presence of openings resulted in significant reduction in ultimate strength and stiffness, however, when both openings and gaps are present, the strength and stiffness reductions as a result of gaps is not as significant.

The cyclic loading scheme revealed dynamic characteristics of masonry infilled frames. It was found that masonry infilled frames had greater ductility than that recommended by NBCC 2015 for unreinforced masonry. The ductility of the infilled frame specimens is comparable to that of a RC bare frame. The 0.5 reduction proposed by MSJC 2013 proved to be overly conservative for both ultimate strength and stiffness of infilled frames with gaps.

LIST OF ABBREVIATIONS AND SYMBOLS USED

Symbols

A	Compressive area of infill diagonal strut
A_{nv}	Net shear area
A_o	Area of infill opening
A_p	Surface area of infill
A_w	Horizontal cross section of the infill
c	Empirical constant that varies with in-plane displacement
C	Multiplication factor accounting for infill aspect ratio
d	Diagonal length of infill
e	Eccentricity of the load
E_f	Modulus of elasticity of frame
E_m	Modulus of elasticity of masonry
f'_m	Compressive strength of masonry
$f'_{m\text{-}0}$	Masonry strength parallel to bed joints
$f'_{m\text{-}90}$	Masonry strength perpendicular to bed joints
f_{bs}	Shear bond strength between the masonry and mortar
f_t	Tensile strength of masonry infill
h, h'	Height of infill, frame
H_{cc}	Corner crushing strength of infill

H_{dc}	Diagonal cracking strength of infill
H_{ss}	Sliding shear strength of infill
H_{ult}	Ultimate load strength of infill
I_b	Second moment of area of beam
I_c	Second moment of area of column
k	Stiffness
K_{cr}	Dimensionless empirical constant for diagonal cracking mean value of 0.066
K_{ult}	Empirical constant for ultimate load strength with mean value 246 mm
l	Length of infill
m	Dimensionless parameter relating to beam and column stiffness
M_f	Factored moment at section
M_p	Plastic moment capacity of either the frame beam or column
M_{pb}	Plastic moment capacity of beam
M_{pc}	Plastic moment capacity of column
M_{pj}	Plastic moment capacity of the joint
N_u	Factored compressive force
P_r	Factored axial load resistance
P_w	Vertical load acting on infilled frame
R_f	Reduction factor of infill diagonal strut width due to opening
t	Thickness of infill
t_e	Effective thickness of infill
μ	Coefficient of friction between the interface of the infill and frame

v	Poisons ratio
v_m	Shear strength of masonry
V_f	Factored shear at section
V_n	Nominal shear strength
V_r	Ultimate load of different failure modes
w	Width of the diagonal strut
α_b, α_l	Contact length between the beam and the infill
α_c, α_h	Contact length between the column and the infill
θ	Angle whose tangent is the infill height to length aspect ratio, in radians
λ	Dimensionless infill relative stiffness parameter
γ	Effective width factor
ϕ_m	Masonry resistance factor
Δ_y	Yield displacement
χ	Factor to account for direction of compressive stress in masonry member relative to the direction used for determination of f'_m

Abbreviations

ASTM	American Society for Testing and Materials
ATC	Applied Technology Council
BF	Bare frame
CC	Corner crushing
CMU	Concrete masonry unit

CSA	Canadian Standards Association
CV	Coefficient of variation
DC	Diagonal cracking
FEMA	Federal Emergency Management Agency
LVDT	Linear variable differential transformer
MSJC	Masonry Society Joint Committee
NBCC	National Building Code of Canada
RC	Reinforced concrete
SS	Sliding shear

ACKNOWLEDGEMENTS

I would like to first and foremost start by thanking my supervisor Dr. Yi Liu for her irreplaceable guidance, generous support, and constant encouragement. Without her leadership this dissertation would not have not been possible.

I would also like to thank my committee members, Dr. Hany El-Nagger and Dr. Steve Zou, for taking the time to review this dissertation and providing valuable feedback.

I would like to thank my fellow colleagues, Reza Rahimi, Ehsan Nasiri, Reza Sepasdar, Chongyang Wang, and Chuanjia Hu for their helpful collaboration during literature research and lab testing, and for their lasting friendship.

I would like to thank Mr. Blair Nickerson, Mr. Brian Kennedy, and Mr. Jesse Keane, for their assistance during specimen construction, building the test set up, and during specimen testing. I would like to thank Mr. Garry Hubley for the construction of the masonry infilled walls. I would also like to the thank Mr. Brian Liekens for creating the LabView program which enable the hydraulic jack to initiate quasi-static cyclic loading.

My thanks also go to the Canadian Concrete Masonry Products Association for providing financial assistance.

Lastly, I would like to thank my parents for their vital support, inspiration, and unconditional love.

CHAPTER 1 INTRODUCTION

1.1 BACKGROUND OF MASONRY

Masonry is one of the oldest construction materials with sundried clay masonry structures dating as far back as 10000 years (Drysdale and Hamid 2005). Since then, masonry has evolved to include building materials such as calcium silicate units, oven dried clay, and more recently, concrete masonry units. Until 1900's, masonry has been the predominant material for construction for various structures. The introduction of structural steel and reinforced concrete in the early 20th century pushed masonry aside by offering more cost-efficient construction material accompanied with advanced design codes while design of masonry was still largely governed by centuries old "rules of thumb". Structural masonry construction then fell behind in terms of competitiveness and marketability for a period of time. With the introduction of modern masonry design codes in 1950's and 1960's, such as the American Standards Association Building Code Requirement for Masonry (ASA A41.4-1953) and the National Building Code of Canada (1965), masonry construction experienced a resurgence. In the past six decades, the masonry design standards and codes in both the US and Canada have been developed from allowable stress design to a more rational limit state design philosophy. Together with the creation of commercial concrete masonry blocks in 1900 (Palmer 1900), masonry has regained its competitiveness and popularity as one of the main building materials in the 21st century.

1.2 MASONRY INFILL FRAMES

Concrete masonry block walls are commonly used in frame building structures as infill walls as shown in Figure 1.1 as an example. They fulfill the function of either partitions to separate spaces or claddings to complete the building envelope. Despite their large in-plane stiffness, the common North American industry practice has been to treat them as non-structural elements and to use other structural elements (steel bracing, concrete shear walls) for lateral load resisting.

Figure 1.1 Masonry Infill Wall Example (World House Encyclopedia)

The decision to neglect the impact of infill is due to a lack of codified design guidelines on how to quantify the exact interaction between the infill and its bounding frame. Despite the large strides made in the field of masonry research, the topic of masonry infilled frames has been one area which has received limited attention. However, the danger of ignoring the infill contribution to the frame system is that contrary to the conventional belief of

being conservative, the resulted design might be unsafe. If the infill is built tight against the bounding frame, its large in-plane stiffness will affect the lateral load distribution and change the dynamic characteristics of the whole structure. If not accounted for properly, the large force attracted to the frame region by the infill could have an adverse effect on the stability of frame system.

Experimental research on masonry infilled frames began in the 1960's and reached its prime in the 1980's-90's. The findings from this period have formed the basis for several key international masonry standards on the design of infills. In the last 20 years, with the advancement of computer technology, the numerical modeling techniques have been used as an effective tool for masonry infill research. In general, these studies have shown that behaviour of the masonry infilled frames is complex and is influenced by many factors such as the geometric and material properties of both the infill and its bounding frame, the interfacial condition, and loading conditions to just name a few. While some factors were studied quite extensively, the presence of interfacial gaps between the infill and its bounding frame, is less researched and there is no sufficient technical information available on how to evaluate their effect in an infill design. The presence of interfacial gaps is not uncommon, which can be due to the shrinkage and settlement of the infill or defects in workmanship and total elimination of interfacial gaps is difficult to achieve in practice. The uncertainty on the effect of a gap on the infill contribution to the system stiffness and strength is believed to be a primary reason that the masonry industry chooses to ignore the infill contribution all together in an infilled frame design. Also to that effect, the Canadian

masonry standard CSA S304-14 (2014) requires that there be no gaps between an infill and its bounding frame for the infill to be considered to participate in the lateral load resisting. On the other hand, the American masonry design standard, MSJC 2013, recommends that an infill may be considered as participating infill with a gap less than 9.5 mm between the infill and the top frame beam, provided that a reduction factor of 0.5 is applied to the stiffness and strength of the infill. However, the standard makes no recommendation for stiffness or strength reduction with gaps between the column and the infill or a full gap separating the infill and bounding frame; nor does the standard provide information on the background of the size and location of gap given. The question as to what gap width on the side, top and all around the infill can be permitted to consider the infill as participating and by what degree of strength or stiffness is affected with gaps present remains unanswered. To augment the existing body of knowledge of masonry infills with the focus on the interfacial effect, a research program was developed in the Department of Civil and Resource Engineering at Dalhousie University under the supervision of Dr. Yi Liu. An experimental testing of six masonry infilled reinforced frame (RC) specimens under a static lateral load applied at the frame beam level was conducted in 2015 (Hu 2015). As an extension of that study, this research was conducted to include more gap sizes and location scenarios. In addition, the load was applied as quasi-static to provide general understanding of infill behaviour under earthquake-like loading which has important practical relevance.

1.3 RESEARCH OBJECTIVES

This research is focused on concrete masonry infilled RC frames subjected to quasi-static cyclic loading. The following lists main objectives to be completed within this study:

1. To design test specimens and test setup to be used in the quasi-static testing program.

2. To conduct testing of concrete masonry infilled RC frames subjected to a quasi-static cyclic lateral loading as well as all essential auxiliary tests on specimen components.

3. To analyze the hysteretic behaviour and failure mode of each specimen with a focus on the effect of gap magnitude and location on the stiffness, strength, ductility, and energy dissipation of the infilled frames.

5. To present appropriate conclusions and recommendations resulted from this study.

1.4 OUTLINE OF RESEARCH

The thesis contains six chapters. Chapter 1 presents an introduction to the subject matter as well as defining the research objectives. Chapter 2 contains a comprehensive review of available literature pertaining to the strength and stiffness of masonry infilled frames, as well as a review of current North American design specifications. Chapter 3 gives a detailed description of the experimental program including the auxiliary test of materials, construction of masonry infilled RC frames, test specimens and test set-up and procedures. Chapter 4 discusses the results obtained from the current experiment program and their

comparison with the static results obtained from Hu (2015). Chapter 5 presents a summary and final conclusions drawn from this study.

CHAPTER 2 LITERATURE REVIEW

2.1 INTRODUCTION

There is a considerable amount of research conducted on the in-plane behaviour of concrete masonry infilled steel or RC frames in the past six decades. However, most studies were conducted on infilled frames subjected to monotonic lateral loading. Nevertheless, the general behaviour trend and failure mechanisms of these infilled systems were established. While providing a description of the general behaviour of infilled frames and a summary of existing analytical methods for design, this chapter focuses on the review of available literature on masonry infilled frames subjected to quasi-static loading and the effect of interfacial gaps.

2.2 MASONRY INFILL BEHAVIOUR

Masonry infills, when built tight against the bounding frame, may act together with the frame during low levels of in-plane lateral load offering a maximum level of stiffness. However, as load increases, the interaction between the infill and the frame changes as the frame deforms which creates two contact regions between the frame and the infill located at two loaded corners in the diagonal direction. These contact regions form a compression zone, creating a bracing action equivalent to a diagonal strut. Figure 2.1 provides a visual representation of the contact corners and zone of compression forming the diagonal strut. Using the diagonal strut to replace the entire infill in the determination of system stiffness

and strength is known as the "diagonal strut method" which was originally proposed by Polyakov (1960). Since then, the method has been modified and developed into various forms of formulations. It has become the predominant method of analysis for masonry infill walls and has been adopted in most masonry design standards across the world.

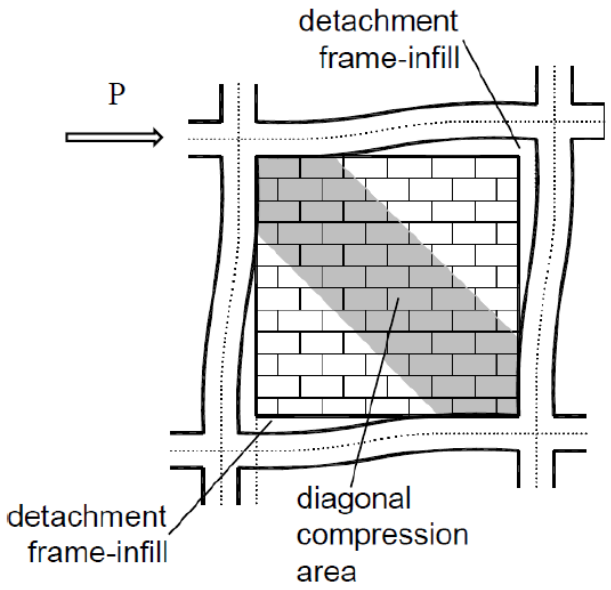

Figure 2.1 Zone of Compression Forming the Equivalent Diagonal Strut

(Adapted from Asteris et al. 2011)

2.2.1 DIAGONAL STRUT METHOD

The key to the diagonal strut method is to determine the width of the diagonal strut which can simulate the stiffness and strength of the infilled system. Once the width is known, a simple frame analysis can be performed to obtain the system stiffness. Both experimental and analytical studies have been conducted to develop analytical models for calculating the strut width. A detailed literature review of these models can be found in Xi (2016). Table

2.1 provides a summary of these models for ease of reference, and the following sections provide a brief background description of each model. It is noted that most models presented were developed with monotonic lateral loading. Figure 2.2 illustrates the geometric variables defined in Table 2.1.

Table 2.1 Summary of Analytical Models of the Equivalent Diagonal Strut Width

Author	Equation	
Holmes (1961)	$w = d/3$	[2-1]
Stafford -Smith and Carter (1969)	$w = \sqrt{\alpha_c^2 + (\frac{l'}{2})^2}$ $\frac{\alpha}{h} = \frac{\pi}{2\lambda h}$ $\lambda = \sqrt[4]{\frac{E_I t sin(\theta)}{4E_c I h'}}$	[2-2]
Mainstone (1971)	$w/d = 0.175(\lambda h')^{-0.4} 4 \leq \lambda h' \leq 5$ $w/d = 0.16(\lambda h')^{-0.3} \quad \lambda h' \geq 5$	[2-3]
Liauw and Kwan (1984)	$w = \frac{0.86 h cos\theta}{\sqrt{\lambda h}}, or\ 0.45 h cos\theta$	[2-4]
Durrani and Luo (1994)	$w = \gamma d sin(2\theta)$ $\gamma = 0.32\sqrt{\sin(2\theta)}\ (H^4 E_I t / m E_c I_c h)^{-0.1}$ $m = 6\left(1 + 6tan^{-1}\left(\frac{E_b I_b H}{E_c I_c L}\right)/\pi\right)$	[2-5]
Flanagan and Bennet (1999)	$w = \frac{\pi t}{c\lambda \cos\theta}$	[2-6]
Al-Chaar (2002)	$w = 0.0835 C d(1 + 2.574/\lambda_l h') for\ l/h \geq 1.5$ $w = 0.1106 d(1 + 6.027/\lambda h') for\ l/h = 1$ $C = -0.3905(l'/h) + 1.7829$	[2-7]
El-Dakhakhni et al. (2003)	$A = \frac{(1 - \alpha_c)\alpha_c h' t}{\cos\theta}$	[2-8]

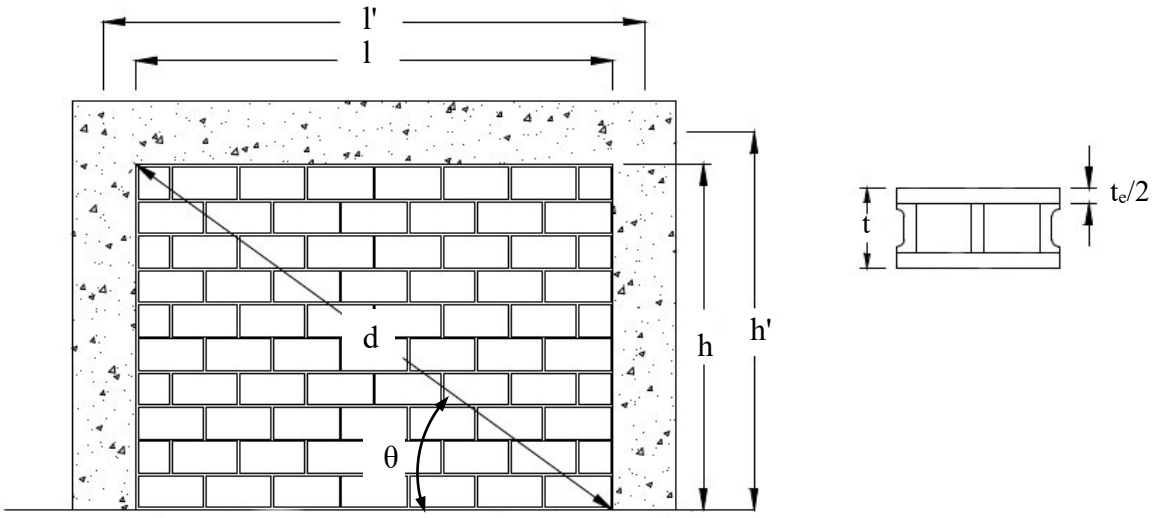

Figure 2.2 Masonry Infill Geometric Variables Definition

Holmes (1961) (Eqn [2-1]) performed experiments on thirteen small scale infilled steel frames and proposed the width of the diagonal strut, w, as a function of the length of the diagonal, d.

Stafford -Smith and Carter (1969) (Eqn [2-2]) conducted experiments on diagonally loaded square infill frames and found that the contact length along the height of the infill, α, is governed by the relative stiffness of the masonry infill to the frame, which is defined using a dimensionless parameter "λ". This term evaluates the relative stiffness through the height of the infilled frame, h, the thickness of the infill, t, the Young's modulus of the infill, E_I, the Young's modulus of the frame column, E_c, and the slope of the infill diagonal to the horizontal, θ. By combining the defined contact length along the column and assuming the contact length along the top of the infill, l', is half the beam span the width of the diagonal

strut can be defined.

Mainstone (1971) (Eqn [2-3]) conducted a series of experiments on concrete infilled steel frames and using curve-fitting technique; it was proposed the semi-empirical equations incorporating the stiffness parameter λ defined by Stafford-Smith and Carter (1969).

Liauw and Kwan (1984) (Eqn [2-4]) conducted an analytical study using the finite element method to analyze the behaviour of masonry infilled frames. A key feature of this analytical study was that the friction forces between the frame/column interfaces were neglected. The resulted strut width equation still incorporated stiffness parameter λ but in a slightly simpler formulation.

Durrani and Luo (1994) (Eqn [2-5]) conducted a finite element study to calculate the diagonal strut width. They proposed a new equation to evaluate the relative stiffness where the effect of stiffness of frame beam and column is considered more explicitly.

Flannagen and Bennet (1999) (Eqn [2-6]) conducted a series of experimental testing on clay tile infilled steel frames under in-plane loading. They proposed a simplified formula based on a new empirical constant, c, which is designed to reflect the different damage states sustained by the infill during the loading history.

Al-Chaar (2002) (Eqn [2-7]) proposed equations for calculating the strut width for infills with different aspect ratios. Based on curve-fitting technique on results obtained from a finite element study, the equations indicate the diagonal strut can only develop for short

and squat infills with aspect ratio greater or equal to unity.

El-Dakhakhni et al. (2003) (Eqn [2-8]) introduced a three-strut method to depict the infill and frame interaction. It was proposed that the diagonal strut is composed of two diagonal regions instead of a single diagonal strut, as illustrated in Figure 2.3. The two regions of diagonal compression are defined by the contact lengths along the height and length of the infill, $\alpha_c h$ and $\alpha_c l$ respectively, as follows:

$$\alpha_c h = \sqrt{\frac{2\left(M_{pj} + 0.2M_{pc}\right)}{f'_{m-0}t}} \leq 0.4h \qquad [2\text{-}9]$$

$$\alpha_b l = \sqrt{\frac{2(M_{pj} + 0.2M_{pb})}{f'_{m-90}t}} \leq 0.4l \qquad [2\text{-}10]$$

where M_{pc} and M_{pb} are the plastic moment capacity at the column and beam respectively; M_{pj} is the plastic moment capacity of the joint taken as the least capacity of the column, beam, or connection; $f'_{m\text{-}0}$ and $f'_{m\text{-}90}$ are the masonry strength parallel and perpendicular to the bed joint, respectively.

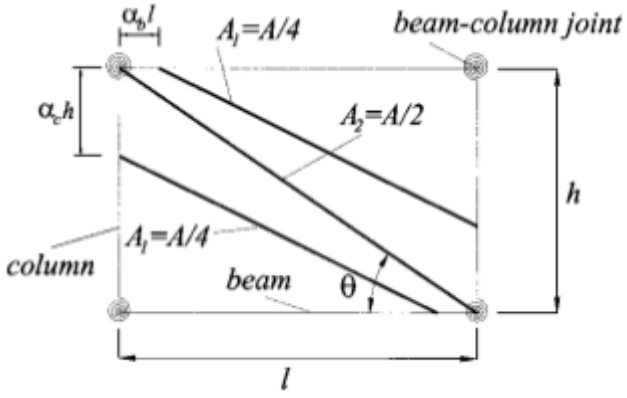

Figure 2.3 Three-Strut Infilled Frame Model

(Adapted from El-Dakhakmi 2003)

2.2.2 FAILURE MODES AND STRENGTH ANALYSIS

Previous research has shown that laterally loaded masonry infilled frames have five potential failure modes (Liauw and Kwan 1983, Flanagan and Bennett 1999). Schematic representations of these failure modes are shown in Figure 2.4.

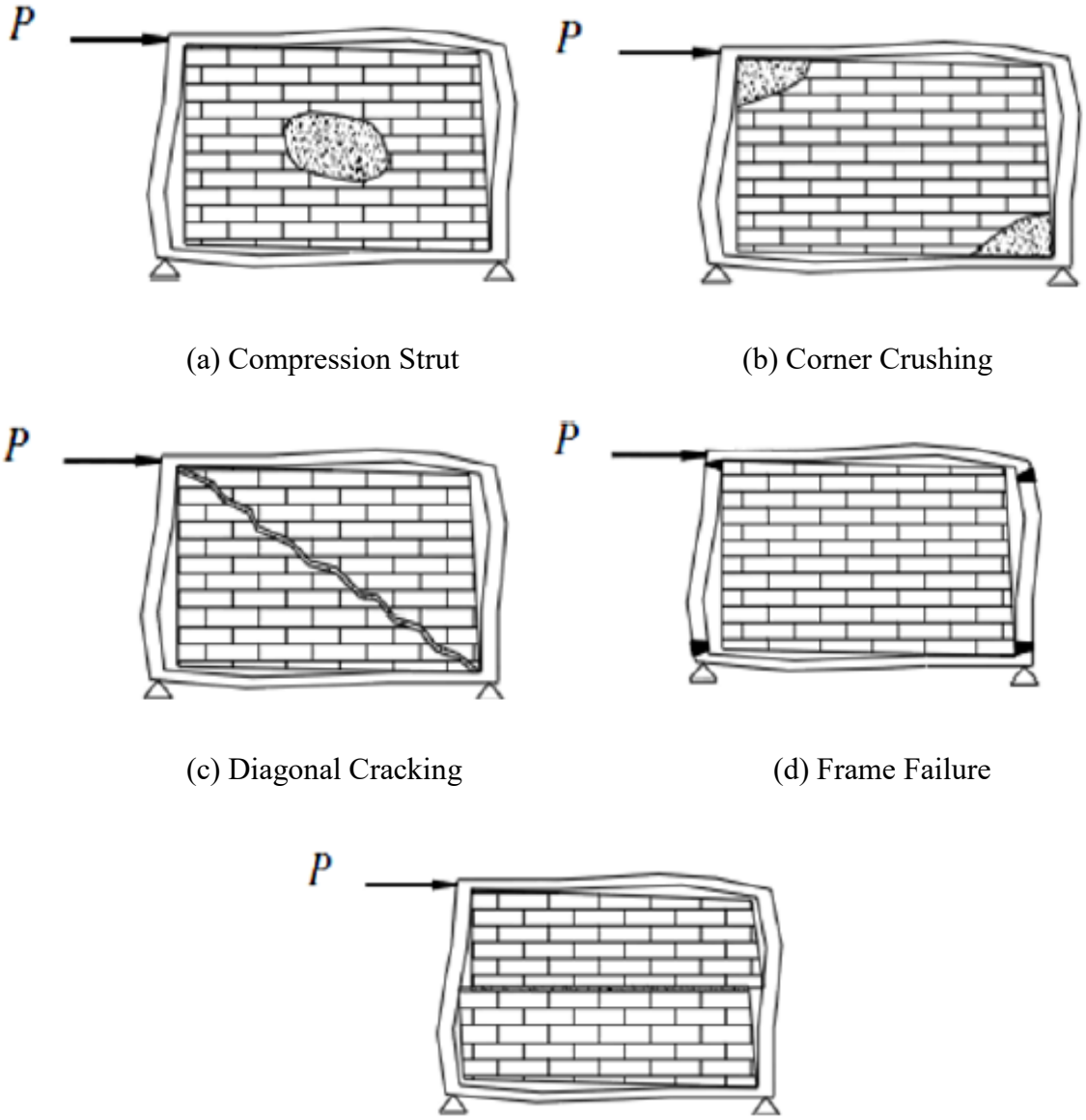

(a) Compression Strut

(b) Corner Crushing

(c) Diagonal Cracking

(d) Frame Failure

(e) Sliding Shear

Figure 2.4 Failure Modes for Infilled Frames

(Adapted from El-Dakhakhni 2003)

Figure 2.4 (a) depicts the compression strut failure mode which occurs when a crushing region forms in the centre of the infill, resulting in an out-of-plane buckling of the masonry

infill wall. Compression strut failure is caused by a compressive strut that is too slender. Figure 2.4 (b) depicts the corner crushing failure mode which occurs when the masonry infill blocks fail in compression in each of the contact corners. This failure mode occurs when a strong frame is paired with weak masonry infill. Figure 2.4 (c) depicts the diagonal tension (or diagonal cracking) failure mode which occurs when the diagonal tension forces create cracks in the diagonal strut. Figure 2.4 (d) depicts the frame failure mode which occurs when a weak frame is paired with a strong masonry infill. This results in a failure of the columns of the bounding frame. Figure 2.4 (e) depicts the sliding shear (or knee brace) failure mode which occurs when a horizontal shearing action occurs along the bedjoint of the masonry infill. This can be attributed to a weak mortar joints and a strong frame

It is also identified that for infilled frames of typical material and geometry encountered in practice, corner crushing failure is the most predominant failure mode. Several researchers have developed infill strength equations that define the capacity of the failure modes defined above. A summary of these equations are presented in Table 2.2 with brief background information given in the following sections.

Table 2.2 Summary of Strength Evaluation Equations for Masonry Infilled Frames

Author	Equation	
Mainstone (1971)	$H_{cc} = 0.56(\lambda h)^{-0.875} f'_m h' t\cot(\theta)$ $4 \le \lambda h' \le 5$ $H_{cc} = 0.52(\lambda h)^{-0.8} f'_m h' t\cot(\theta)$ $\lambda h' \ge 5$	[2-11]
Woods (1978)	$H_{ult} = \frac{4M_p}{h} + \frac{1}{2}\sigma_c I t$	[2-12]
Rosenbluth (1980)	$H_{ss} = \left(0.9 + 0.3\frac{l}{h}\right) f_{bs} h t$	[2-13]
	$H_{cc} = \frac{2}{3}\alpha_c t f'_m sec\theta$	[2-14]
	$\alpha_c = \frac{\pi}{2}\sqrt[4]{\frac{4E_f I_c h}{E_I t_c sin2\theta}}$	
Liauw and Kwan (1983)	$H_{CC} = \sigma_c t h' \sqrt{\frac{2(M_{pj} + M_{pb})}{\sigma_c t h'^2}}$	[2-15]
	$H_{CC} = \frac{\sigma_c t h'}{tan\theta} \sqrt{\frac{2(M_{pj} + M_{pb})}{\sigma_c t h'^2}}$	[2-16]
	$H_{DC} = \frac{4M_{pj}}{h'} + \frac{\sigma_c t h'}{6}$	[2-17]
	$H_{DC} = \frac{4M_{pj}}{h'} + \frac{\sigma_c t h'}{6tan\theta}$	[2-18]
Mehrabi (1996)	$H_{ss} = 0.34A_w + 0.9P_w$	[2-19]
Stafford-Smith and Coull (1991)	$H_{cc} = f'_m t \frac{\pi}{2}\sqrt[4]{\frac{4E_f I h'}{E_I t}}$	[2-20]
	$H_{cr} = 1.72\ell t f_t$	[2-21]
Flanagan and Bennett	$H_{DC} = K_{DC} l t \sqrt{f'_m}$	[2-22]
	$H_{cc} = K_{cc} t f'_m$	[2-23]

Note: Hss is the sliding shear capacity; Hcc is the corner crushing strength; H_{DC} is the diagonal cracking strength, and H_{ult} is the ultimate load of the infilled frame

Mainstone (1971) (Eqn [2-11]) proposed an equation to calculate the capacity of the corner crushing load, $H_{cc,}$ of brick masonry infill which was formulated to relate to the stiffness parameter λ, the compressive strength of the masonry infill f'_m, and the height of the frame column.

Woods (1978) (Eqn [2-12]) developed an equation to calculate the ultimate load of infilled RC frames as a combination of the strength of the infill and the surrounding frame. The equation utilizes the corner crushing strength, σ_c, and the lesser of the plastic moment capacity of the frame beam or the column, M_p.

Rosenbluth (1980) (Eqn [2-13, 2-14]) described two failure mode equations, sliding shear and corner crushing, for masonry infilled RC frames. Sliding shear was described as a function of the aspect ratio and shear strength of the mortar while the corner crushing was defined as a function of the contact length and compressive strength of the masonry blocks. The equation utilizes the shear bond strength between the masonry and mortar, f_{bs}, and the contact length of the infill and column, $\alpha_{c.}$

Liauw and Kwan (1983) (Eqn [2-15, 2-16, 2-17, 2-18]) applied the plastic analysis method to describe two failure modes, corner crushing, and diagonal compression. The equation utilizes the plastic moment capacity of the joint and beam M_{pj} and M_{pb}. Equations [2-15, 2-16] calculates corner crushing failure in the columns and infill-beam connection and beam and infill-beam connection respectively. Equations [2-17, 2-18] calculates failure diagonal cracking infill-beam connection and infill-column connection respectively.

Mehrabi (1996) (Eqn [2-19]) conducted a study assessing the effect of biaxial loading on masonry infilled RC frames and defined the sliding shear failure resistance of infilled frames under biaxial loading as a function of the horizontal cross section of the infill, $A_{w,}$ and the vertical load acting on the infill, P_w.

Stafford-Smith and Coull (1991) (Eqn [2-20, 2-21]) proposed equations for the corner crushing and diagonal cracking strength of masonry infilled frames based on diagonal strut concept.

Flanagan and Bennett (1999) (Eqn [2-22, 2-23]) argued that the frame geometry and properties had little impact on corner crushing strength and that a more simplified method could prove just as effective. They proposed a simplified formula to calculate corner crushing strength and diagonal cracking strength with two empirical constants. K_{CC} is an empirical constant for corner crushing with a value of 246 mm, and K_{DC} is an empirical constant with a value of 0.066.

2.3 NORTH AMERICAN DESIGN STANDARDS AND CODES

The diagonal strut method is widely adopted in various international masonry design standards, albeit with different formulation of strut width calculation. The following section provides descriptions of design guidelines in the current Canadian and American design standards for the design of masonry infill walls.

2.3.1 CSA S304-14

The design of masonry infilled frames can be found in CSA S304-14, Clause 7.13.3 where the equivalent diagonal strut method is defined. The code adopts a modified version of the method first proposed by Stafford-Smith and Carter (1969) to determine the width of the diagonal strut, w, which is defined as the following:

$$w = \sqrt{\alpha_h^2 + \alpha_L^2} \qquad [2\text{-}24]$$

where α_h and α_L are the vertical and horizontal contact length between the frame and the diagonal strut respectively. The contact lengths of the infilled frames are defined as follows:

$$\alpha_h = \frac{\pi}{2}\sqrt[4]{\frac{4E_f I_c h}{E_I t_e \sin 2\theta}}; \alpha_L = \pi\sqrt[4]{\frac{4E_f I_b l}{E_I t_e \sin 2\theta}} \qquad [2\text{-}25]$$

where t_e is the effective thickness of the masonry infill, E_f is the elastic modulus of the frame material, I_c is the moment of inertia of the column, I_b is the moment of inertia of the beam, and remaining terms are as defined in Figure 2.2 The effective diagonal strut width, w_{eff}, for the calculation of the compressive capacity of the diagonal strut shall be taken as w/2 and shall not exceed one-quarter the length of the diagonal. However, S304-14 requires a further reduction for the effective strut width used for stiffness calculations with a factor of 0.5.

The in-plane strength of masonry infills in CSA S304-14 is determined with respect to three failure modes, i.e., diagonal strut compression, shear sliding, and diagonal tension cracking. Formulae for CSA S304-14 strength evaluation methods are presented in Appendix A.

2.3.2 MASONRY STANDARDS JOINT COMMITTEE

The Masonry Standards Joint Committee (MSJC) has been given a mandate from The Masonry Society (TMS), The American Concrete Institute (ACI), and the Structural Engineering Institute of the American Society of Civil Engineers (SEI/ASCE) to determine masonry design provisions in accordance with American National Standards Institute (ANSI) consensus procedures. The resulted standard is referred to as MSJC 2013 in (TMS 402-13/ACI 530-13/ASCE 5-13) to represent the American masonry design standard. The standard utilizes the equivalent strut method and calculates the width, w, as the following:

$$w = \frac{0.3}{\lambda_{strut} \cos\theta_{strut}} \qquad [2\text{-}26]$$

where θ_{strut} is the same angle as θ defined earlier. λ_{strut} is the stiffness parameter as defined in Stafford-Smith and Carter (1969). This expression was based on work conducted by Flanagan and Bennett (1999) on structural clay tile infilled steel frames.

Similar to CSA S304-14, the infill strength in MSJC 2013 is also evaluated based on three failure modes while slightly different failure modes are defined. They are corner crushing,

sliding shear and 25 mm lateral displacement of the infilled frame. For the predominant corner crushing failure mode, MSJC 2013 simply uses a constant term of 6 inches as the diagonal strut width to account for the compressive capacity of the diagonal strut where the lateral strength of the infill is expressed as the following:

$$V_r = (6.0\text{in.})t_e f'_m \qquad [2\text{-}27]$$

It is worth noting that both codes (CSA S304-14 and MSJC 2013) use the effective thickness, t_e, of the infill instead of the total thickness, t, of the infill adopted by previous studies. In the case of ungrouted infills, the effective thickness is considered as the face shell thickness of the masonry units.

2.3.3 FEDERAL EMERGENCY MANAGEMENT AGENCY-306

The Federal Emergency Management Agency- 306 (FEMA 306), presented a definition of the width of the diagonal strut as well as four failure modes for masonry infilled frames (i.e. sliding shear, compression failure, diagonal tension failure and general shear failure of panel.) The definition of the geometry of equivalent strut follows the method proposed by Mainstone (1971) with the width of the diagonal strut, w, defined as follows:

$$w = 0.175(\lambda_{strut}\mathrm{h}')^{-0.4} r_{inf} \qquad [2\text{-}28]$$

where r_{inf} is the diagonal length of the infill panel.

2.3.4 SEISMIC DESIGN

It is well recognized in seismic design that the elastic seismic design force can be reduced if structural elements are expected to develop inelasticity. The reduction in design seismic force is realized through the use of ductility factor. This design philosophy is commonly adopted in the seismic design codes (NBCC 2015, ASCE 7). Ductility is a measure of the capacity of a structure or a member to undergo deformation beyond yield level while maintaining most of its load-carrying capacity. When seismic loads are considered, structures or members are always designed to have a certain amount of ductility so that they are able to absorb and dissipate earthquake energy by plastic deformations. The higher the ductility, the higher reduction of the design seismic force. NBCC 2015 permits that the design seismic loads be reduced by a factor of 1 to 5 depending on the type of seismic resisting systems used. The typical ductility factors used in design for moderately ductile moment-resisting RC frames, and unreinforced masonry are 2.5, and 1.0, respectively. The low ductility factor of unreinforced masonry results in a much larger seismic design force than a concrete or steel lateral resisting frame system, and thus using the unreinforced masonry becomes non-economical in seismic regions. Due to the lack of scientific information on their seismic performance, the masonry infilled frames are not explicitly listed as a type of seismic load resisting system in NBCC 2015, despite experimental evidence that masonry infilled frames can exhibit marked ductility in simulated seismic loading. One objective of this study is to demonstrate the behaviour and performance of masonry infilled RC frames through quasi-static loading.

2.4 QUASI-STATIC LOAD TESTING

Quasi-static cyclic load testing is an effective method for analyzing seismic performance of a component or subassembly of a structure. Quasi-static cyclic loading can be defined as a testing procedure where slow cycles of loading, simulating seismic activity, are applied in order to study the performance of structures and structural members for crack propagation, hierarchy of collapse, and associated levels of damage. In comparison to monotonic loading, which assesses a material's yielding point, quasi-static cyclic gives insight into the hysteric characteristics such as strength and stiffness deterioration, energy dissipation, and ductility. The ultimate load obtained from a monotonically loaded specimen usually is greater than that of a cyclically loaded specimen due to the deterioration and degradation of the specimen. The quasi-static loading is considered a good alternative for understanding the structural seismic performance in lieu of more sophisticated and advanced testing strategies such as pseudo-dynamic or shaking table testing. Specifications of loading histories for quasi-static loading have been standardized by the Applied Technology Council (ATC) and FEMA to provide more effective seismic simulation. While a majority of experimental research has been conducted using monotonic loading, the following section provides a review of several cyclic loading experimental programs conducted for masonry infilled frames.

Mehrabi et al. (1994) conducted in-plane monotonic and cyclic load testing of 14 half-scale masonry infilled RC frames. The parameters investigated in the study included the infill-

to-frame stiffness, infill panel aspect ratio, lateral load history, and multi-bay infilled frames. It was found that specimens subjected to cyclic loading showed lower lateral resistance and faster strength degradation than their monotonically loaded counterparts and that strong infills provided better energy dissipation, especially when combined with strong frames. Multi-bay specimens showed an increase in lateral load resistance up to 1.85 times larger than similar single bay specimens, and aspect ratio had little effect on performance.

Mosalam (1996) performed in-plane experimental studies of infilled multi-bay and multi-storey steel frames with and without openings. Frames were subject to cyclic quasi-static loading and pseudo-dynamic loading conditions. Results from quasi-static testing concluded that solid infill walls resulted in brittle failure and openings led to more ductile behaviour; the larger the opening, the larger post-cracking force.

Moghaddam (2004) performed an experimental investigation on five brick infilled steel frames subjected to cyclic racking load. Two types of brick infill were tested, perforated and solid units. In this study, it was found that the perforated units showed higher shear rigidity in comparison to the solid units but did not influence the overall shear strength of the infill.

Calvi & Bolognini (2008) conducted experimental tests on the in-plane behaviour of single story infilled RC frames with infill reinforcements under quasi-static cyclic loading. Results showed that a significant reduction in strength deterioration was observed in all reinforced infills when compared with un-reinforced infills; infilled specimens showed

lower energy dissipation at low amplitude cycles in comparison to bare frames, and infilled specimen response was similar to that of the bare frame at drift values close to collapse.

Harris (2013) performed an experimental and numerical testing of 15 two-storey single bay masonry infilled RC frames under monotonic, and quasi-static loading. The loading protocol was force-controlled based on previously determined monotonically loaded yield points. It was found that by increasing the strength of the mortar, a considerable increase in lateral displacement was seen at identical load intensity prior to failure of cyclically loaded specimens.

Al-Nimry (2014) performed quasi-static cyclic load testing on 1/3 scale RC frames with limestone masonry infills. Three infill conditions were tested including window and door openings, presence of axial loading, and use of reinforcing dowels. Experimental results showed a substantial decrease in ductility with the presence of axial load; reduced load capacity with the presence of openings; and the presence of dowels improved the load capacity of the infilled frames without reducing ductility.

2.5 MASONRY INFILL WITH INTERFACIAL GAP

While considerable experimental studies have been conducted to study the masonry infilled frame behaviour in general, those focusing on the interfacial gap effect is limited and to the best knowledge of the author, none were conducted in a quasi-static loading condition. The general findings of previous studies show that gaps between the infill and the bounding frame can significantly affect the stiffness and strength of the infilled system. The CSA

S304-14 does not allow any gaps between the masonry infill and the bounding frame for design of a participating infill. MSJC 2013, however, permits the use of infills with a top beam-to-infill gap less than 9.5 mm, but in such a case the stiffness and strength of gapped infill shall be reduced by 50%. It is, however, not clear whether this also applies to the case of side gaps and the background of the gap size limit and reduction factor was not provided. The following provides a review of most relevant research involving initial gaps between frames and masonry infills.

Abdul-Kadir (1974) conducted the first experimental tests of masonry infilled frame with an initial gap. Two infilled steel frames with a 1.6 mm top gap between the infill and the frame beam were tested and the tests yielded no significant effect of the gap on the strength or stiffness of the infill.

Riddington (1984) conducted a series of tests on full-scale concrete masonry infilled steel frames with initial gaps. The gap conditions included a 3 mm top beam-to-infill gap, and a 3 mm top beam-to-infill gap along and a 1.5 mm column-to-infill on each side of the infill. Results showed that in comparison with the control specimen with no gaps, a 3 mm top gap paired with the strong frame resulted in a 7% reduction in ultimate strength, and a 5% reduction when paired with the weak frame. The infilled frame with the 3 mm top gap and 1.5 mm side gaps resulted in a ultimate strength reduction of 12% and 20% for the strong frame and weak frame respectively.

Yong (1984) investigated two full-scale infill specimens both with a 20 mm top gap

between the infill and the frame beam. The first gap specimen was built tight to the column with mortar and the second specimen utilized flat bar ties that were welded to the column and embedded into the mortar at alternating courses. In comparison to a similar full contact specimen, specimen one showed a reduction of ultimate strength of 62% and a reduction of initial cracking load of 53%. Specimen two showed a 10% increase in ultimate load strength and a 15% increase in initial cracking load in comparison to specimen one.

Richardson (1986) investigated one specimen in an experimental study of masonry infilled steel frames with a 20 mm top gap. The gap resulted in a 75% reduction in initial stiffness and 30% reduction in first crack loading in comparison to a full contact specimen. Ultimate strength was also reduced by 39% in comparison to a full contact specimen.

Dawe and Seah (1989) tested 28 concrete masonry infilled steel frames with two specimens having a 20 mm top beam-to-infill gap. They found a significant decreased in stiffness and strength in both gapped specimens in comparison to specimens with full contact. It was concluded that a top infill gap reduced cracking and ultimate loads by roughly 50%.

Flanagan and Bennett (1999) tested clay tile infilled steel frames with a 25 mm column-to-infill gap. The presence of a gap reduced stiffness in the early stage of loading; however, once the gap was closed the stiffness increased drastically. They noted that the ultimate strength of the gapped specimen was roughly the same as the specimen with no gap.

Ng'andu (2006) tested two calcium silicate wall infilled steel frames with a 12 mm top beam-to-infill gap. When compared with full contact infilled counterparts, the gapped

specimens showed an average reduction of 20% in stiffness and of 2% in average first cracking load.

Nazief (2014) conducted a finite element study on the effect of initial infill gaps for both steel and RC frames. The gaps tested were 5 mm, 7 mm, 10 mm, 15 mm between the top of the infill and the frame beam, and 5 mm, 7 mm, 10 mm, and 15 mm full separation around the infill and the frame members. It was concluded that the top gap of less than 15 mm had virtually no effect on the strength and stiffness of the infill while a 15 mm top gap caused a 25% strength reduction. It was also found that the lateral load resistance of the infill should be neglected when a 10 mm or greater full separation gap is present.

Hu (2015) conducted an experimental investigation of four concrete masonry infilled RC frames with top beam-to-infill and side column-to-infill gaps. The investigated gap widths were 7 mm and 12 mm in both cases. The investigation found little reduction in ultimate strength with a 7 mm top gap but a 21% reduction with a 12 mm top gap. A reduction in ultimate strength for specimens with side gaps was found to be 11% and 36% for 7mm and 12mm side gap respectively. In the case of stiffness, average reductions of 28.2% and 31.8% were observed for the top gap and side gap respectively.

For ease of reference, Table 2.3 provides a summary of aforementioned findings for the gap effect on strength and stiffness reduction.

Table 2.3: Summary of Previous Studies on Gap Effects

Reference	Frame	Gap	Stiffness Change (%)	Strength Change (%)
Riddignton (1984)	Steel	3 mm top gap	-50	-7
		3 mm top & 1 mm side gap	-70	-15
Richardson (1986)	Steel	20 mm top gap	-75	-39
Dawe &Seah (1989)	Steel	20 mm top gap	-50	-60
Ng'andu (2006)	Steel (calcium silicate infill)	12 mm top gap	-20	-2
Nazief (2014)	Steel	5, 7 mm top gap	-27	-9
		10, 15 mm top gap	-41	-24
		5, 7 mm full gap	-37	-15
		10, 15 mm full gap	-71	-50
	RC	5, 7 mm top gap	-1	-12
		10, 15 mm top gap	-5	-19
		5, 7 mm full gap	-64	-31
		10, 15 mm full gap	-90	-58
Hu (2015)	RC	7 mm top gap	-28.1	-1.9
		12 mm top gap	-28.3	-21
		7 mm side gap	-31.6	+1.2
		12 mm side gap	-32.1	-15

2.6 MASONRY INFILL WITH AN OPENING

It is commonly accepted that the presence of infill openings reduces the lateral stiffness and strength of the infilled system. Based on the diagonal strut approach for solid infills, the simple and practical way of taking into account of opening effect is to apply a reduction factor, R_F, to the width of the corresponding solid infill, w, resulting in an effective width of $R_f \times w$. Several analytical methods have been proposed to calculate the reduction factor to account for openings in infills. Table 2.4 provides a summary of these equations when analyzing infilled specimens with an opening.

Table 2.4 Proposed Diagonal Strut Width Reduction Factors for Infill with Openings

Author	Equation	Frame	
Durrani and Luo (1994)	$R_F = 1 - (\frac{A_d}{H \times L})^2$ $A_d = H \times L - \frac{[Rsin(2\theta) - R_o \sin(\theta + \theta_o)]^2}{2\sin(2\theta)}$ $R_o = \sqrt{{H_o}^2 + {L_o}^2} \quad R = \sqrt{H^2 + L^2}$	Steel &RC	[2-31]
Al-Chaar et al. (2003)	$R_F = 1 + 0.6(A_o/A_p)^2 - 1.6(A_o/A_p)$	Steel &RC	[2-32]
Mondal and Jain (2008)	$R_F = 1 - 2.6(A_o/A_p)$	Steel &RC	[2-33]
Tasnimi and Mohebkhah (2011)	$R_F = 1 + 1.49(A_o/A_p)^2 - 2.238(A_o/A_p)$	Steel &RC	[2-34]
Asteris et al. (2012)	$R_F = 1 - 2(A_o/A_p)^{0.54} + (A_o/A_p)^{1.14}$	Steel &RC	[2-35]
Mohammadi and Nikfar (2013)	$R_F = 1 + 1.1163(A_o/A_p)^2 - 1.6534(A_o/A_p)$ $R_F = 1 - 2.21(A_o/A_p)$ $R_F = 1 - 1.05(A_o/A_p)$	Steel RC	[2-36]

In these equations, H and L are the height and lengths of the infill, respectively; H_0 and L_0 are the height and length of the opening, respectively; θ and θ_0 are the angles of the infill diagonal and opening diagonal, respectively; A_p and A_o are the infill area and the opening

area respectively.

2.7 CONCLUDING REMARKS

Previous studies have resulted in several analytical models to evaluate the strength and stiffness of RC/steel infilled frames. The equivalent diagonal strut method has been the most accepted method of analysis for infilled frames due to its simplicity and reasonable accuracy. A variety of formulae were proposed for the determination of the strut width. However, the existing analytical equations were developed using masonry infills subjected to monotonic loading and they are only intended for "regular" infills where gaps are not present. Despite that the presence of interfacial gaps has been reported to significantly affect the strength and stiffness, and sometimes even alter the failure mode of the infilled frame, no definable relationship between the magnitude and location of the gap and stiffness and strength of the infill was generated from those studies. In addition, the majority of the existing research on gap effects was focused on infilled steel frames and results on RC bounding frames are limited. As quasi-static loading has been established as an effective method for understanding seismic performance of infilled frames, this study is motivated to investigate further the effect of interfacial gaps on masonry infilled RC frames subjected to quasi-static loading.

CHAPTER 3 EXPERIMENTAL PROGRAM

3.1 GENERAL

This experimental program was designed to assess the effect of interfacial gaps on the behaviour of masonry infilled RC frames under quasi-static in-plane loading. A total of five specimens were tested to failure using displacement controlled quasi-static loading, of which four were given a pre-defined interfacial gap between the infill and frame, and one was a bare frame without infill. Of the four gapped specimens, two also had window openings in the infill.

In addition to infilled frame testing, auxiliary tests were also performed to obtain the material properties of concrete, masonry units, mortar, and masonry prisms. The following sections provide detailed descriptions of the infilled frame specimens, fabrication of specimens, test set-up, and testing procedures as well as relevant auxiliary tests on masonry components.

3.2 INFILLED FRAME SPECIMENS

Table 3.1 provides a description of the test specimens used in this experimental program. All four infilled specimens had a pre-defined gap located in three scenarios: 1) at top beam-infill interface (Top Gap), 2) at two column-infill interfaces (Side Gap), 3) at both beam and column-infill interfaces (Full Separation Gap). In addition to the predefined gap, two infilled specimens had a window opening accounting for 16% of the infill area and with an

opening aspect ratio of 1:1.5 (IF-W-SG12 and IF-W-TG12).

Table 3.1 Summary of Frame Specimens

Number	Specimen ID	Gap	Window Opening
1	BF	-	-
2	IF-TG25	25 mm Top Gap	-
3	IF-FG12	12 mm Top Gap & 12 mm Side Gap (6 mm each side)	-
4	IF-W-TG12	12 mm Top Gap	16%
5	IF-W-SG12	12 mm Side Gap (6 mm each side)	16%

The dimensions of the frame specimen are shown in Figure 3.1. It is noted that a similar test program was conducted in the same research group (Hu 2015) on the gapped infilled RC frames but subjected to static loading. In order to compare results, the geometry and reinforcing details of specimens were kept to be the same. The infill had a height to length aspect ratio of 0.73. All pre-defined gap magnitudes were achieved by adjusting mortar thickness with the exception of specimen IF-TG25 in which case the height of the top layer of blocks was trimmed in addition to adjusting mortar thickness. The masonry infill blocks used were custom-made, half-scale standard 200 mm CMUs laid in a running bond pattern. Infills were unreinforced and ungrouted in specimens without window openings. The masonry blocks surrounding the window opening were grouted in accordance with CSA A179 while all other remaining blocks remained ungrouted. The nominal dimensions of the masonry block units are given in Figure 3.2. Half blocks were obtained by cutting

stretcher blocks in half.

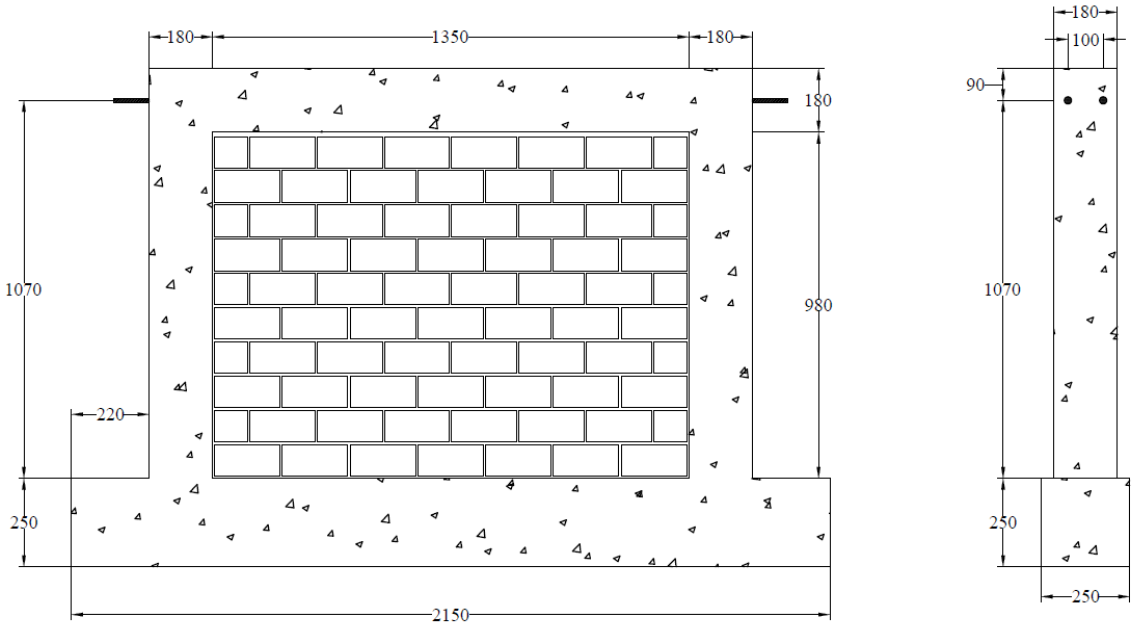

Figure 3.1 Details of RC Infilled Frame Specimens (unit: mm)

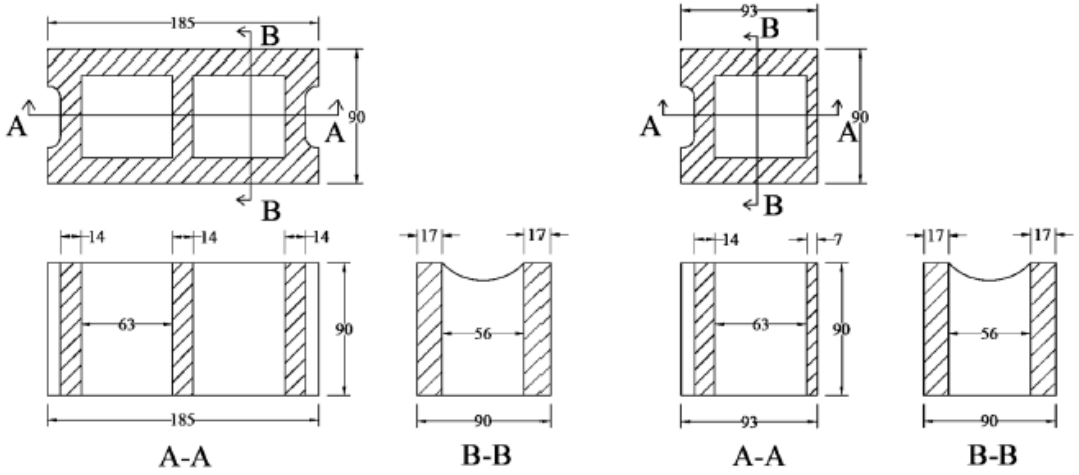

Figure 3.2 Dimensions of Half Scale Concrete Masonry Units (unit: mm)

The frame beam and columns are 180 mm by 180 mm square sections reinforced with four 10M deformed rebars and 10M stirrups spaced at 100 mm centre-to-centre. Additional strengthening was added to the top beam-column corners with four 300 mm by 300 mm 10M L-shaped rebars. The base beam of the frame was a 250 mm by 250 mm square section reinforced with four 15M deformed rebars and 10M stirrups spaced at 100 mm centre-to-centre. Reinforcement details are provided in Figure 3.3.

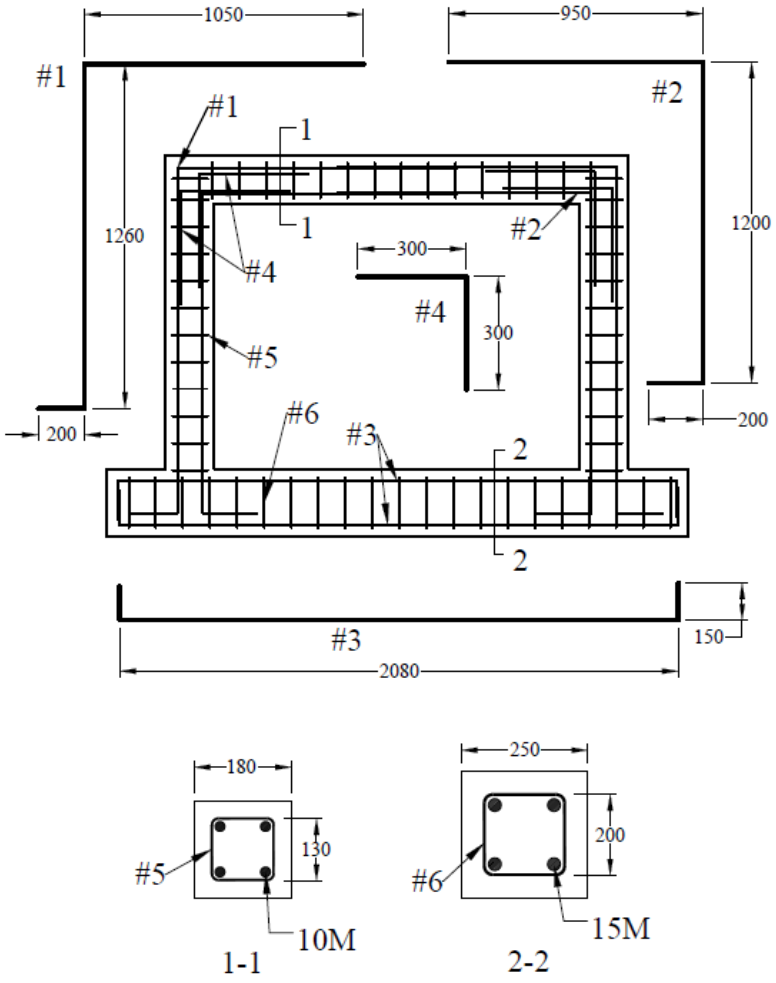

Figure 3.3 Reinforcing Rebar Detail (unit: mm)

3.2.1 CONSTRUCTION OF RC FRAMES

Construction of the RC frames began with forming reinforcement steel cages followed by building concrete formwork (Figure 3.4), placing the reinforcement cage into formwork (Figure 3.5), and casting the concrete (Figure 3.8 and Figure 3.9). The forms were constructed with oriented strain board to specified geometry. The reinforcing rebar cage was then positioned into the formwork, where plastic chairs were utilized to maintain a 25 mm cover. To enable cyclic loading on the specimen, two threaded rods running the full length of the frame beam were implemented as shown in Figure 3.6 and 3.7. The rods were placed on the neutral axis of the beam so their effect to the frame in-plane resistance is negligible. The ready mix concrete was specified with a compressive strength of 25 MPa and maximum coarse aggregate size of 12 mm. Concrete was poured on 15th December 2015 and the onsite slump test showed a falling height of 157 mm satisfying the required 150 mm. The slump test was completed in accordance with ASTM C143/C143M (2012) Standard Test Method for Slum of Hydraulic-Cement Concrete. Concrete was then poured into the formwork and vibrated with a vibrator (Figure 3.8). Once the concrete was thoroughly vibrated the surface was smoothed over using concrete trowels (Figure 3.9). Concrete cylinders were poured simultaneously and prepared in accordance with ASTM C39/C39M (2014).

Figure 3.4 Formwork Overview

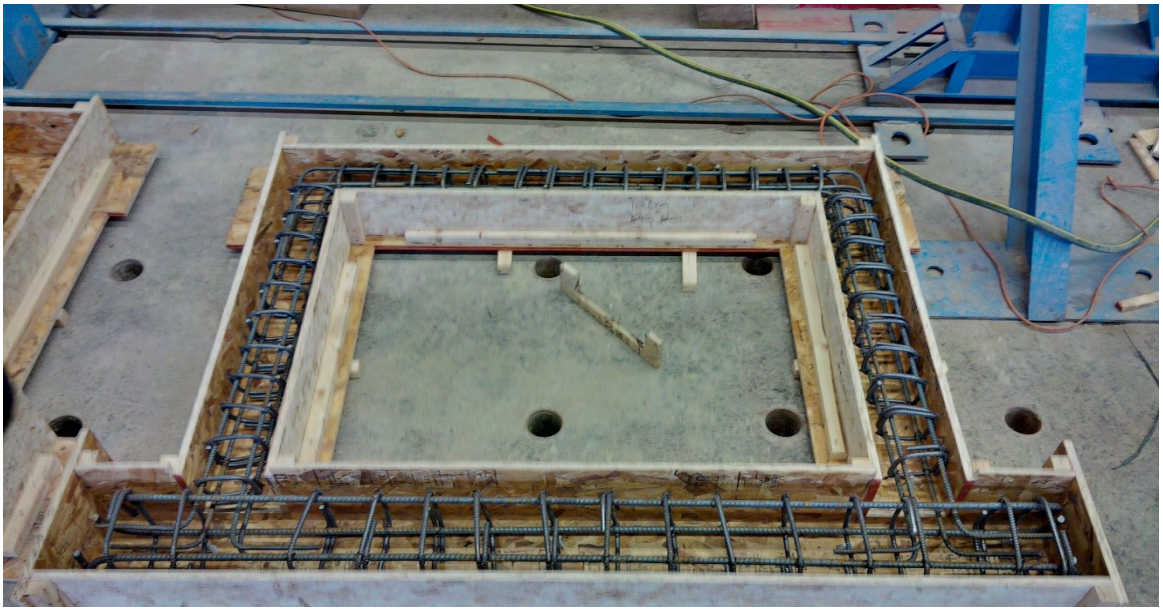

Figure 3.5 Reinforcing Steel Placed in Formwork

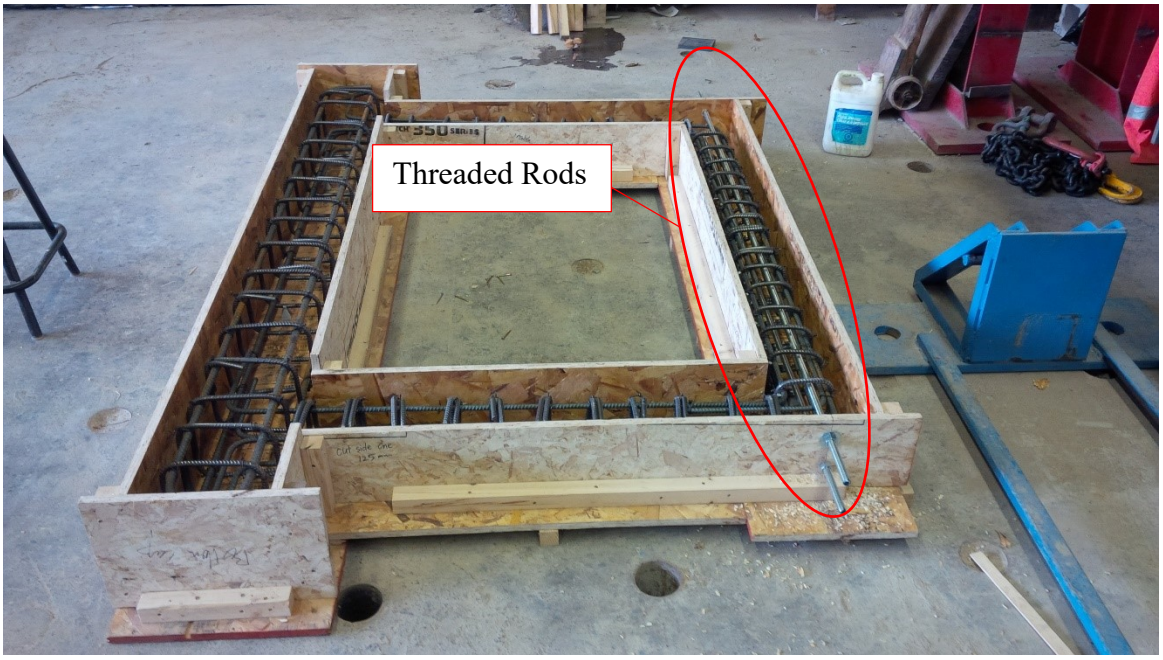

Figure 3.6 Threaded Rods Placed in Formwork

Figure 3.7 Formwork with Reinforcement and Threaded Rod Detail

Figure 3.8 Concrete Casting with Vibration

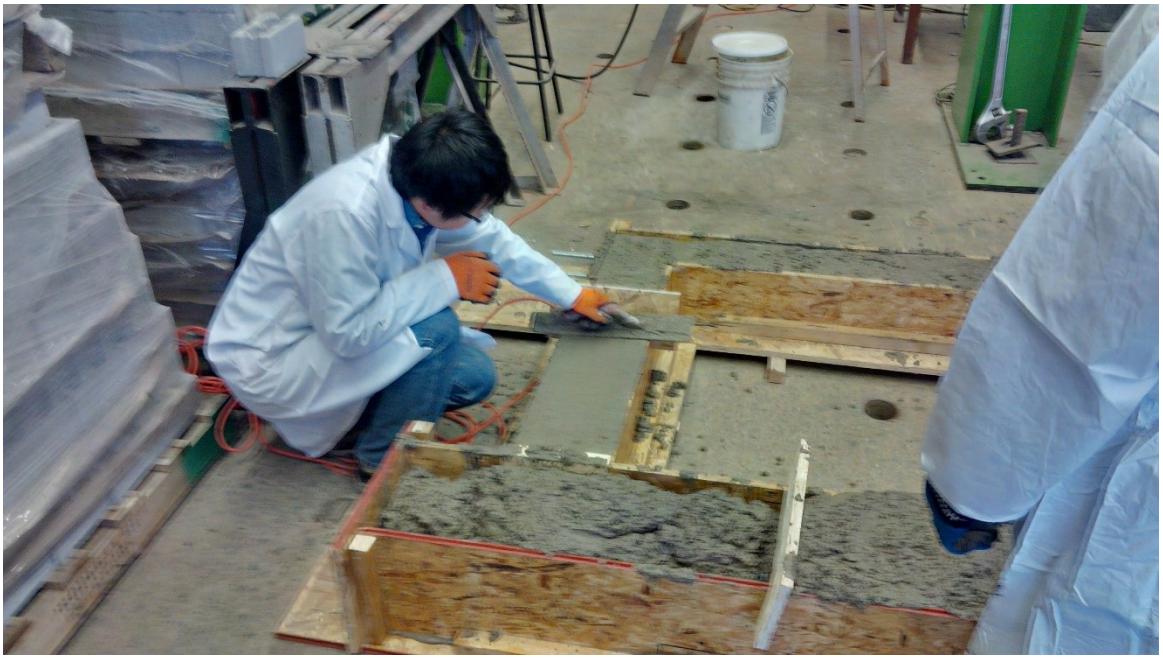

Figure 3.9 Concrete Surface Smoothing with Trowel

3.2.2 MASONRY INFILL CONSTRUCTION

The masonry infill walls were constructed on the 19th and 20th of January, 2016 by an experienced mason to the standard practice. Specimens IF-FG12 and IF-TG25 were constructed on the 19th with mortar batch A, while IF-W-SG12 and IF-W-TG12 were constructed on the 20th with mortar batch B. Figure 3.10 illustrates the typical construction process of a masonry infill. Construction of the infill began with cutting the stretcher block in half with a concrete saw creating half blocks for the running bond pattern as shown in Figure 3.10 (a). This was followed by carefully marking course lines outlining the height and width of the infill on the RC column and base so that the specified gap size can be achieved as shown in Figure 3.10 (b). Following the establishment of the references lines, CMUs and mortar were carefully placed in a running bond pattern, as illustrated in Figure 3.10 (c). A level and plumb were used throughout the construction to ensure that the walls were level and plumb, as shown in Figure 3.10 (d). Masonry blocks in the course above the window openings were grouted as per construction practice illustrated in 3.10 (e). All specimens and masonry prisms were moist cured under the same conditions for 28 days and then air cured until the day of testing.

(a)

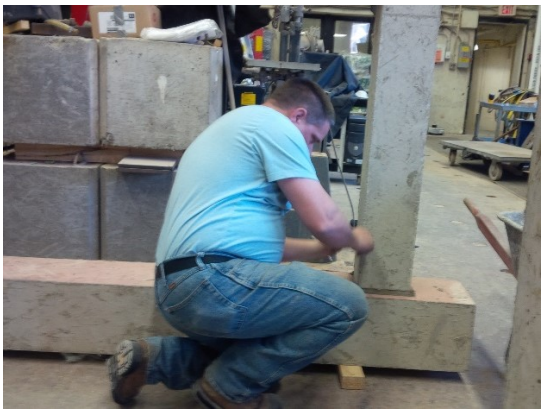

(b)

(c)

(d)

(e)

Figure 3.10 Masonry Infill Wall Construction

3.3 TEST SET-UP

A hydraulic actuator with a capacity of 100 kN was used to apply lateral cyclic loading. The actuator was housed in an independent frame which was then attached to the column of a reaction frame as shown in Figure 3.11. To realize the pulling and pushing action on the specimen, the two threaded rods running the full length of the frame beam were used as a simple measure. The actuator head was connected to the specimen through a steel plate and threaded rod assembly where a steel plate was secured to the specimen with two bolt holes for which the two threaded rods of the specimen were bolted through while a threaded rod connected to the actuator head was also welded to the steel plate at its center, as depicted in Figure 3.12. Between the plate and the frame, a pair of incompressible rubber pads were placed to prevent crushing of the concrete. The bottom beam of the frame was held in place with two w-shape steel beams clamping to the strong floor using threaded rods at stem ends of the beam as illustrated in Figure 3.13 (a) and (b). Two additional hydraulic rams were placed tightly against the frame bottom beam and the reaction frame column to further restrain the in-plane sliding of the frame bottom beam as shown in Figure 3.14 (a) and (b). Hydraulic pressure of the rams were monitored throughout testing.

Figure 3.11 Test Set-up

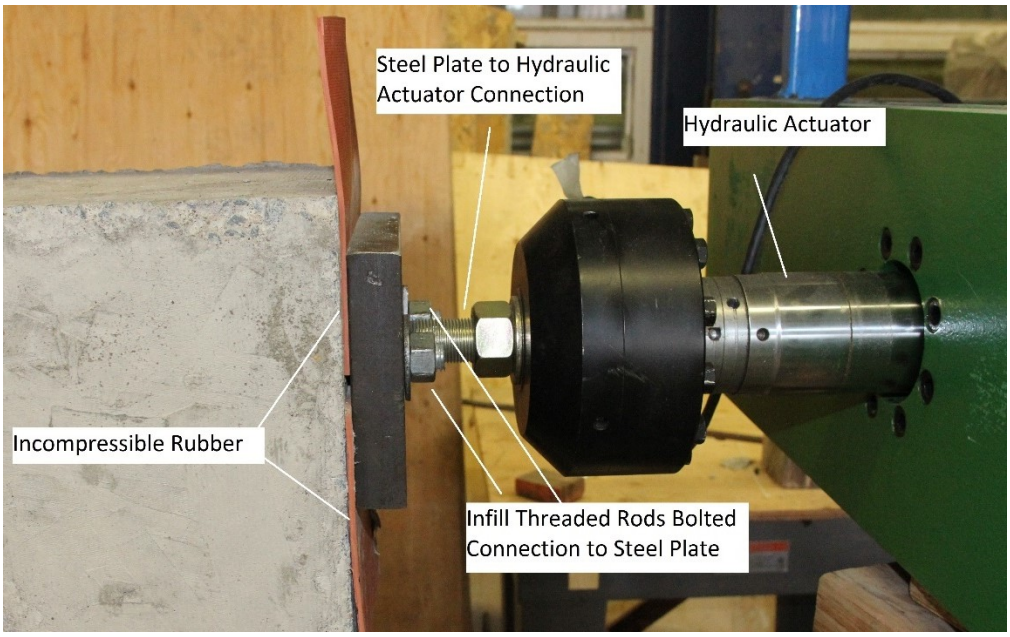

Figure 3.12 Hydraulic Actuator Connection to Test Specimen

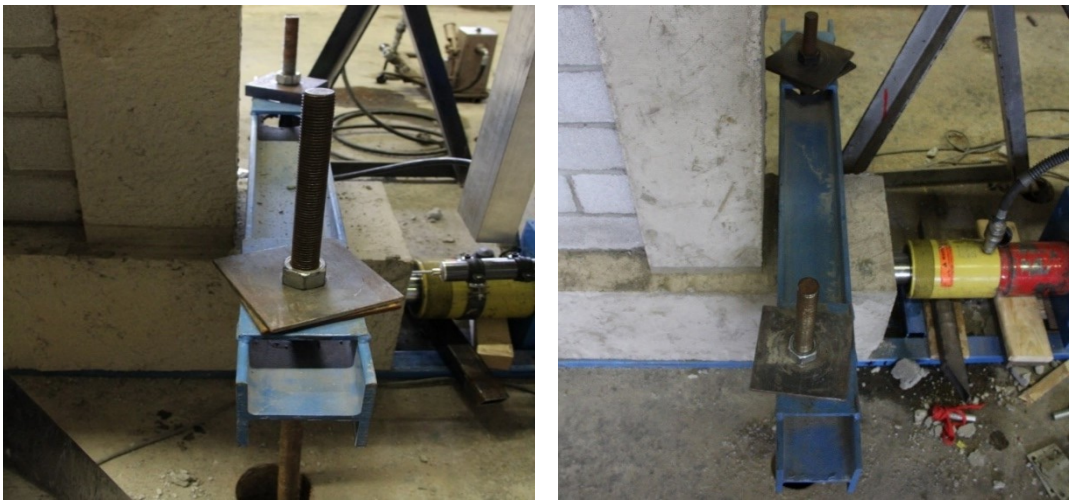

(a) (b)

Figure 3.13 Frame to Floor Connection Side and Top View

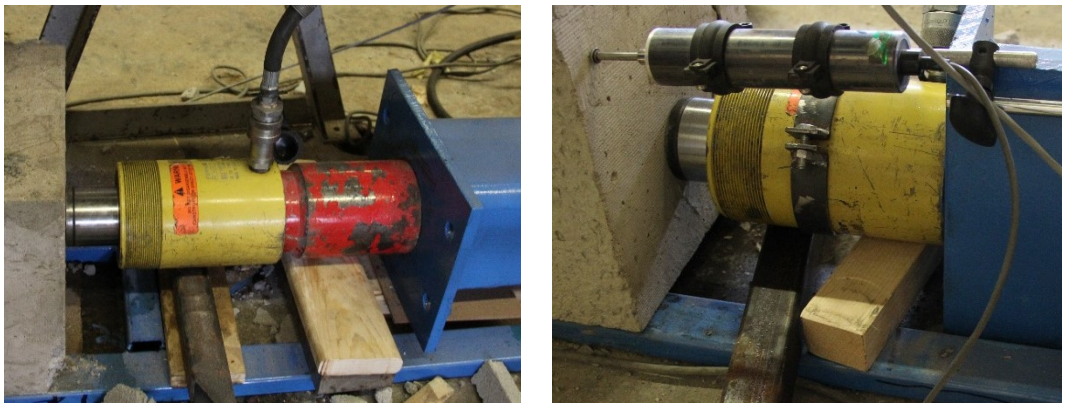

(a) (b)

Figure 3.14 Right Hand (a) and Left Hand (b) Hydraulic Base Support Jack

Four displacement transducers were used to monitor the specimen displacement. Transducer 1 (String potentiometer displacement transducer) and LVDT 2 (linear variable differential transformers, LVDT) were used to measure the lateral displacement of the specimen, where transducer 1 was to measure the frame top beam lateral displacement and

LVDT2 was mounted to measure the lateral displacement of the bottom beam of the specimen as shown in Figure 3.15 and 3.16. LVDT 3 and 4 were used to measure potential out-of-plane movement of the specimen where LVDT 3 was placed perpendicular to the centre of the frame beam and LVDT 4 was placed perpendicular to centre of the frame infill as shown in Figure 3.17.

Figure 3.15 Placement of Transducer 1

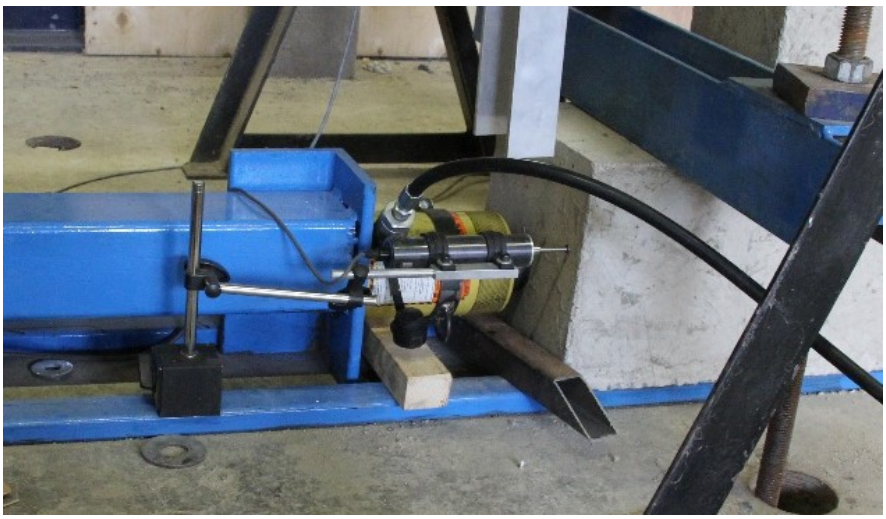

Figure 3.16 Placement of LVDT 2

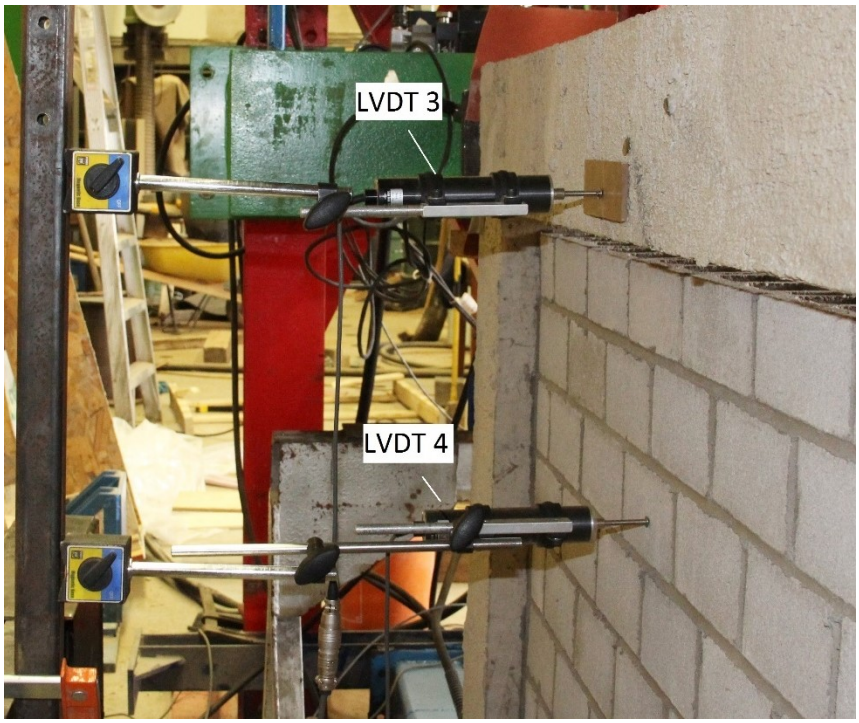

Figure 3.17 Placement of LVDT 3 & 4

3.4 LOADING PROTOCOL

The cyclic loading protocol used in this study was in accordance with ATC-24 (Applied Technology Council-24 1991) loading protocol specified for cyclic testing of steel structures. Although intended for steel structures, ATC-24 has often been used for the loading procedure of concrete masonry infill RC frames in several experimental programs (Mehrabi et al. 1994, Mosalam 1996, El-Dakhakhni 2002, Al-Nimry 2014). The ATC loading protocol uses the yield deformation reference Δ_y to determine the increase in amplitudes for each set of cycles.

Testing begins with six elastic cycles with at least three of which are performed at 0.75 Δ_y.

Following the elastic cycles, three cycles at Δ_y, $2\Delta_y$, and $3\Delta_y$, respectively are performed. If the specimen has not failed by $3\Delta_y$ cycles, the loading would continue with sets of two cycles starting at $4\Delta_y$ increasing by increments of Δ_y until failure.

The calculated Δ_y for the RC frame in this study is 7 mm, which occurs at approximately 34 kN of the in-plane lateral force. The loading protocol of the infilled frame used in this study can be seen in Figure 3.18.

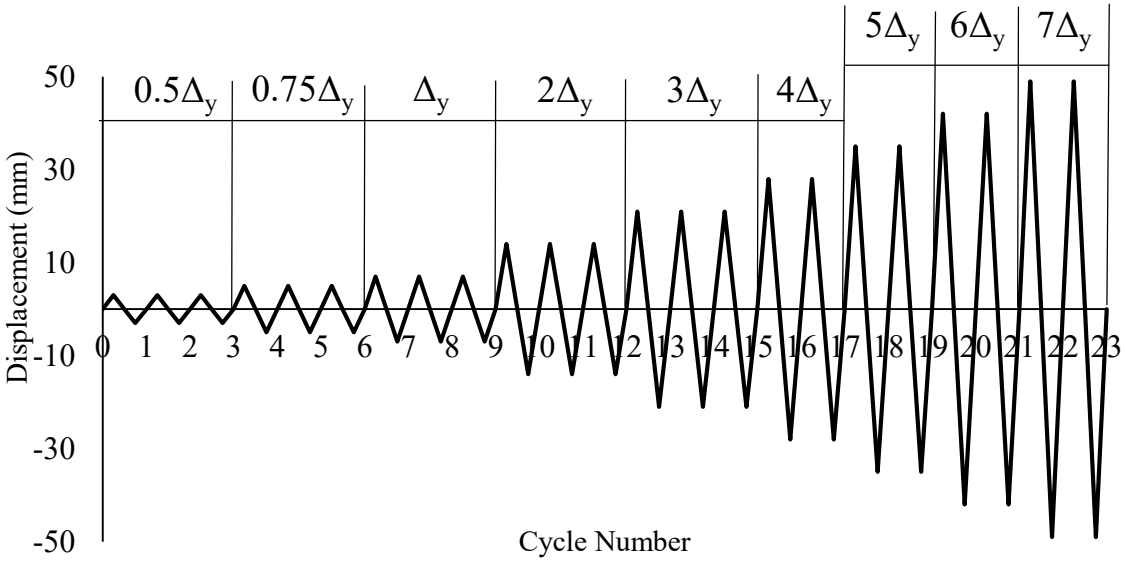

Figure 3.18 Loading Protocol for the Quasi-Static Loading

3.5 TESTING PROCEDURE

Prior to testing, each specimen was first positioned in the testing place and was aligned carefully in both in-plane and out-of-plane directions. The displacement transducers were then checked for functionality and were zeroed for initial recording. The reading of the

load and displacement was set to record at 0.2 second intervals using an electronic data acquisition system. Lateral displacement corresponding to each cycle was input into a LabVIEW program that controls the actuator to move to the prescribed position at a rate of 10 mm/minute. After each set of cycles, the displacement readings were verified with the LabView displacement indicator to ensure that the accuracy of the loading and data collecting system. For each specimen, a minimum set of 9 cycles were performed. Throughout the testing, the cracking pattern and failure mode as loading progressed were noted for each specimen.

3.6 AUXILIARY TESTS

3.6.1 CMUs

The compressive strength and physical properties of the scaled CMUs used in this study were measured in accordance with ASTM C140/C1140M (2014) Standard Test Methods for Sampling and Testing Concrete Masonry Units and Related Units. Physical properties obtained included percentage absorption, moisture content, and density. Three blocks were selected at random for both compression and physical properties testing. Compressive testing was conducted using the Instron universal testing machine as seen in Figure 3.19. Fiberboards were used as capping material on both ends of the unit specimen to provide a smooth surface for even load distribution.

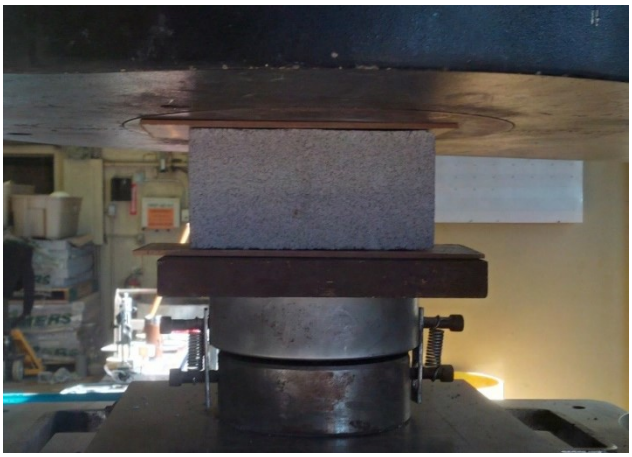

Figure 3.19 CMU Compression Test

3.6.2 MORTAR

Mortar specified for the masonry infill walls was Type S mortar. The mortar mix volume aspect ratio used was 1:1:6 volume ratio for Type N mortar, Portland cement and sand. Traditionally a mix volume aspect ratio of 1:3:12 of Type N mortar, Portland cement, and sand is used for Type S Mortar. Two batches of mortar (batch A and B) were mixed for the construction of masonry infill walls and mortar cubes. Mortar cubes were demolded 48 hours after curing in the non-absorbent mold; the mortar cubes were then cured in hydrated lime water for 26 days as per specification of ASTM C109/C109M Standard Test Method for Compressive Strength of Hydraulic Cement Mortars. Compressive testing was conducted using the Instron compression machine as shown in Figure 3.20.

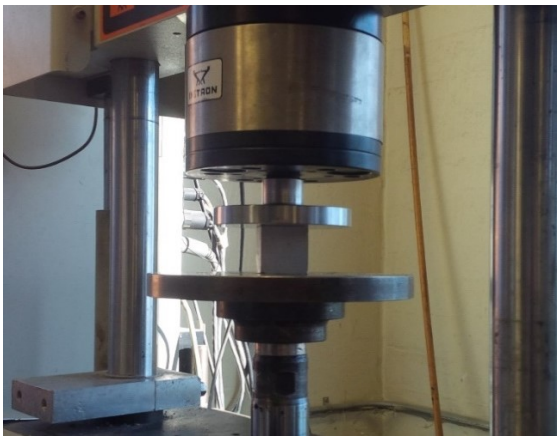

Figure 3.20 Mortar Cube Compression Test

3.6.3 MASONRY PRISMS

A total of twenty 3-course high masonry prisms were constructed and tested for compressive strength in accordance with ASTM C1314 Standard Test Method for Masonry Prisms. The prisms were produced at the same time as the masonry infill walls and cured under the same condition. Figure 3.21 illustrates the production of masonry prisms. In the prism construction, mortar was applied only to the faceshell of the masonry block. Compressive testing was conducted using the Instron universal testing machine with specimens capped with two pieces of fiberboard on the loading surface, as shown in Figure 3.22.

Figure 3.21 Masonry Prism Construction

Figure 3.22 Masonry Prism Test

3.6.4 CONCRETE CYLINDERS

The ready mix concrete used for concrete frames construction was specified to have a

compressive strength of 25 MPa. The frame specimens were cast on December 15th, 2015 and six 100x200 mm and three 150x300 mm cylinders were poured. Small cylinder (100x200 mm) were tested on 14 day, and 28 day for compressive strength. Large cylinders were tested on the day of frame testing for both compressive strength and modulus of elasticity. All testing procedures were conducted in accordance with ASTN C39/C39M (2014) Standard Test Method for Compressive Strength of Cylinder Concrete Specimens. Figure 3.23 shows a typical setup for prism testing for compressive strength and modulus.

Figure 3.23 Concrete Modulus and Compression Test

3.6.5 REINFORCING STEEL

Reinforcing steel data was collected from Hu (2015) and is used in this study since the reinforcement used in both studies was from the same batch. Three coupons from the 10M

longitudinal reinforcing steel used in the frame member were cut at random and tested for modulus of elasticity and strength. Details of the reinforcing coupons used are presented in Figure 3.24. Testing was conducted in accordance with ASTM E8 (2008) Standard Test Methods for Tension Testing of Metallic Materials for their mechanical properties using Instron universal testing machine. Figure 3.25 depicts a typical test setup for steel coupon testing. The stress-strain relationship of the steel was measured by obtaining the strain of the steel using the extensometer.

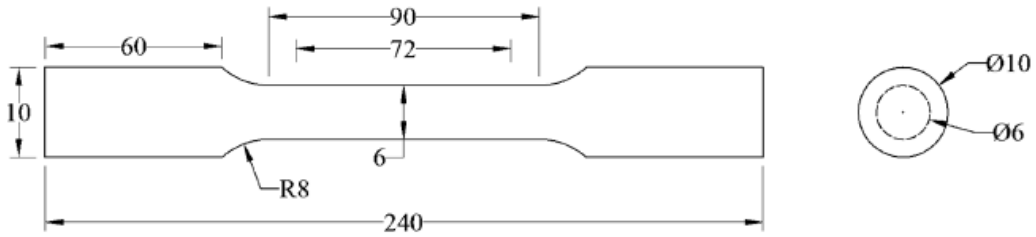

(a) (b)

Figure 3.24 Steel Coupon Detailing (Hu 2015)

Figure 3.25 Tension Test Set-up for Steel Coupons (Hu 2015)

CHAPTER 4 EXPERIMENTAL RESULTS

4.1 INTRODUCTION

This chapter presents results of both the auxiliary and infilled frame tests. Auxiliary test results detail physical and mechanical properties of CMUs, mortar, masonry prisms and concrete cylinders. The results of the infilled frame tests are focused on presentation and discussions of infilled frame failure mode, strength, stiffness, ductility, energy dissipation, and strength/stiffness deterioration as affected by interfacial gaps between the infill and the bounding frame.

4.2 RESULTS OF AUXILLARY TESTS

4.2.1 CMUs

The physical properties of CMUs including net area, weight, density, absorption rate, and moisture content were determined in this study. Three CMUs were selected at random and were used for this purpose. The net area of the CMUs, shown as the hatched area in Figure 4.1, was calculated to be 9128 mm^2. The moisture content, absorption, and density were determined in accordance with ASTM C140/C140M (2015). For each randomly selected CMU, the initial mass (weight received) was first measured. The specimen was then submerged in 150 mm of water for 24 hours at which point, its weight was measured in water. The specimen was then removed from the water and surfaced dried and its weight was recorded at this point (saturated weight). The specimen was then oven dried at 100 °C

for 24 hours and final mass was recorded (dry weight). The masses obtained were used to calculate the absorption, moisture content, and density. Average absorption was determined to be 141.6 kg/m with a coefficient of variation (CV) of 3%; average moisture content was determined to be 4.8% with a CV of 8%; and the average density was 2022.3 kg/m^3 with a CV of 1%. The CAN/CSA A165 Standard for Masonry Units requires that standard 200 mm hollow blocks shall have a density greater than 2000 kg/m^3, moisture content below 45% at a relative humidity of above 75%, and an absorption less than 175 kg/m^3. All average physical properties of the CMUs meet these criteria.

Table 4.1 CMU Physical Properties

ID	Received Weight (g)	Immersed Weight (g)	Saturated Weight (g)	Dry Weight (g)	Absorption		Moisture Content (%)	Density (kg/m^3)
					kg/m^3	(%)		
A	1598.8	913.7	1701.1	1593.3	136.9	6.8	5.1	2023.5
B	1606.7	919.4	1714.5	1601.0	142.7	7.1	5.0	2013.6
C	1640.3	946.7	1752.3	1635.3	145.2	7.2	4.3	2029.9
				Avg.	141.6	7.0	4.8	2022.3
				CV (%)	3	3	8	1

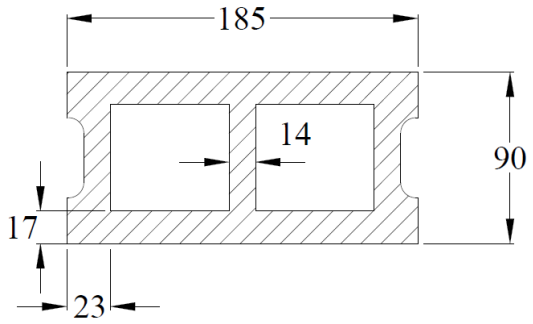

Figure 4.1 Net Area of the CMU Block

Table 4.2 summarizes the compressive strength of the CMUs. The net area of 9128 mm^2 was used in the calculation of the compressive strength. The average compressive strength was determined to be 12.3 MPa with a CV of 7%. Failure modes seen for CMUs included conical shear and spalling shown in Figure 4.2.

Table 4.2 Compressive Strength of CMUs

ID	Ultimate Load (kN)	Compressive Strength (MPa)
CMU1	123.5	13.5
CMU2	107.8	11.8
CMU3	105.6	11.5
	Avg.	12.3
	CV (%)	7

Figure 4.2 Typical Failure Mode of the CMUs

4.2.2 MORTAR

Mortar batch A was used in the construction of IF-G12 and IF-TG25 and mortar batch B was used in the construction of IF-W-TG12 and IF-W-SG12. As shown in Table 4.3, mortar batch A showed a compressive strength of 49.4 MPa and a CV of 7% whereas mortar batch B showed a compressive strength of 48.8 MPa and a CV of 3%. Both batches' CV were well below the limit of 15% specified by CSA S304-14, indicating the mortar used was consistent for both batches. Figure 4.3 illustrates a specimen with conical failure mode, typical for mortar cube compressive tests.

Figure 4.3 Typical Failure Mode of the Mortar Cubes

Table 4.3 Compressive Strength of Mortar Cubes

ID	Length (mm)	Width (mm)	Area (mm^2)	Ultimate Load (kN)	Compressive Strength (MPa)
MA1	49.9	50.6	2510	128.4	51.1
MA2	50.8	51.0	2591	133.3	51.4
MA3	50.5	51.8	2616	141.2	53.9
MA4	50.9	51.5	2621	119.3	45.5
MA5	50.2	51.0	2560	116.0	45.3
				Avg.	49.4
				CV(%)	7
MB1	50.0	50.8	2540	126.1	49.6
MB2	50.3	51.2	2545	130.9	50.8
MB3	50.1	50.5	2560	124.5	49.2
MB4	50.4	50.0	2520	117.9	46.7
MB5	51.0	50.0	2550	122.0	47.8
				Avg.	48.8
				CV(%)	3

4.2.3 MASONRY PRISMS

Prism batches A and B were constructed with mortar from batches A and B respectively. Since mortar was applied only to the face shell of CMUs for prisms to mimic the actual wall construction, compressive strength was calculated using the faceshell area, A_e. The faceshell area of the prism was calculated to be 6290 mm^2, and is shown as the hatched area in Figure 4.4. A list of resulted compressive strength can be found in Table 4.4. Prism

batch A showed a compressive strength of 11.1 MPa and a CV of 14% whereas prism batch B showed a compressive strength of 10.0 MPa and a CV of 11%. Again, the CVs of both batches are below the required 15%, indicating a consistent prism strength. Masonry prisms typically failed in a diagonal cracking pattern as shown in Figure 4.5 (a) and (b) where cracking was through the web of the prism.

Table 4.4 Masonry Prism Compressive Test Results

ID	P_{ult} (kN)	f'_m (MPa)	ID	P_{ult} (kN)	f'_m (MPa)
PA1	74.2	11.8	PB1	68.0	10.8
PA2	63.2	10.1	PB2	58.3	9.3
PA3	60.7	9.7	PB3	67.9	10.8
PA4	86.9	13.8	PB4	67.5	10.7
PA5	66.1	10.5	PB5	51.0	8.19
	Avg.	11.1		Avg.	10.0
	CV(%)	14		CV(%)	11

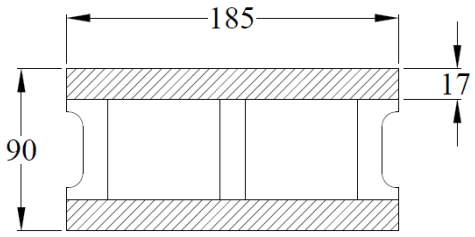

Figure 4.4 Effective Cross-sectional Area of Prisms

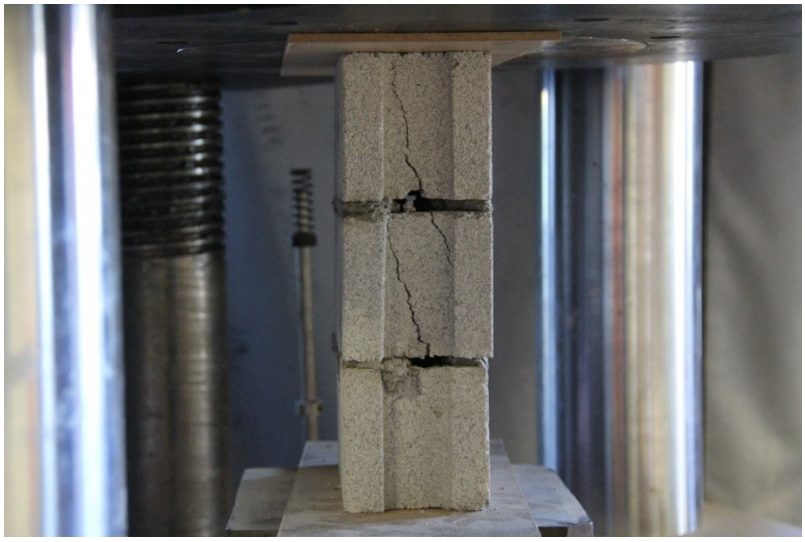

(a)

(b)

Figure 4.5 Typical Failure Mode of Masonry Prisms

4.2.4 CONCRETE

Concrete cylinders were tested for compressive strength at 14, and 28 days of curing as well as on the day of the infilled frame testing (120 days). Table 4.5 summarizes the results

of concrete strength at different days of curing. The average compressive strength on 14-day was 21.2 kN with a CV of 3%. The average compressive strength on 28-day was 27.4 MPa. The average compressive strength on the day of testing was 29.2 MPa with a CV of 2.5%. The average modulus of elasticity was found to be 13203 MPa. Figure 4.6 shows the typical failure of the cylinders and Figure 4.7 depicts the initial linear portion of the typical stress vs. strain curve of the concrete cylinders.

Table 4.5 Concrete Cylinder Compression Tests Results

14 Days	P_{ult} (kN)	f'_c (MPa)	28 Days	P_{ult} (kN)	f'_c (MPa)	120 Days	P_{ult} (kN)	f'_c (MPa)	E (MPa)
A1	37.0	20.3	B1	224.2	27.5	C1	514.1	28.2	14023
A2	40.1	22.0	B2	223.5	27.4	C2	541.9	29.8	12876
A3	39.0	21.2	B3	222.7	27.3	C3	543.7	29.7	12710
	Avg.	21.2			27.4			29.2	13203
	CV(%)	3			3			3	4

Figure 4.6 Typical Failure Mode of Concrete Cylinder

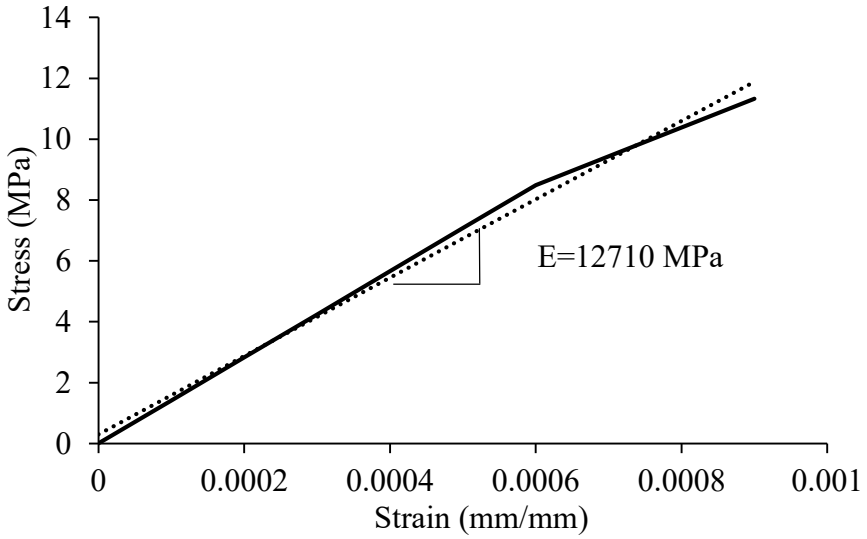

Figure 4.7 Initial Stress vs. Strain Curve of Concrete Cylinders in Compression (Cylinder C3)

4.2.5 SUMMARY OF AUXILARY TEST RESULTS

The steel reinforcement properties were obtained in a previous testing program (Hu 2015) and was reproduced in the table including the yield stress, ultimate stress (in the bracket), and Young's modulus. The mechanical properties of the masonry components used in this study are summarized in Table 4.6. As shown in the table, results indicate that mechanical properties of RC frames in terms of concrete and reinforcement and masonry infills in terms of components and assemblage are similar among all specimens.

Table 4.6 Summary of Auxiliary Tests

		CMUs	Mortar	Prisms	Concrete	Reinforcement Hu (2015)
Batch A	Strength (MPa)	17.8	49.4	11.1	29.2	446 (665)
	Elastic Modulus (MPa)	-	-	9435	13203	247357
Batch B	Strength (MPa)	17.8	48.8	10.1	29.2	446 (665)
	Elastic Modulus (MPa)	-	-	8500	13203	247357

4.3 INFILLED SPECIMEN RESULTS

4.3.1 FAILURE MODE

Table 4.7 summarizes the failure initiation mode, and final failure mode in both the positive (pulling) and negative direction (pushing) for each infilled specimen.

Table 4.7 Summary of Experimental Results

ID	Failure Initiation	Final Failure Mode (+)	Final Failure Mode (-)
IF-FG12	SS	CC	DC
IF-TG25	DC	CC	DC
IF-W-TG12	DC	DC	DC
IF-W-SG12	DC	CC	DC

Note: CC stands for corner crushing; SS stands for sliding shear; DC stands for diagonal cracking.

Corner crushing was the most common failure mode in the pulling action, and diagonal cracking was the most common failure mode in the pushing action. Almost all failure was initiated by diagonal cracking, with the exception of specimen IF-FG12 whose failure was initiated by sliding shear. The failure modes obtained from this study are in line with the findings of similar infilled frames subjected to static loading (Hu 2015) where the formation of diagonal cracking followed by corner crushing was also identified as the most common failure mode. The following section provides detailed failure mode description for each specimen.

4.3.1.1 *IF-FG12*

Corner crushing occurred at 31.9 mm lateral displacement in pulling direction for specimen IF-FG12. With a full gap present, the bounding frame made contact with the infill at the third set of cycles and the infill showed noticeable load carrying at the fourth set of cycles at a displacement of 14 mm. During the 14 mm cycle, sliding was observed along the base of the infill at 22.4 kN in the pulling action and 19.1 kN in the pushing action. Once sliding was initiated, the infill began to form the diagonal strut with opposing corners making contact with the infill. A small area at the bottom right-hand corner began to show corner crushing at 37 kN during the pulling action of the 21 mm cycle. The specimen continued to gain strength and the crushed area grew until ultimate failure was reached at 80.3 kN during the pulling action of the 35 mm cycle. Figure 4.8 (a) provides an overall view of failure pattern. Figure 4.8 (b) depicts corner crushing in the bottom right corner at failure. Following pulling action failure, diagonal cracking failure was observed at 31.5 mm during the pushing action of the 35 mm loading cycle. The ultimate load in the pushing action was 79.5 kN, similar to the pulling action ultimate load. Only one major diagonal crack was observed in the pushing direction. Early signs of spalling/corner crushing in the top right-hand corner were also observed during failure, which then grew to full corner crushing following the completion full corner crushing as depicted in Figure 4.8 (c).

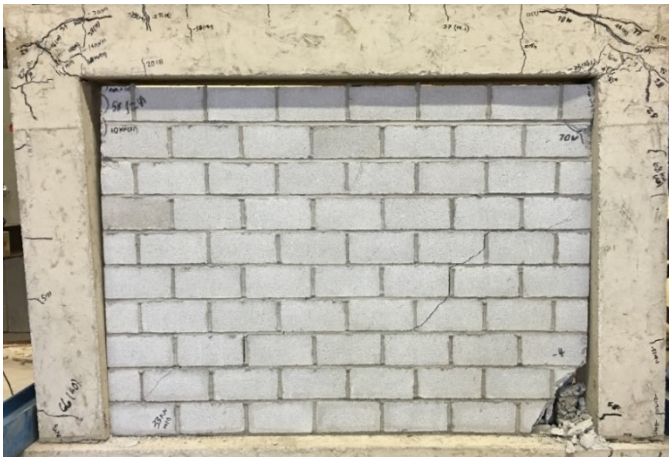

a) Overview of Infilled Frame at Failure

b) Bottom Right Corner

c) Top Right Corner

Figure 4.8 Specimen IF-FG12 Failure Pattern

4.3.1.2 *IF-TG25*

Specimen IF-TG25 failed due to corner crushing during the pulling action of the 14 mm cycle where a sudden diagonal crack initiated failure in the pulling direction at a displacement of 7.7 mm and a lateral load of 75.7 kN. Following shortly after the diagonal cracking, ultimate capacity was reached with corner crushing in the top left corner of the infill at a displacement of 8.4 mm, achieving the ultimate load of 77.9 kN in the pulling action. Figure 4.9 (a) shows the overall failure pattern whereas 4.9 (b) and (c) show the

close-up view of the top left corner and top right corner at failure respectively. Figure 4.9 (b) depicts the corner crushing in the top left corner at failure. Following the corner crushing failure, a sharp drop in load capacity was observed in the pulling action. Upon load reversal, a diagonal crack was also initiated 1.4 mm into the pushing action of the 14 mm cycle, reaching at a load of 21 kN. Failure in the pushing action was more ductile as the specimen continued to gain strength during the 21 mm cycle until reaching ultimate strength in the pushing action of 76.3 kN at a lateral displacement of 20.8 mm. Figure 4.9 (c) shows that no corner crushing at the top right corner.

a) Overview of Infilled Frame at Failure

b) Top Left Corner

c) Top Right Corner

Figure 4.9 Specimen IF-TG25 Failure Pattern

4.3.1.3 *IF-W-TG12*

Diagonal cracking was observed as the initiation failure and final failure mode of specimen IF-W-TG12 while no visible corner crushing was seen. Cracks began to form along the diagonal direction of the infill at 3.5 mm in the pulling action of the 5 mm cycle at a recorded load of 19.4 kN. Similarly, diagonal cracks formed at 2.7 mm in the pushing action of 5 mm cycle at a recorded load of 19.3 kN. Cracks in the infill and the frame

continued to propagate in subsequent cycles and extended to the corner of the opening. The ultimate load was reached during pushing action of the 28 mm cycle at a recorded load of 71.8 kN. Figure 4.10 depicts the overall failure pattern and extent of cracking in the top corners.

a) Overview of Infilled Frame at Failure

b) Top Left Corner

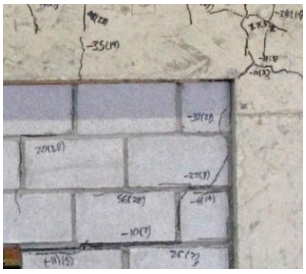

c) Top Right Corner

Figure 4.10 Specimen IF-W-TG12 Failure Pattern

4.3.1.4 *IF-W-SG12*

Failure of specimen IF-W-SG12 was initiated by diagonal cracking during the 14 mm cycle at 31.8 kN. During the previous cycles, contact did not form between the infill and the

bounding frame on opposite corners of the infill. The diagonal crack propagated throughout the remaining cycles and extended to the opening at the 35 mm cycle. The specimen reached the ultimate load of 66.9 kN in the pushing action. In the pulling action the ultimate load of 64.2 kN was reached with loaded top left corner crushing at a lateral displacement of 28 mm. While overall similar cracking pattern to the specimen IF-W-TG 12 was observed, cracking of the side gapped specimen in this case did not necessarily form from the diagonal corner. Figure 4.11 shows the overall and close-up view of the failure pattern.

a) Overview of Infilled Frame at Failure

b) Top Left Corner

c) Top Right Corner

Figure 4.11 Specimen IF-W-SG12 Failure Pattern

Table 4.8 presents a summary of cracking and ultimate loads and displacements for both the pulling and pushing action for all specimens. The pulling direction load and displacement are assigned positive values, and pushing direction load and displacement are assigned negative values. Definition of cracking strength, P_{cr}, and ultimate strength, P_{ult} and their corresponding deflections, Δ_{cr} and Δ_{ult}, are shown in Figure 4.12 using specimen IF-W-TG12 as an example. They were defined using the load vs. displacement hysteric curves which is discussed in detail in Section 4.3.2. In terms of the strength, specimen IF-

FG12 sustained the highest ultimate load, which is 32.7% increase in comparison to the bare frame. Specimen IF-TG 25 also showed an increase in comparison to the bare frame specimens with an ultimate strength of 77.9 kN and also had the highest cracking strength at 75.7 kN. For those two specimens with both interfacial gap and openings, the ultimate strengths were also higher than the bare frame specimen and did not differ significantly from each other.

Table 4.8 Peak Load and Deflections from Hysteric Load-Displacement Curves

ID	P_{cr}^{+} (kN)	Δ_{cr}^{+} (mm)	P_{cr}^{-} (kN)	Δ_{cr}^{-} (mm)	P_{ult}^{+} (kN)	Δ_{ult}^{+} (mm)	P_{ult}^{-} (kN)	Δ_{ult}^{-} (mm)
IF-FG12	22.4	6.9	-19.1	-4.0	80.3	31.9	-79.5	-31.5
IF-TG25	75.7	7.7	-21.0	-1.4	77.9	8.4	-76.3	-20.8
IF-W-TG12	19.4	3.4	-19.3	-2.7	64.8	28.2	-71.8	-26.8
IF-W-SG12	31.8	8.3	-25.1	-4.4	64.2	27.3	-66.9	-31.4
BF	23.7	6.9	-27.9	-7.0	48.1	32.2	-60.5	-50.9

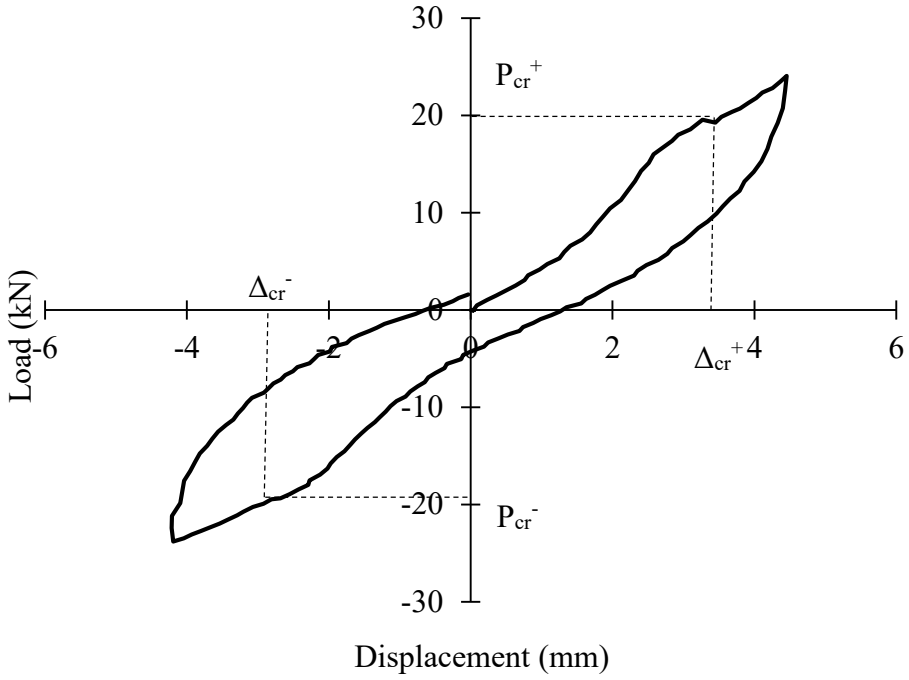

a) Cracking Load and Displacement for Specimen IF-W-TG12 first loop, cycle no. 2

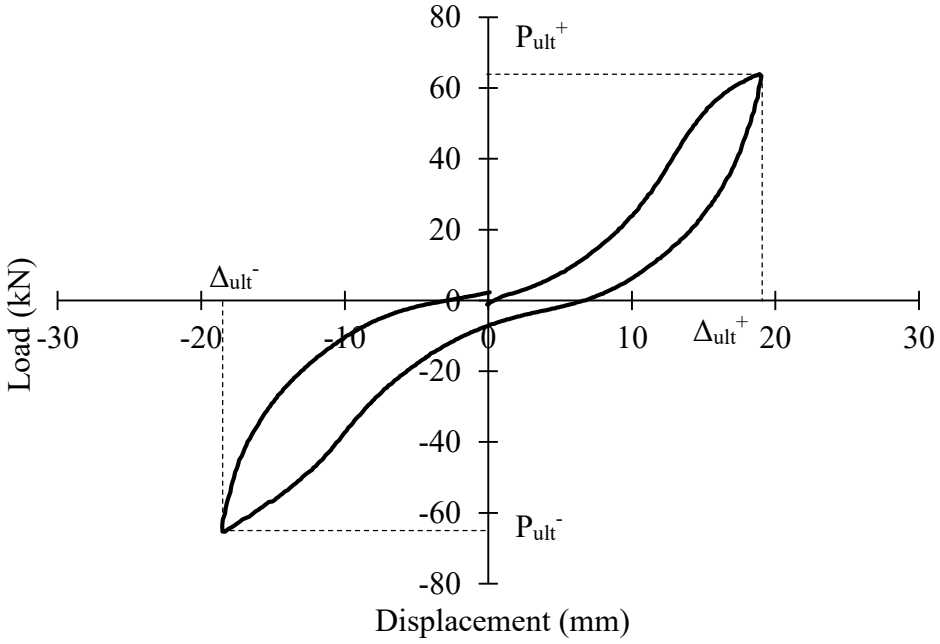

b) Ultimate Load and Displacement for Specimen IF-W-TG12 first loop, cycle no. 5

Figure 4.12 Cracking and Ultimate Load and Deflections

4.3.2 *HYSTERIC RESPONSES*

The lateral load vs. displacement hysteric response for all specimens are presented in this section. To aid the discussion, the following terms are defined and they are the initial stiffness, K_{in}, the average secant initial stiffness, $K_{in\ sec}$, the average secant cracking stiffness, $K_{cr\ sec}$, and the average secant ultimate stiffness, $K_{ult\ sec.}$ Figures 4.13, 4.14, 4.15, and 4.16 depict the definition of these terms.

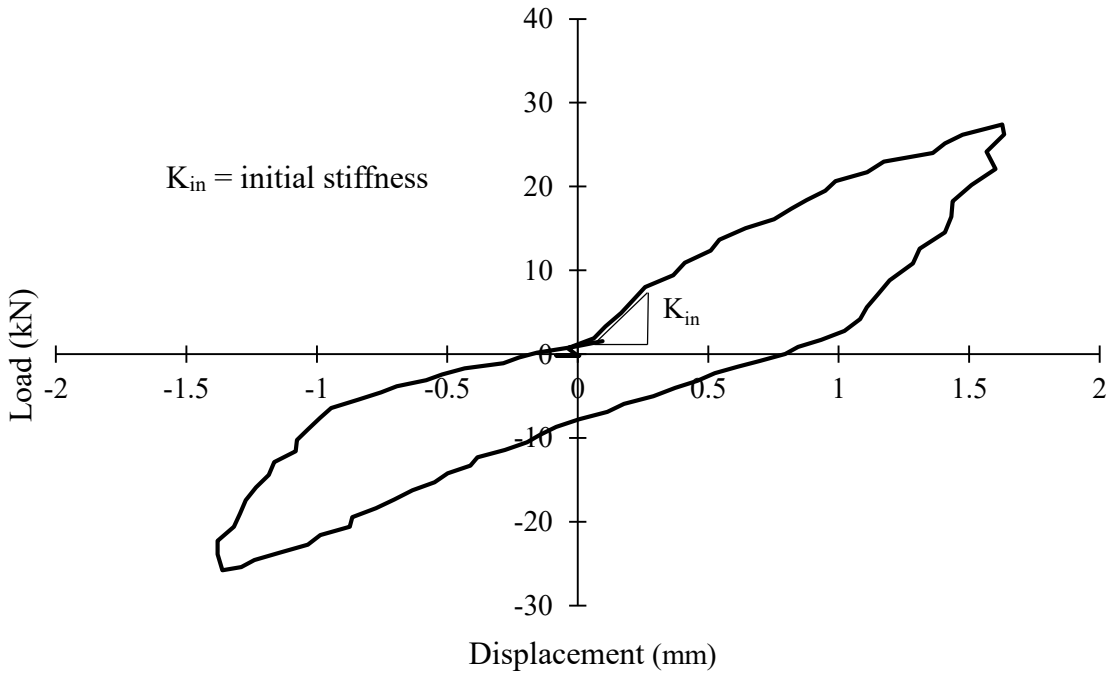

Figure 4.13 Specimen IF-TG25 Cycle No. 1, Loop 1

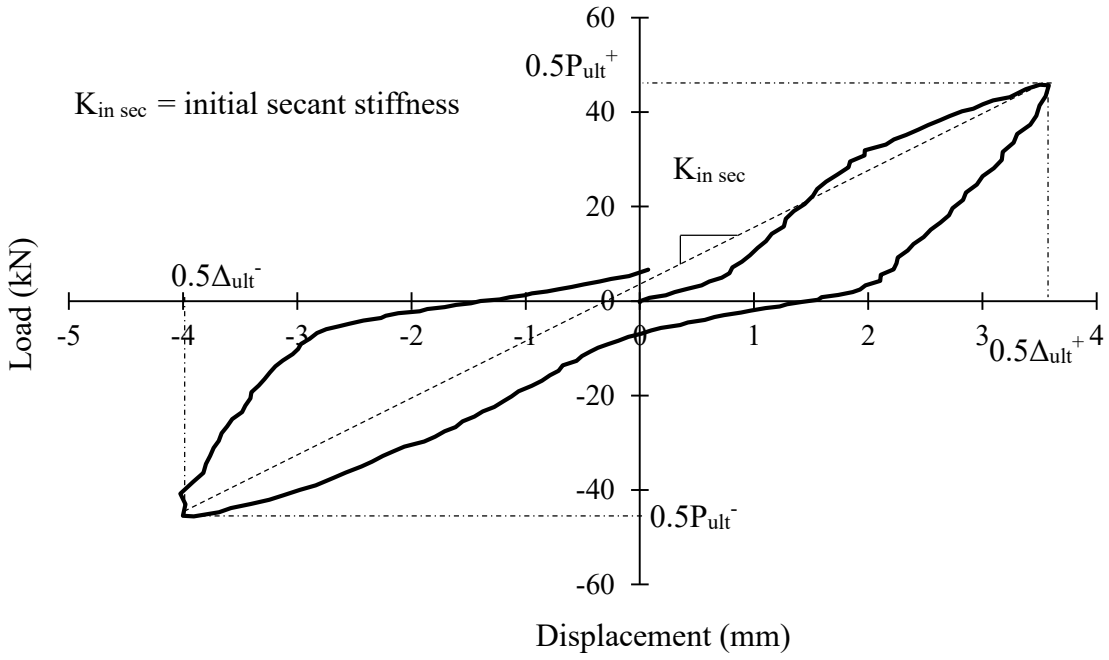

Figure 4.14 Specimen IF-TG25 Cycle No. 2 Loop 1

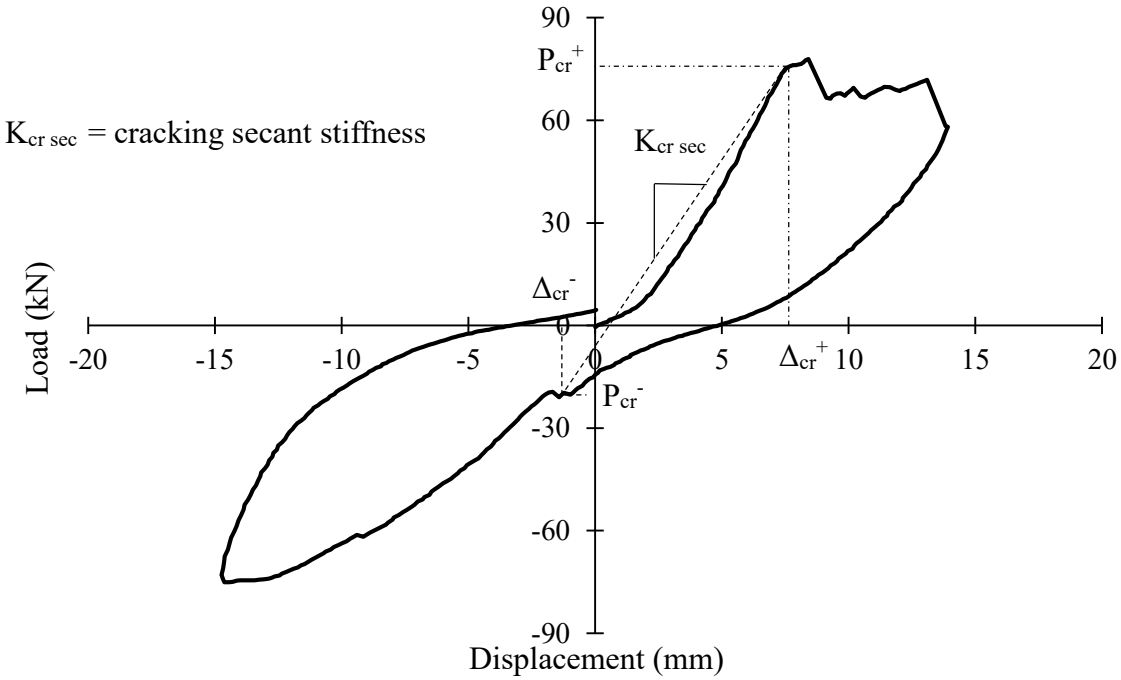

Figure 4.15 Specimen IF-TG25 Cycle No.4 Loop 1

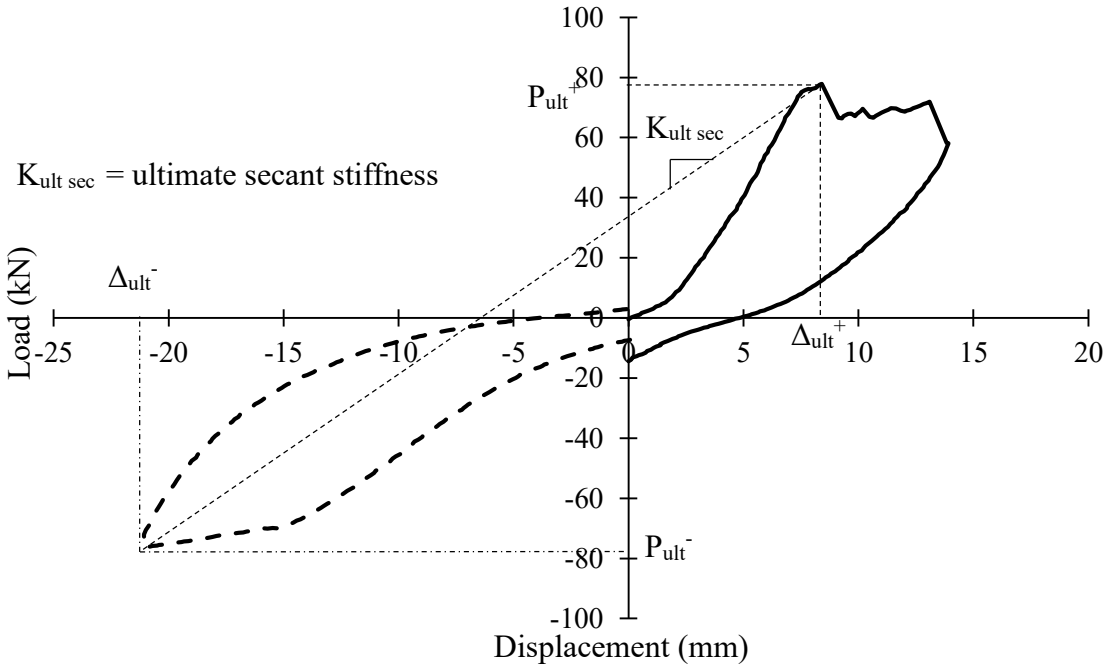

Figure 4.16 Specimen IF-TG25 Cycle No 4 & 5 Cycle Loop 1

Initial stiffness is calculated as the slope of the tangent of the initial linear portion (up to 5% of the ultimate load level) of the first cycle of the load displacement curve. The average secant initial, cracking and ultimate stiffness are defined as the slope of a line connecting extreme points of displacement cycle as depicted in Fig. 4.14 to Fig. 4.16. Average secant stiffness is calculated using the following equation:

$$K_{sec} = \frac{P_{max} + P_{min}}{\Delta_{max} + \Delta_{min}} \qquad 4\text{-}1$$

where P_{max} and Δ_{max} are the largest force and corresponding displacement in the positive action within a cycle, respectively; and P_{min} and Δ_{min} are the lowest force and corresponding displacement within the negative action of a cycle, respectively. Initial average secant

stiffness, $K_{in\ sec}$, is determined by connecting two extreme points within a cycle roughly equal to 50% of the ultimate lateral load (Moslam 1996, Al-Nimry 2014). Cracking and ultimate stiffness, $K_{cr\ sec}$ and $K_{ult\ sec}$ respectively, are calculated in a similar manner as initial stiffness but with P_{max} and Δ_{max} being replaced with cracking force and corresponding displacement, P_{cr} and Δ_{cr}, and ultimate force and corresponding displacement, P_{ult} and Δ_{ult}, respectively. Table 4.9 gives a summary of all average secant stiffness and the initial stiffness of the test specimens.

Table 4.9 Average Secant Stiffness Results of Specimens

ID	K_{in} (kN/mm)	Average Secant Stiffness (kN/mm)		
		$K_{in\ sec}$ (kN/mm)	$K_{cr\ sec}$ (kN/mm)	$K_{ult\ sec}$ (kN/mm)
IF-FG12	-	7.8	3.8	2.5
IF-TG25	26.4	25.5	10.6	5.5
IF-W-TG12	24.7	9.1	6.3	2.5
IF-W-SG12	19.1	8.8	4.5	2.2
BF	12.4	7.2	-	1.3

As shown in Table 4.9, in the comparison of specimens IF-FG12 and IF-TG25, the full separation gap had the greater influence on the stiffness than the top gap in all cases. This is expected as more deformation would be required to close the full separation gap before the infill is engaged in the load sharing. Also noted is that the full separation gap specimen initial secant stiffness is similar to that of the bare frame specimen. Although the top gap specimen (IF-TG25) had a greater size, the load was transferred at the onset of loading through the bearing between the infill and frame columns, leading to a much greater stiffness. In the comparison of specimens IF-W-TG12 and IF-W-SG12, the much lower

stiffness in both specimens was attributed to the presence of openings; however, specimen IF-W-TG 12 still showed a noticeable higher stiffness than specimen IF-W-SG12.

The lateral load vs. displacement hysteric response for all specimens are shown in Fig. 4.17 to Fig. 4.21.

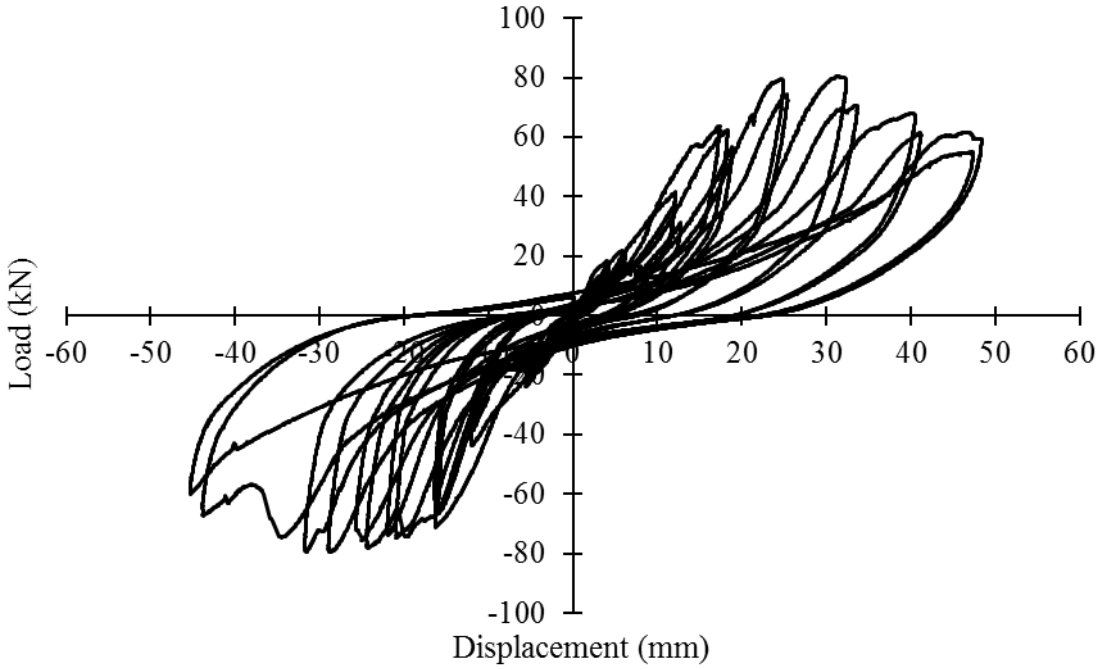

Figure 4.17 Load vs. Displacement Hysteric Curve for Specimen IF-FG12

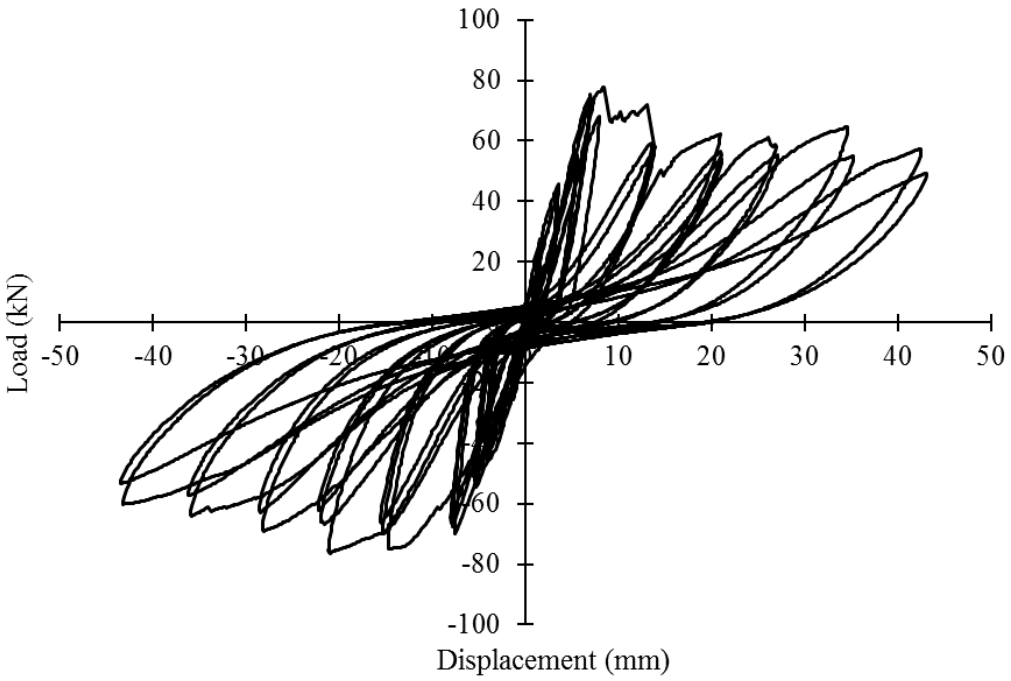

Figure 4.18 Load vs. Displacement Hysteric Curve for Specimen IF-TG25

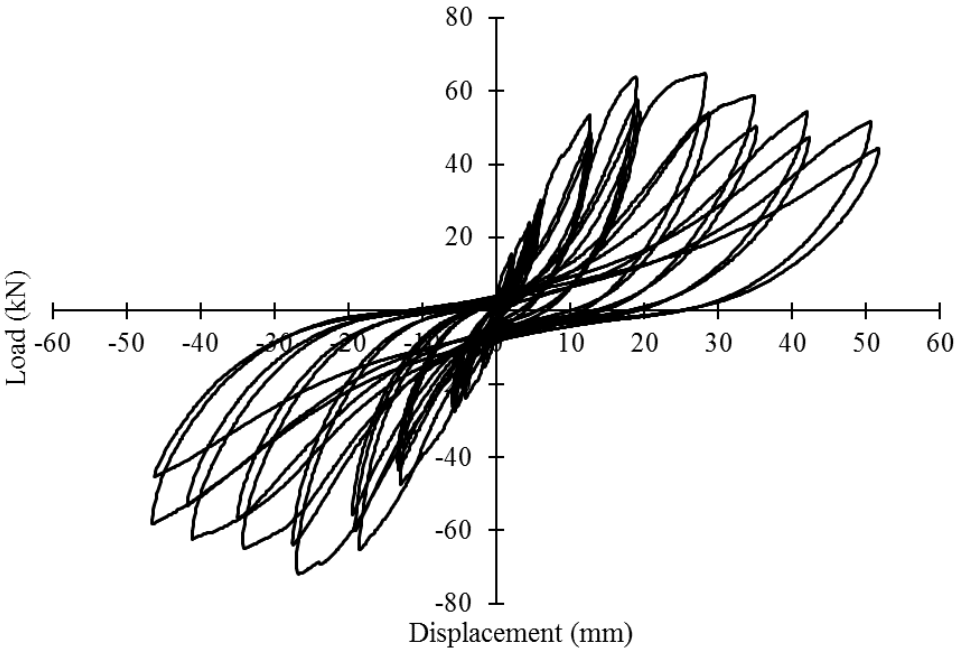

Figure 4.19 Load vs. Displacement Hysteric Curve for Specimen IF-W-TG12

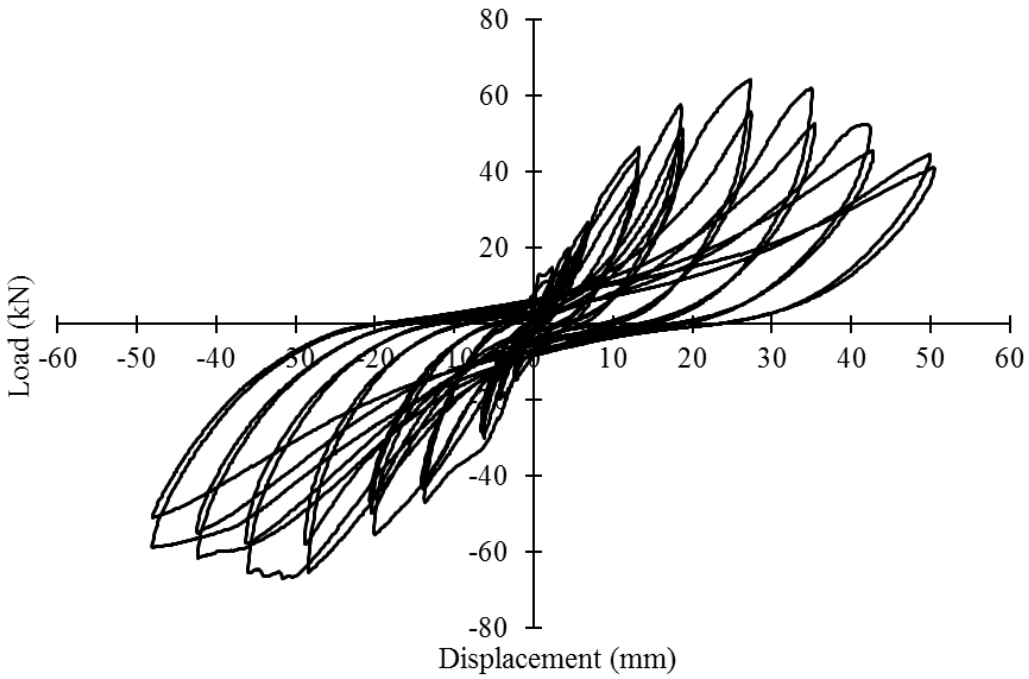

Figure 4.20 Load vs. Displacement Hysteric Curve for Specimen IF-W-SG12

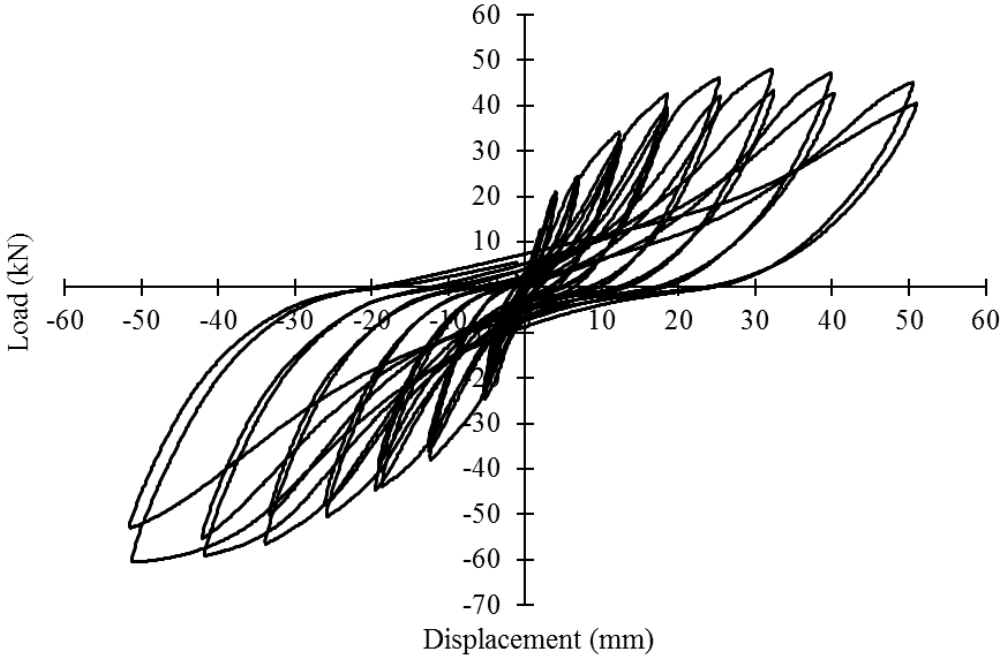

Figure 4.21 Load vs. Displacement Hysteric Curve for Specimen BF

The hysteric curves of all specimens exhibited pinching characteristics which is typical of masonry infilled RC frames subjected to cyclic loading. Pinching characteristics of masonry infilled frames are largely attributed to the opening and closing of cracks (Klinger and Bertero 1976).

For example, hysteric curves of specimens IF-W-TG12, and IF-W-SG12 can be broken into two distinct sections shown in Fig. 4.22 and Fig. 4.23. The first section, which occurs in the early cycles before cracking, exhibits no pinching, and behaves more or less in a linear elastic manner. The second section occurs once cracking of the infill is initiated, typically around 20-30 kN, and the hysteric curve begins to show more pronounced signs of pinching.

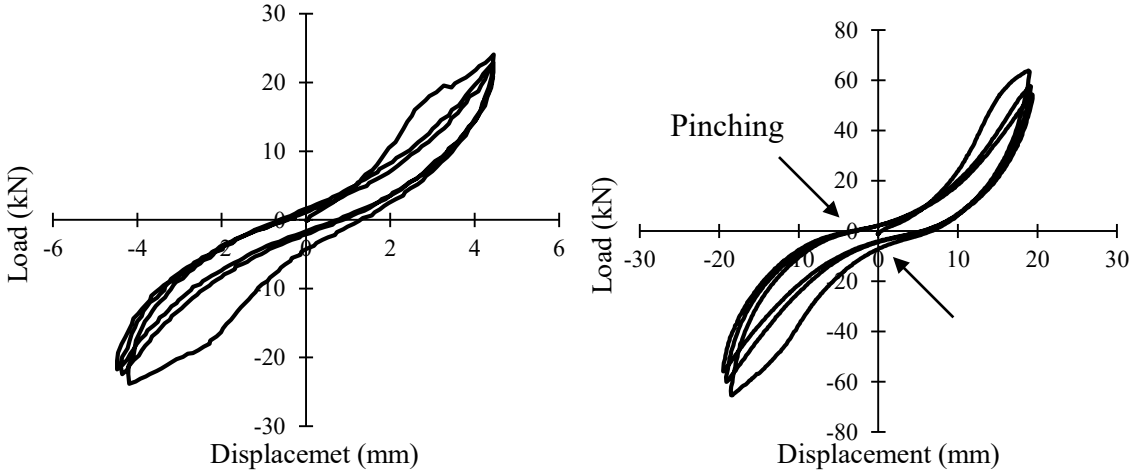

a) Cycle No.2 (At Cracking) b) Cycle No. 5 (Post Cracking)

Figure 4.22 Cyclic Load vs. Displacement Curves Specimen IF-W-TG12

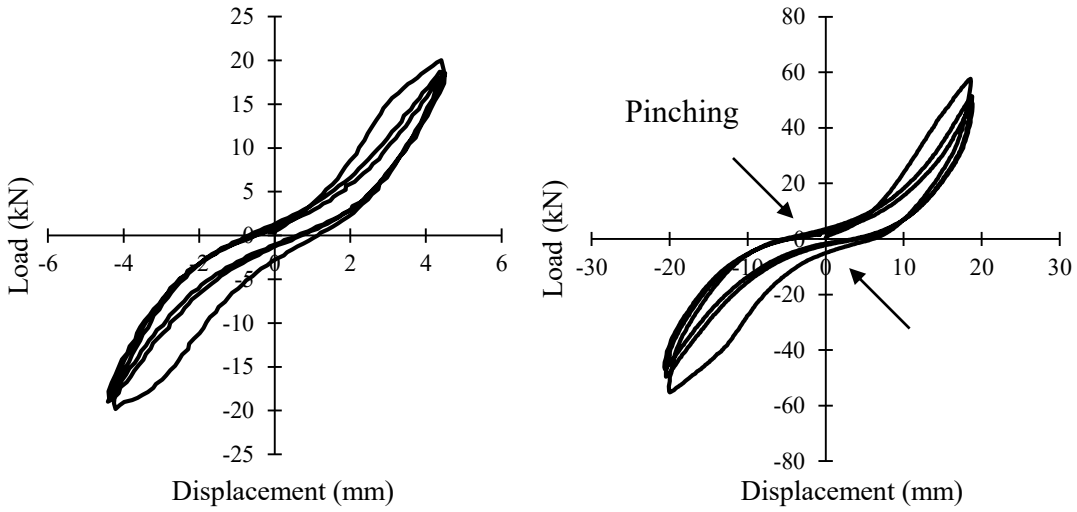

a) Cycle No. 2 (Before Cracking) b) Cycle No. 5 (Post Cracking)

Figure 4.23 Cyclic Load vs. Displacement Curves Specimen IF-W-SG12

Unlike the specimens with windows, hysteric curve for specimen IF-TG25 exhibited pinching characteristics earlier and more pronounced than other specimens, with curves showing a flatter slope approaching zero displacement as illustrated in Figure 4.24. Post cracking, specimen IF-TG25 hysteric curves exhibited similar behaviour as the second section of the specimens with openings, with smooth curves as illustrated in Figure 4.24 (b). Specimen IF-FG12, differs only slightly from the other three specimens. However, the loops are narrower and stiffness is lower due to the lack of contact between the infill and the frame. A zone of zero stiffness, as illustrated in Figure 4.25 (a), is observed at a load around 20 kN. The zone of zero stiffness corresponds to the sliding occurred along the base of the infill. Following the sliding shear, the hysteric curves exhibits a similar pinching pattern as the second section of infilled specimens with openings as illustrated in Figure

4.25 (b).

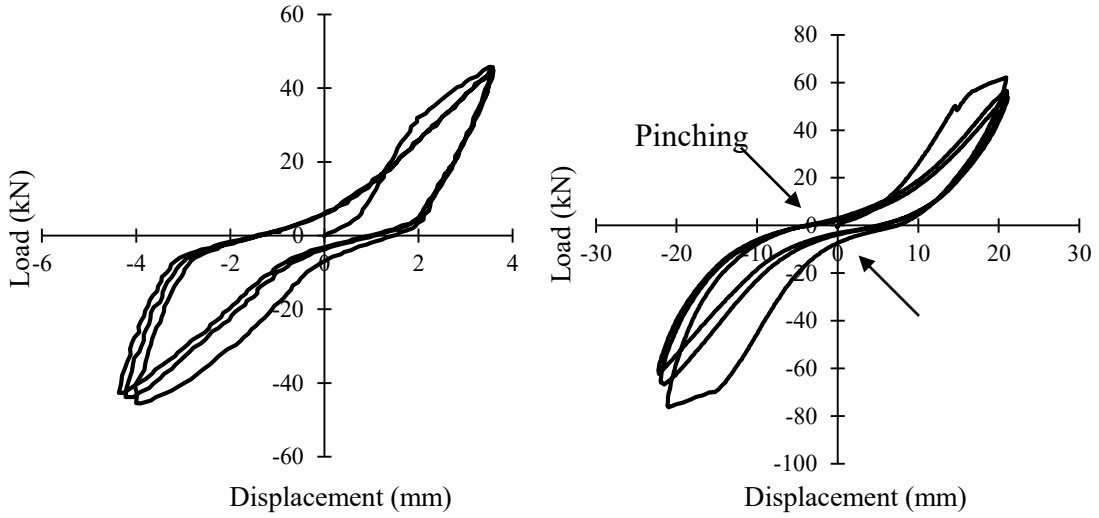

a) Cycle No. 2 (Before Cracking) b) Cycle No. 5 (After Cracking)

Figure 4.24 Cyclic Load vs. Displacement Curves Specimen IF-TG25

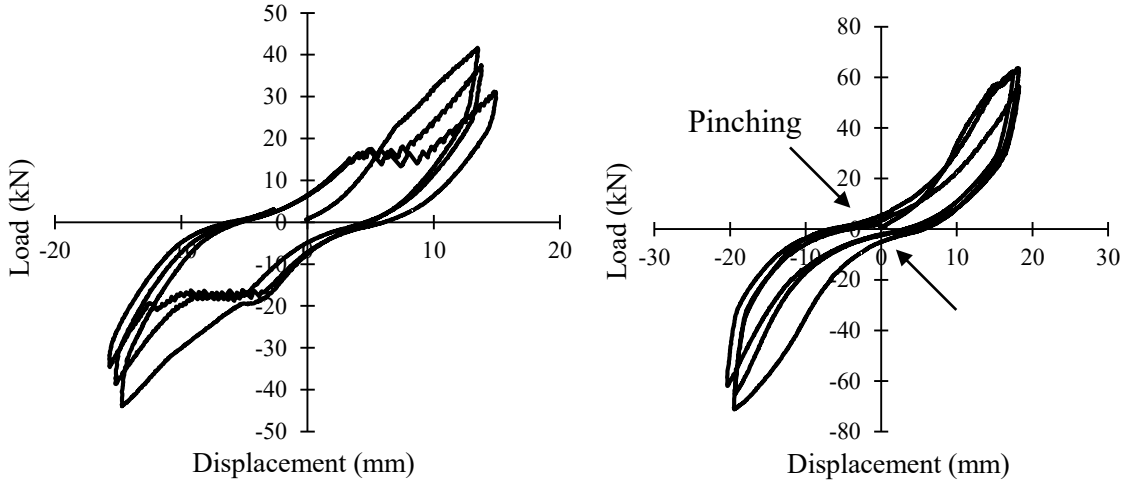

a) Cycle No. 4 (At Cracking) b) Cycle No. 5 (After Cracking)

Figure 4.25 Cycle Load vs. Displacement Curves Specimen IF-FG12

In addition to the peak secant stiffness and hysteric curves, the loading and unloading stiffness degradation of each successive cycle is also an important indicator of specimen behaviour under cyclic loading. The loading and unloading stiffness were calculated using the secant stiffness of the positive and negative portion of the first cycle in each set of cycles. Figure 4.26 details the loading and unloading stiffness in both the positive and negative direction. Loading stiffness was calculated as the secant stiffness from the origin to the peak load of the positive and negative loading direction. Unloading stiffness was taken as the secant stiffness connecting the peak load, in either the positive or negative direction, to the point of zero load within the half cycle.

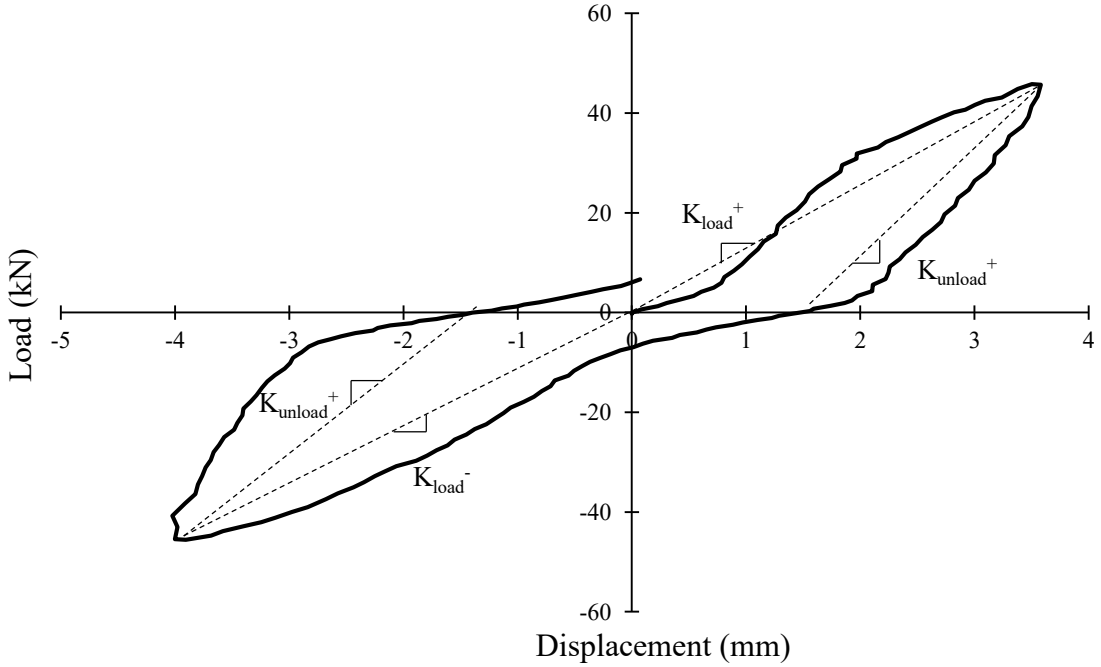

Figure 4.26 Load vs. Displacement of a Single Cycle for Specimen IF-W-SG12

Figures 4.27 (a) to (e) plot the average loading and unloading stiffness from the positive and negative cycles, against the cycle number for each specimen. All except specimen IF-FG12 showed similar stiffness variation trend as cycle number increased.

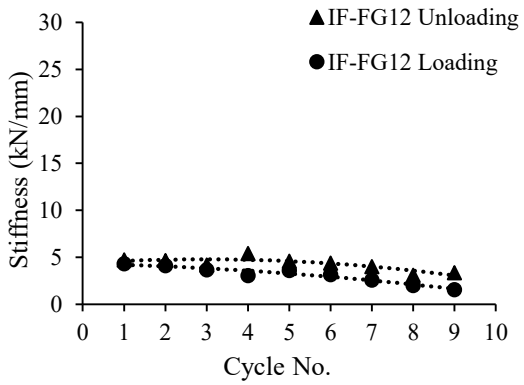

a) Specimen IF-FG12

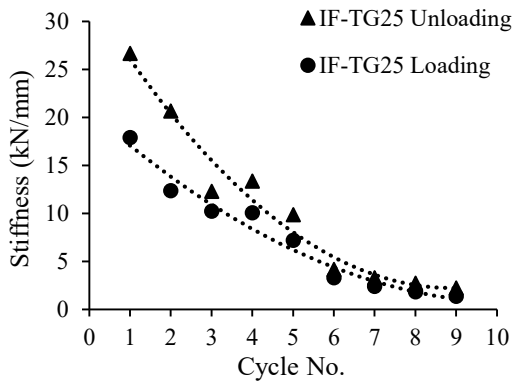

b) Specimen IF-TG25

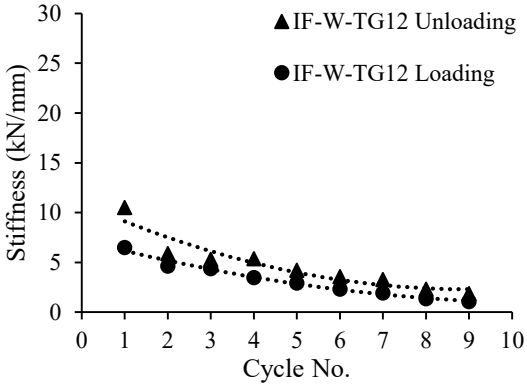

c) Specimen IF-W-TG12

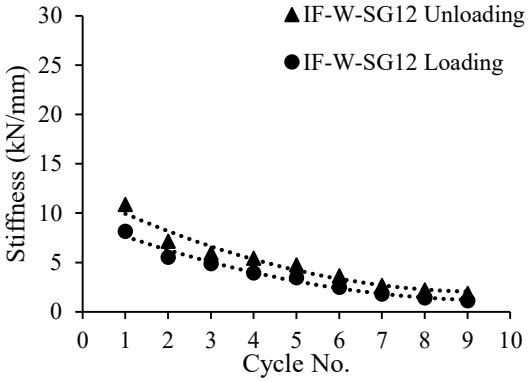

d) Specimen IF-W-SG12

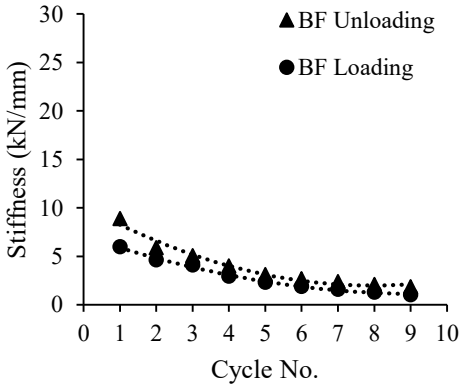

e) Bare Frame Specimen

Figure 4.27 Loading and Unloading Secant Stiffness vs. Cycle No.

Loading secant stiffness of specimens IF-W-TG12 and IF-W-SG12 generally decreased in a more or less linear manner at a similar rate as the bare frame specimen. Both specimens exhibited similar unloading secant stiffness with an average difference of 2% when compared at the same cycle. Specimen IF-TG25 showed the steepest decrease in unloading secant stiffness with 26.7 kN/mm in the first cycle and 2.2 kN/mm in the final cycle. Loading stiffness followed an approximately linear pattern and showed a marked difference in initial stiffness when compared with the unloading stiffness. However, close to failure, difference in loading and unloading stiffness began to diminish. In the case of specimen IF-FG12, the stiffness decreasing trend showed a slightly different curve where an arc pattern was observed, indicating a stiffness increase in the process of loading. This is most notably seen in the increase in unloading secant stiffness during the 4^{th} set of cycles which corresponded to when the frame made contact with the infill. Overall, specimen IF-FG12 showed some of the lowest levels of secant stiffness among all specimens.

4.3.2.1 *BACKBONE CURVES*

From the hysteric curve, a backbone curve can be generated by connecting the peak points of each successive cycle of the hysteric curve. The backbone curve provides an equivalent monotonic load vs displacement relationship of a cyclically loaded specimen. Although monotonically loaded specimens typically have a higher ultimate load than cyclically loaded counterparts, backbone curves are a good indicator of characteristics of cyclically loaded specimens using familiar monotonic-like curves. The monotonic backbone curves for all specimens are shown in Figure 4.28. One apparent finding seen in the figure is that

benefit of the infill to the stiffness and strength of the frame is still valid under the quasi-static loading condition. The presence of infill, regardless of whether there are openings or interfacial gaps, results in a significant increase in both the stiffness and strength of infilled frames when compared with the bare frame specimen.

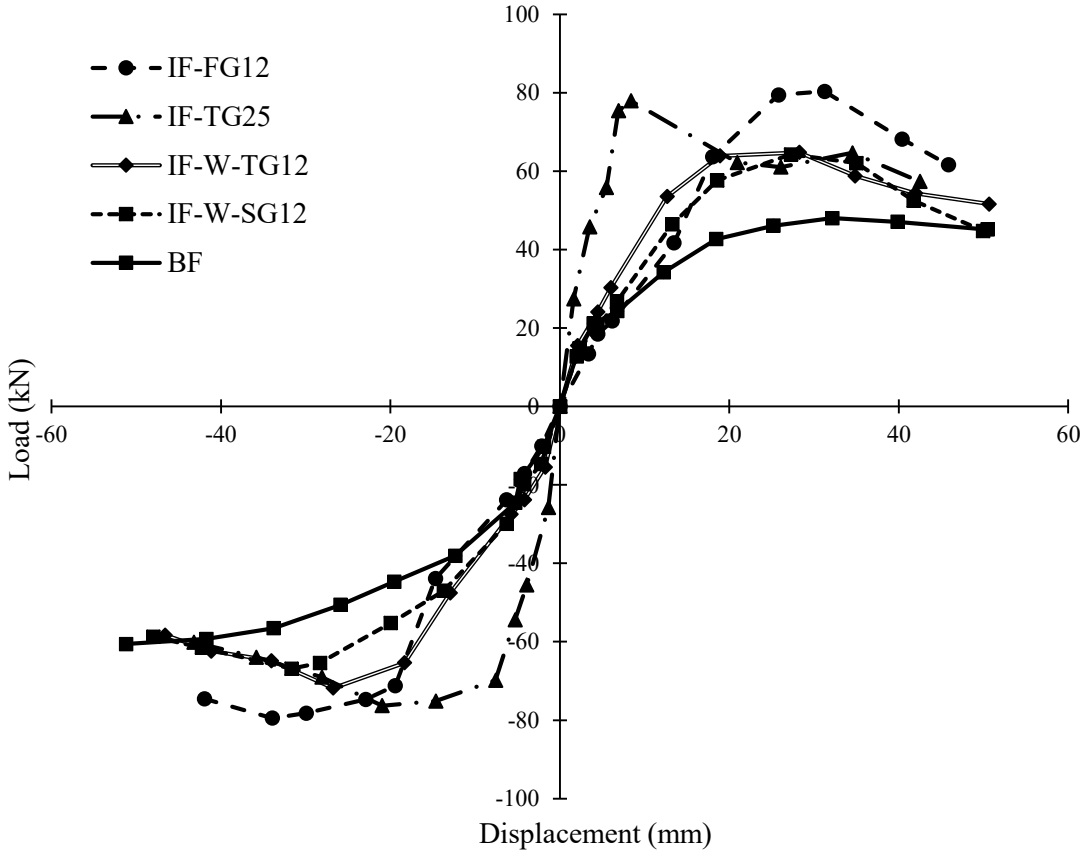

Figure 4.28 Equivalent Monotonic Load-Displacement Back Bone Curves

In order to further evaluate the effect of interfacial gaps, a specimen without interfacial gaps is required. However, such an infilled specimen would require a high capacity hydraulic actuator which is beyond the capability of the available testing facility. The

following alternatives are therefore sought to aid the evaluation process. The bare frame specimen of this experimental program and the bare frame tested by Hu (2015) were compared to determine the reduction in strength capacity due to quasi-static loading. The bare frame specimen used in two studies had the same dimensions and reinforcement details, and the final frame and infill strengths were also similar in two studies.

Figure 4.29 shows a comparison of monotonically and cyclically loaded bare frame specimens. Both curves exhibited similar behaviour with the difference being that the quasi-static loaded bare frame reached a lower ultimate load. In this case, a reduction of 17% in ultimate strength were observed. With a 17% reduction factor applied to the monotonic bare frame, the two curves seem to agree quite well with one and other.

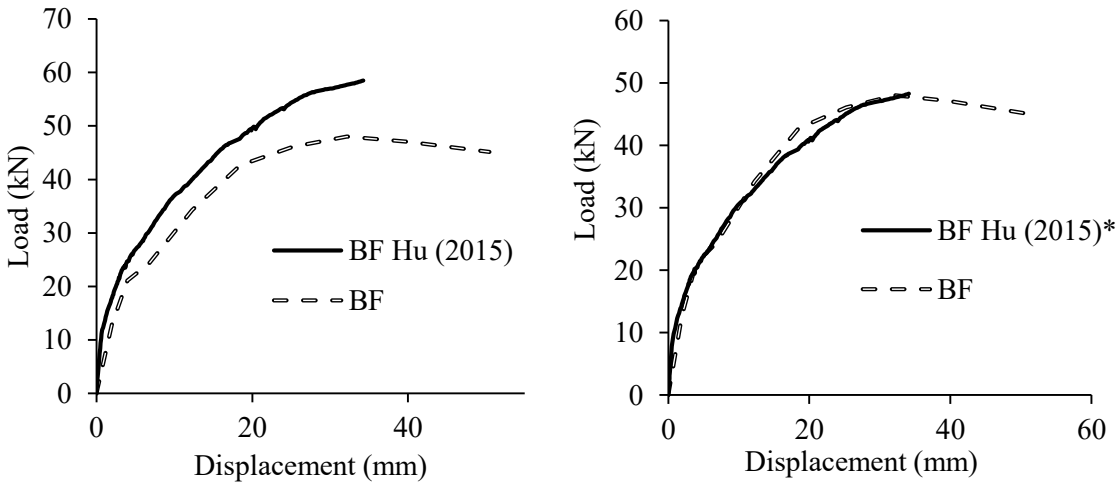

a) Before Reduction b) After Reduction

Figure 4.29 Load-Displacement Curves of Monotonic and Cyclic Loaded BF

Available literature was also consulted in determining a strength correlation between

monotonically and cyclically loaded infill specimens. Mehrabi et al. (1994) reported a similar reduction in ultimate strength when comparing monotonically loaded infilled specimens and cyclically loaded ones under quasi-static loading. In that study, two pairs of similar infilled specimens were tested with one of each pair subjected to quasi-static cyclic loading (specimens 4 and 5) and the remaining pair subjected to monotonic loading (specimen 8 and 9). The quasi-static loaded specimens showed reductions of 10% and 17% in ultimate strength, respectively, when compared to their monotonic counter-parts. Load vs. displacement curves obtained from Mehrabi et al. (1994) are presented in Figure 4.30. It is therefore determined that a 17% reduction factor be applied to monotonically loaded specimens to obtain their ultimate strength under quasi-static loading condition.

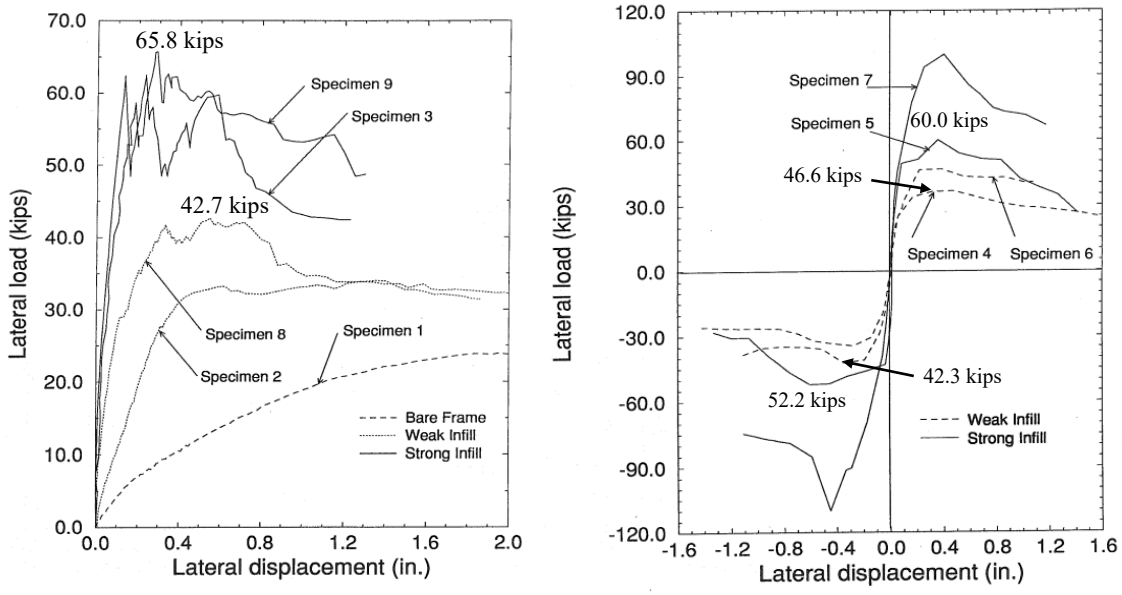

a) Monotonic Loaded b) Hysteretic Backbone Curves

Figure 4.30 Load-Displacement Curves Adapted from Mehrabi et al. (2014)

Adopting this approach, Figures 4.31 to 4.34 depict a comparison of the modified monotonic load vs. displacement curves (Hu 2015) with those quasi-static loaded curves obtained from this study. Table 4.10 lists specimens and original test results in Hu (2015) for ease of reference. Ten specimens were tested in Hu (2015) including one bare frame specimen, (BF), one infilled specimen with no gaps (IFNG), four gap infill specimens, and four specimens with openings. Specimen details are illustrated in Table 4.10 and those used in the comparison with the current study are identified with "*".

Table 4.10 Test Results of Hu (2015)

ID	Top Gap (mm)	Side Gap (mm)	Opening Ratio (%)	Opening Style	K_{in} (kN/mm)	P_{ult} (kN)
BF	-	-	-	-	20.2	57.7
*IFNG	-	-	-	-	39.9	133.6
IFTG6	6	-	-	-	28.7	129.6
*IFTG12	12	-	-	-	28.6	103.6
IFSG6	-	6 (3 on each side)	-	-	27.3	135.2
*IFSG12	-	12 (6 on each side)	-	-	27.1	114.2
IFW8	-	-	8	Window	35.6	108.2
*IFW16	-	-	16	Window	35.3	108.2
IFW22	-	-	22	Window	50.8	86.4
IFD19	-	-	19	Door	38.8	96.0

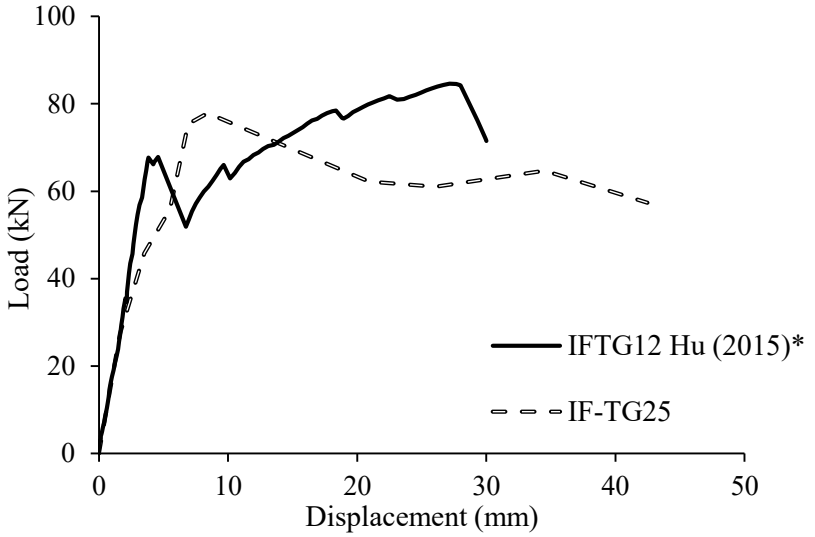

Figure 4.31 Load-Disp. Curves of IF-TG25 and Reduced IFTG12 (Hu 2015)

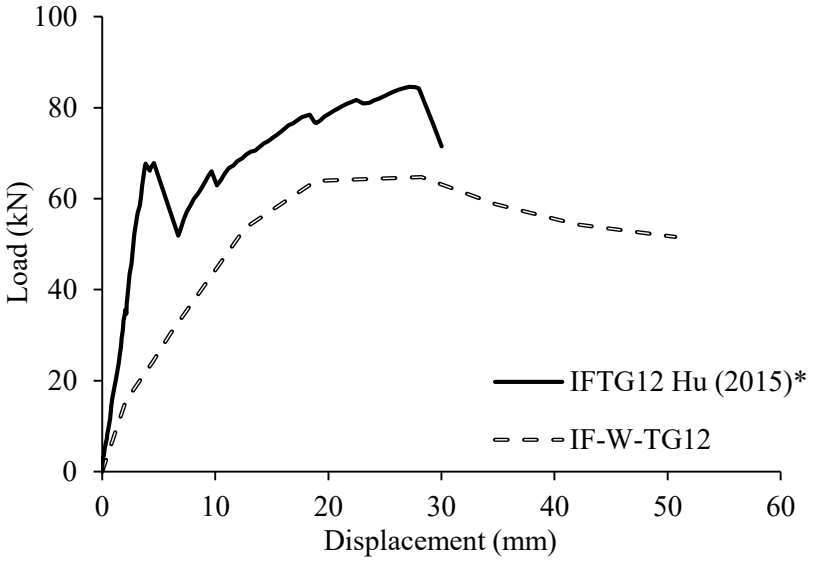

Figure 4.32 Load-Disp. Curves of IF-W- TG12 and Reduced IFTG12 (Hu 2015)

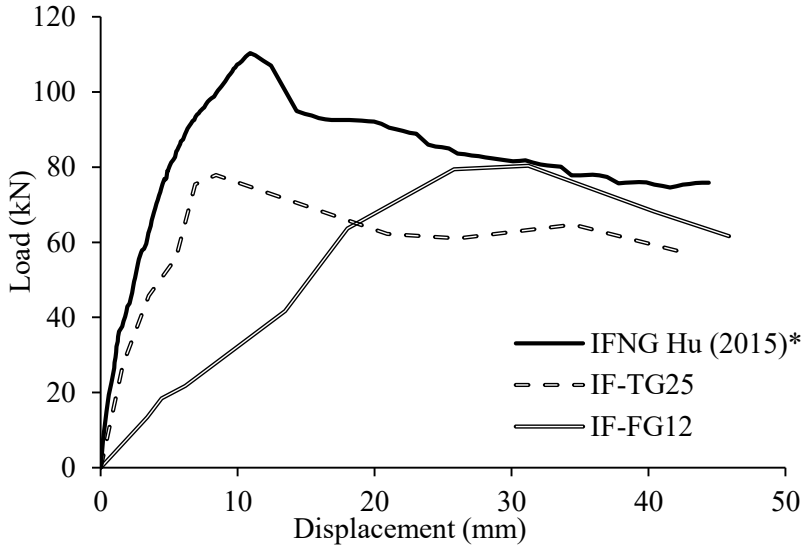

Figure 4.33 Load-Disp. Curves of IF-TG25, IF-FG12 and Reduced IFTG12 (Hu 2015)

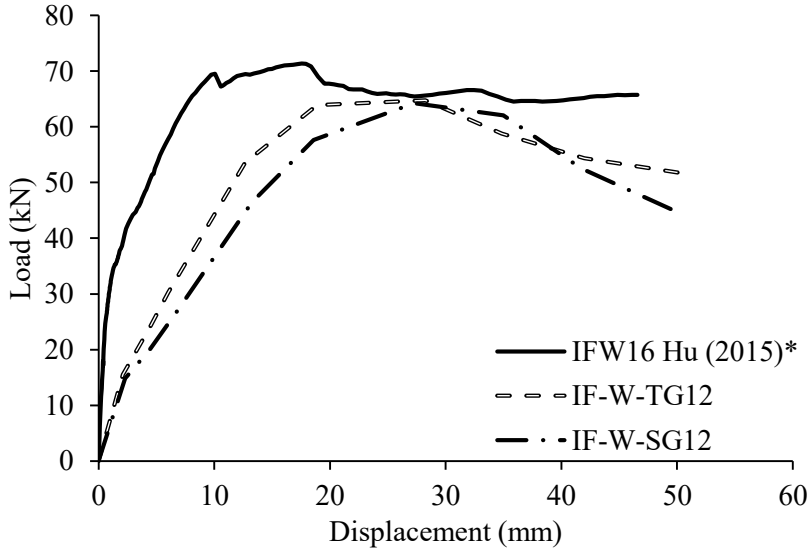

Figure 4.34 Load-Disp. Curves of IF-W-TG12, IF-W-SG12 and Reduced IFW16 (Hu 2015)

4.4 EVALUATION OF INTERFACIAL GAP AND OPENING EFFECTS

A comparison of reduction of the strength and stiffness of infill specimens due to interfacial gaps and/or openings is discussed in this section. In addition, the validity of standard provisions for specimens with gaps and several analytical models for the opening effect is examined. Table 4.11 presents a summary of ultimate strength test results from the current study and those of Hu (2015) with the 17% reduction applied. The reductions in both strength and stiffness due to gap and opening are determined in three groups. Group "a" and "b" show the reduction due to gaps where "a" is for infills without openings and "b" is for infills with openings (all around 16%). Group "c" shows the reduction due to opening where the gap was kept at a constant 12 mm in all specimens.

Table 4.11 Summary of Test Results of Infilled Frames with Gaps and Openings

	ID	P_{ult}^{+} (kN)	P_{ult}^{-} (kN)	K_{in} (kN/mm)	Gap Strength Reduction (%)	Opening Strength Reduction (%)	Gap Stiffness Reduction (%)	Opening Stiffness Reduction (%)
Current study	IF-FG12	80.3	-79.5	-	28[a]	-	-	-
	IF-TG25	77.9	-76.3	26.4	31[a]	-	34[a]	-
	IF-W-TG12	64.8	-71.8	24.7	5[b]	21[c]	30[b]	14[c]
	IF-W-SG12	64.2	-66.9	19.1	8[b]	31[c]	46[b]	30[c]
Hu (2015)	[a]IFNG	111.3	-	39.9	-	-	-	-
	[c]IFTG12	86.3	-	28.6	-	-	-	-
	[c]IFSG12	95.1	-	27.1	-	-	-	-
	[b]IFW16	71.7	-	35.3	-	-	-	-

4.4.1 INTERFACIAL GAPS

4.4.1.1 ULTIMATE STRENGTH

The ultimate strength of infilled specimens with gaps and without an opening (Group "a") showed a significant reduction when compared to the normalized specimen without gaps and openings. Ultimate strength for specimen IF-FG12 showed a reduction of 28% when compared to the ultimate strength of normalized specimen with no gap IFNG (Hu 2015). The ultimate strength of specimen IF-TG25 showed an average reduction of 31% when compared to the normalized strength of IFNG (Hu 2015). When comparing the ultimate strength of the normalized specimen IFW16 to specimen IF-W-TG12 and IF-W-SG12 (Group "b"), a much smaller reduction in ultimate strength was observed. Specimens IF-

W-TG12 and IF-W-SG12 exhibited an average reduction 5% and 8% in ultimate strength when compared to specimen IFW16 Hu (2015). Figure 4.35 depicts the reduction of ultimate strength of infill specimens with gaps compared to specimens without gaps.

4.4.1.2 STIFFNESS

Specimens in Hu (2015) experienced an average reduction of 30% for both 6 mm and 12 mm specimens. Specimen IF-TG25 experienced a similar reduction to initial stiffness observed in Hu (2015) with a 34% reduction when compared to specimen IFNG Hu (2015). Stiffness of specimens with openings and gaps exhibited a larger decrease in stiffness in comparison to specimen IFW16. Specimen IF-W-TG12 saw a 30% reduction in initial stiffness and specimen IF-W-SG12 saw a reduction of 46% when compared to specimen IFW16. Figure 4.36 presents the reduction of initial stiffness of infill specimens with gaps compared to specimens without gaps.

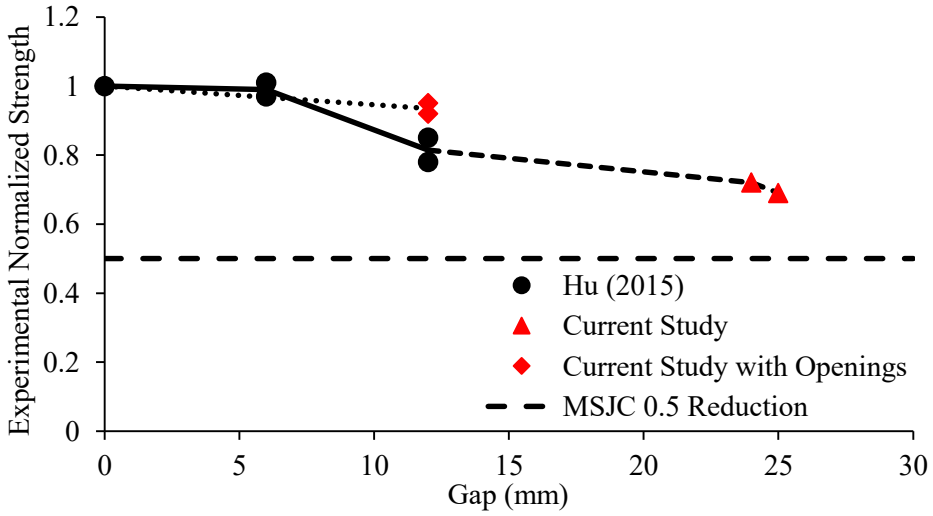

Figure 4.35 Relationship Between Gap Size and Normalized Strength

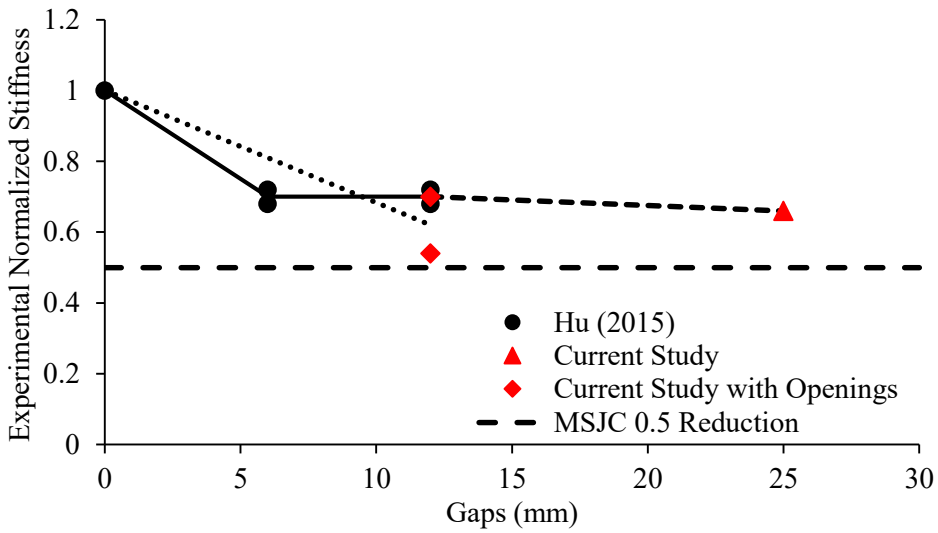

Figure 4.36 Relationship Between Gap Size and Normalized Stiffness

In both curves, a reduction line of 0.5 proposed by MSJC 2013 is also shown. As mentioned previously, the MSJC 2013 provides a guideline in addressing the effect of one interfacial gap situation on the infill design. Gaps along the top beam-infill interface that are less than or equal to 9.5 mm are permitted provided that a 50% reduction is applied to the calculated strength and stiffness of the infilled frame. However, upon examination of Figures 4.35 and 4.36, the 0.5 factor overestimates the reduction of strength and stiffness of specimens. It suggests that a blanket reduction factor of 0.5 specified in MSJC 2013 for a gap size up to 9.5 mm is conservative on both the reduction factor and the allowed gap size. As opposed to the MSJC 2013 provisions, the infilled specimens still have appreciable strength and stiffness when the gap size reaches 25 mm (30% of reduction in both cases). For an assumed linear correlation, the figure shows a reduction factor of around 0.9 for strength and 0.7 for stiffness for a gap of 9.5 mm. Hence, applying the 0.5 reduction factor seemed

to be harsh for the infilled frames with gap size studied. In the case of specimens with both opening and gap, the conservatism of MSJC 2013 reduction factor as discussed above is still valid.

4.4.2 WINDOW OPENING

4.4.2.1 ULTIMATE STRENGTH

Referring to Table 4.11 for Group "c" comparison, a clear reduction in ultimate strength is observed with the addition of window openings. Specimen IF-W-TG12 with an opening-to-infill ratio of 16% showed a reduction of 21% when comparing the normalized ultimate strength of specimen IFTG12 from Hu (2015). Specimen IF-W-SG12 showed a 31% reduction when compared to the normalized ultimate strength of specimen IFSG12 from Hu (2015). Similar reductions in ultimate strength were observed when comparing the ultimate strength of specimen from Hu (2015). As shown in Table 4.10, the reduction in ultimate strength, when comparing IFNG to IFW8, IFW16, and IFW22 were 19%, 35%, and 35% respectively (Hu 2015). Figure 4.37 depicts the relationship of strength reduction due to openings.

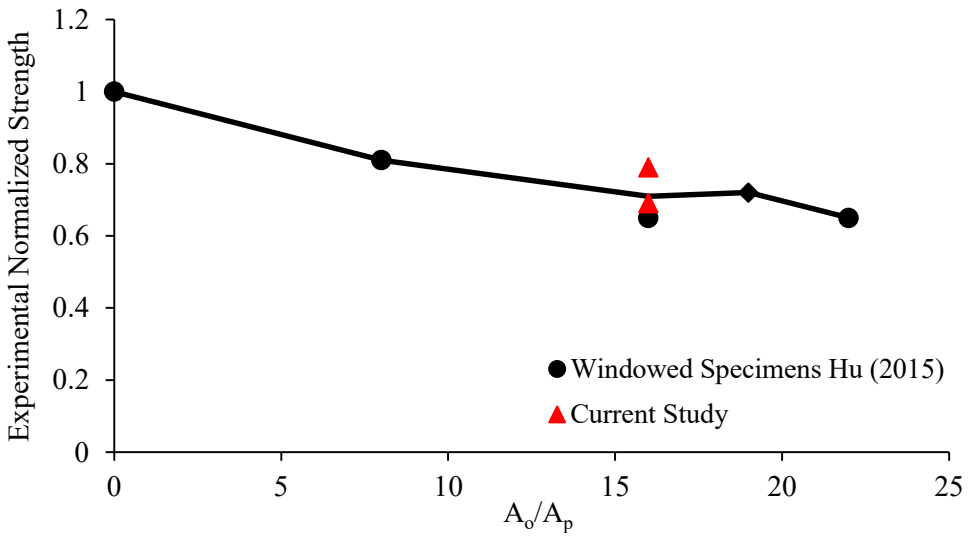

Figure 4.37 Relationship Between Opening Size and Normalized Strength

4.4.2.2 STIFFNESS

When comparing the initial stiffness of specimens IFTG12 and the initial stiffness of IF-W-TG12, a reduction of 14% was observed. The reduction in initial stiffness was more pronounced when comparing specimen IFSG12 with IF-W-SG12, where a reduction of 30% was observed. Specimens of Hu (2015) (Table 4.10) showed the initial stiffness reduction due to openings but the reduction is less pronounced than the specimens of this study. Both specimens IFW8 and IFW16 showed a reduction of approximate 11% (Hu 2015). Figure 4.38 presents the relation of stiffness reduction due to openings. Specimen IFW22 showed abnormally high initial stiffness, possibly due to issues during the experiment setup and was excluded from Figure 4.38.

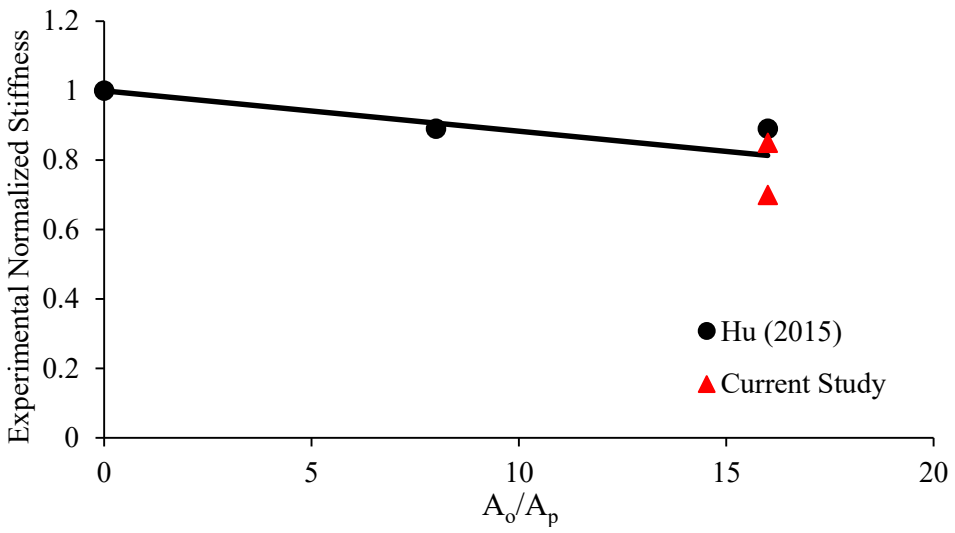

Figure 4.38 Relationship Between Opening Size and Normalized Stiffness

4.4.2.3 EVALUATION OF ANALYTICAL METHODS

As discussed previously in Chapter 2, numerous reduction equations have been proposed to account the presence of openings in masonry infill walls. For ease of reference, Tables 4.12 and 4.13 present a summary of proposed equations to diagonal strut width to account for the presence of openings for strength and stiffness reduction respectively.

Table 4.12 Proposed Strength Reduction Equations

Author	Strength Reduction Equations
Durrani and Luo (1994)	$R_F = 1 - (\frac{A_d}{H \times L})^2$ $A_d = H \times L - \frac{[R\sin(2\theta) - R_0 \sin(\theta + \theta_0)]^2}{2\sin(2\theta)}$ $R_0 = \sqrt{H_0^2 + L_0^2}$ $R = \sqrt{H^2 + L^2}$
Al-Chaar et al. (2003)	$R_F = 1 + 0.6(A_o / A_p)^2 - 1.6(A_o / A_p)$
Mondal and Jain (2008)	$R_F = 1 - 2.6(A_o / A_p)$
Tasnimi and Mohebkhah (2011)	$R_F = 1 + 1.49(A_o / A_p)^2 - 2.238(A_o / A_p)$
Mohammadi and Nikfar (2013)	$R_F = 1 + 1.1163(A_o / A_p)^2 - 1.6534(A_o / A_p)$ $R_F = 1 - 2.12(A_o / A_p)$ For Steel Frames $R_F = 1 - 1.05(A_o / A_p)$ For RC Frames

Table 4.13 Proposed Stiffness Reduction Equations

Author	Stiffness Reduction Equations
Durrani and Luo (1994)	$R_F = 1 - (\frac{A_d}{H \times L})^2$ $A_d = H \times L - \frac{[R\sin(2\theta) - R_0 \sin(\theta + \theta_0)]^2}{2\sin(2\theta)}$ $R_0 = \sqrt{H_0^2 + L_0^2}$ $R = \sqrt{H^2 + L^2}$
Al-Chaar et al. (2003)	$R_F = 1 + 0.6(A_o / A_p)^2 - 1.6(A_o / A_p)$
Mondal and Jain (2008)	$R_F = 1 - 2.6(A_o / A_p)$
Asteris et al. (2012)	$R_F = 1 - 2(A_o / A_p)^{0.54} + (A_o / A_p)^{1.14}$
Mohammadi and Nikfar (2013)	$R_F = 1 + 1.1163(A_o / A_p)^2 - 1.6534(A_o / A_p)$ $R_F = 1 - 2.12(A_o / A_p)$ For Steel Frames $R_F = 1 - 1.05(A_o / A_p)$ For RC Frames

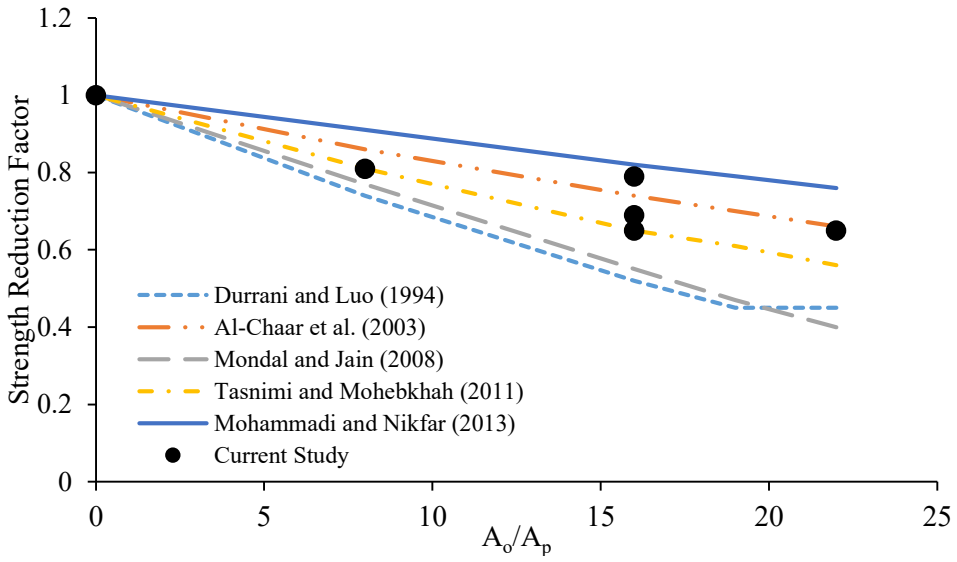

Figure 4.39 Proposed Analytical Strength Reductions Due to Openings

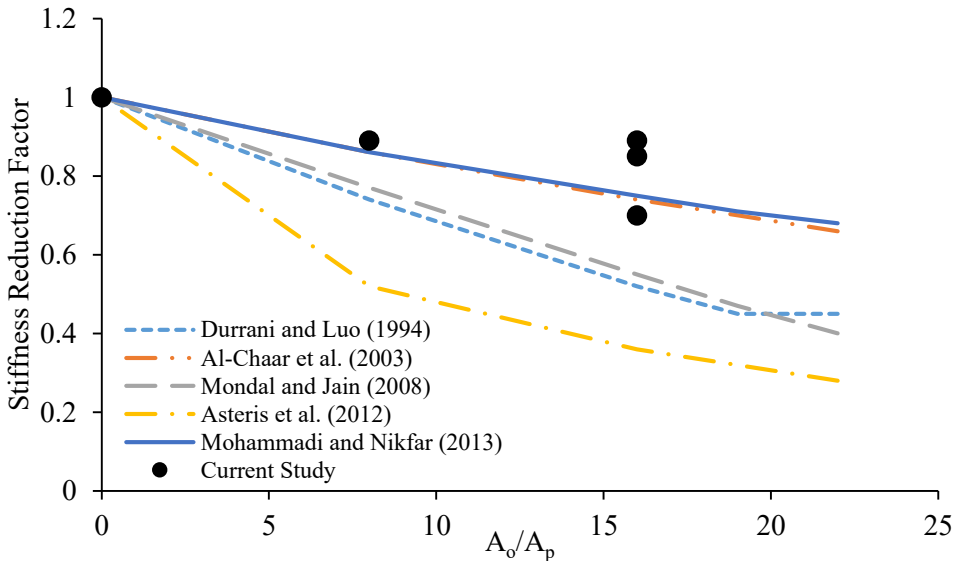

Figure 4.40 Proposed Analytical Stiffness Reductions Due to Openings

As shown in Figure 4.39, the strength reductions observed from this study correlate well with reductions with proposed by Al-Chaar et al. (2003), and Tasnimi and Mohebkhah (2011). Reductions proposed by Mondal and Jain (2008) and Durrani and Luo (1994) have good correlation for smaller window openings, the reductions become overly conservative as opening size increases. The reductions proposed by Mohammadi and Nikfar (2013), proved to be unconservative and underestimate the strength reductions due to openings.

As shown in Figure 4.40, the reductions proposed by Mondal and Jain (2008), Durrani and Luo (1994), and Asteris et. al. (2012) we overly conservative in estimating the stiffness reductions observed from this study and Hu (2015). The stiffness reduction proposed by Mohammadi and Nikfar (2013), and Al-Chaar et al. (2003) were closest to resembling the reduction in initial stiffness observed in this study.

4.4.3 DUCTILITY

Ductility is the measure of a structure's ability to undergo plastic deformation while maintaining its load carrying capacity. As discussed previously, NBCC 2015 allows for a reduction of seismic loading by a factor from 1 to 5 based on the seismic resisting system implemented. Typical ductility factors for RC frames and unreinforced masonry are 2.5 and 1.0, respectively. Although there is no uniform formulation on ductility calculation, the approach presented in the following has been commonly used to calculate ductility of infilled frames (Hu, 2015; Carrillo et al., 2014; Tawfik et al., 2014). In this method as expressed in Eqn [4-2], the ductility factor, R, is calculated as the ratio of the displacement occurs at ultimate load and the displacement corresponding to 80% of the ultimate load in the ascending portion of the monotonic backbone curve, as depicted in Figure 4.41.

$$R = \frac{\Delta_{ult}}{0.8\Delta_{ult}} \qquad [4\text{-}2]$$

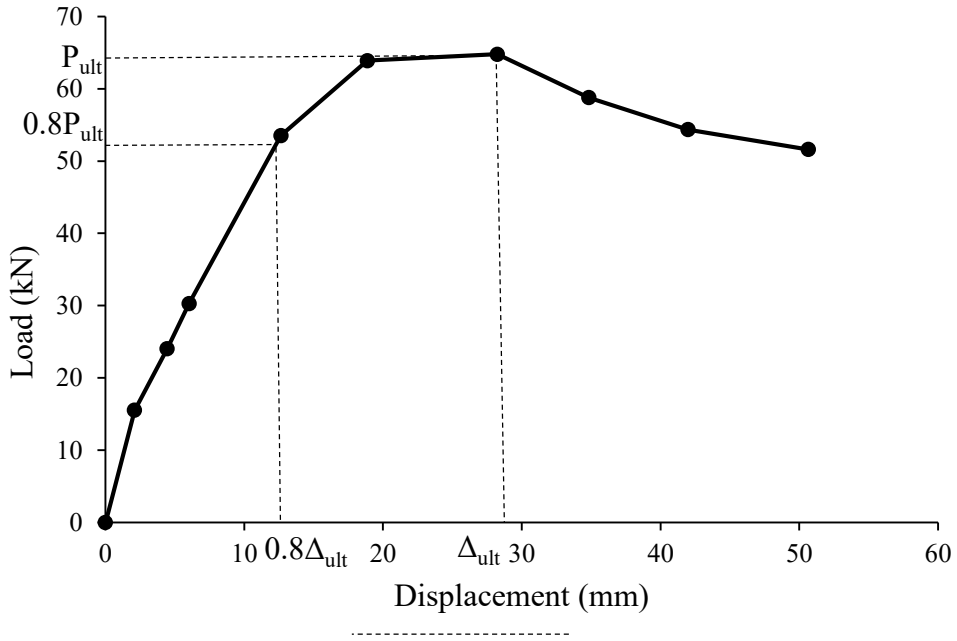

Figure 4.41 Load vs. Displacement Backbone Curve Specimen IF-W-TG12

Table 4.14 summarizes the ductility factor R for each specimen in this study as well as the ductility factors obtained from Hu (2015).

Table 4.14 Summary of Specimens Peak Deflections and Ductility Factors

ID		$0.8\Delta_{ult}$ (mm)	Δ_{ult} (mm)	$0.8P_{ult}$ (kN)	P_{ult} (kN)	R
Current study	IF-FG12	20.7	31.9	64.3	80.4	1.5
	IF-TG25	7.1	8.4	62.3	77.9	1.2
	IF-W-TG12	16.1	28.2	57.2	71.9	1.8
	IF-W-SG12	19.1	27.3	53.5	66.9	1.4
	BF	18.2	41.5	50.9	60.5	2.3
Hu (2015)	IFNG	6.8	11.0	106.9	133.6	1.6
	IFTG6	10.5	17.7	103.7	129.6	1.7
	IFTG12	16.8	30.8	82.9	103.6	1.8
	IFSG6	14.7	20.7	108.2	135.2	1.4
	IFSG12	23.8	45.0	91.4	114.2	1.9
	BF	16.9	33.5	46.2	57.7	2.0
	IFW16	6.1	17.6	69.1	86.4	2.9

As shown in Table 4.14 the ductility of all the masonry infilled RC frames with gaps in this study are greater than 1.0 with an average of 1.5, which is greater than the assigned factor of 1.0 for unreinforced masonry by NBCC 2015, indicating that unreinforced masonry bounded by RC frames has much improved ductility. Secondly, the ratio of the ductility of the bare frame and the infilled frames obtained from this study is around 2.3/1.5=1.5, which is much lower than 2.5 as suggested by NBCC 2015. This indicates that the ductility of masonry infilled frames can be comparable to that of the RC bare frame. The factor of 1.0 specified in NBCC 2015 is too harsh for masonry to be designed in seismic region. Similarly, the average ductility factor obtained from Hu (2015) is 1.7 and the ratio of ductility between the bare frame and the infilled frames is 2/1.7=1.2. Although more testing is needed, the current results seem to suggest that monotonic loading condition may

overestimate ductility.

4.4.4 ENERGY DISSIPATION

A desirable seismic load resisting system should be designed to dissipate seismic energy through flexural ductile behaviour and development of plastic deformation. Energy dissipation is calculated as the area under the load-displacement hysteric loop of a single cycle. In a perfectly elastic material, the hysteric loop would show a straight line and energy would not be dissipated. The sum of the energy dissipated over the entire test duration is known as the cumulative energy dissipation (CED). Figure 4.42 plots the cumulative energy dissipated (MN/mm) for each cycle of the frame specimens.

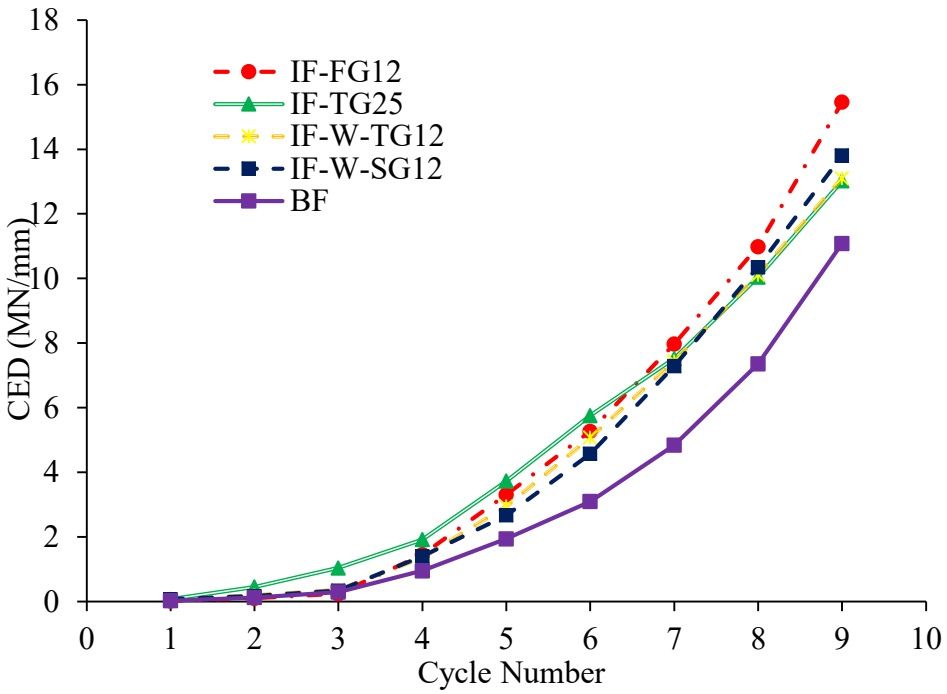

Figure 4.42 Cumulative Energy Dissipated vs. Cycle Number

As illustrated in Figure 4.42, all infilled specimens dissipate more cummulitive energy than the bare frame specimen. Specimen IF-TG25 dissipated most cumulative energy in early cycles when compared to other infill specimens. By the third set of cycles, specimen IF-TG25 had dissipated more cumulative energy than the next highest specimen, IF-W-TG12, by 65%. During the first three cycles, all specimens with the exception of IF-TG25 dissipated energy at roughly the same rate as the bare frame. At the fourth set of cycles, each specimen deviates from the bare frame as cracks in the infill begin to propagate further. Beginning from the seventh set of cycles, the cumulative energy dissipated by specimen IF-FG12 and specimens IF-W-TG12 and IF-W-SG12 increased at a greater rate than specimen IF-TG25. This could be due to the early failure of specimen IF-W-TG12. In the case of specimens with a window opening, the early cracking helped specimen IF-W-TG12 dissipate more energy than specimen IF-W-SG12 during the first seven cycles. However, post failure, IF-W-SG12 dissipated the second most amount of cumulative energy by the final cycle with 13.8 MN/mm which was 1.7 MN/mm less than specimen IF-FG12 with the most energy dissipated by the final cycle of 15.5 MN/mm.

4.4.5 DRIFT

Since seismic design permits the lateral load resisting structure to develop plastic deformation to dissipate energy, the control of storey drift is important to ensure stable behaviour in the inelastic range of response. NBCC 2015 allows for a 1%, 2%, and 2.5% story drift in post-disaster relief structures, schools, and all other buildings respectively.

The displacement corresponding to the 1%, 2%, and 2.5% drift ratios of the frame used in this experimental program are 12.0, 23.9, and 29.9 mm. Table 4.15 summarizes the loads at the three drift levels as P_{d1}, P_{d2}, $P_{d2.5}$, respectively for both pulling and pushing. For comparison purposes, the % drift ratio of the full contact specimen IFNG from Hu (2015) and the full contact specimen IFW16 are also presented in Table 4.15. Strengths at each prescribed drift have a 17% reduction applied to compare the monotonic results with quasi-static results.

Table 4.15 Story Drift Results

	ID	P_{d1}^{+} (kN)	P_{d1}^{-} (kN)	P_{d2}^{+} (kN)	P_{d2}^{-} (kN)	$P_{d2.5}^{+}$ (kN)	$P_{d2.5}^{-}$ (kN)	P_{ult} (kN)
Current study	IF-FG12	37.7	-37.5	75.6	-75.2	80.1	-53.6	80.3
	IF-TG25	73.4	-73.1	61.5	-73.3	62.7	-66.1	77.9
	IF-W-TG12	51.3	-45.0	64.4	-69.6	63.3	-68.1	71.9
	IF-W-SG12	42.7	-43.1	61.7	-60.0	63.5	-67.8	66.9
Hu (2015)	IFNG	108.5	-	86.4	-	83.0	-	111.3
	IFTG12	67.1	-	81.3	-	85.5	-	86.3
	IFSG12	46.5	-	76.3	-	82.4	-	95.1
	IFW16	69.1	-	66.0	-	66.1	-	71.7

Loads corresponding with the percentage drift were obtained from load vs. displacement backbone curve as shown in Figure 4.43.

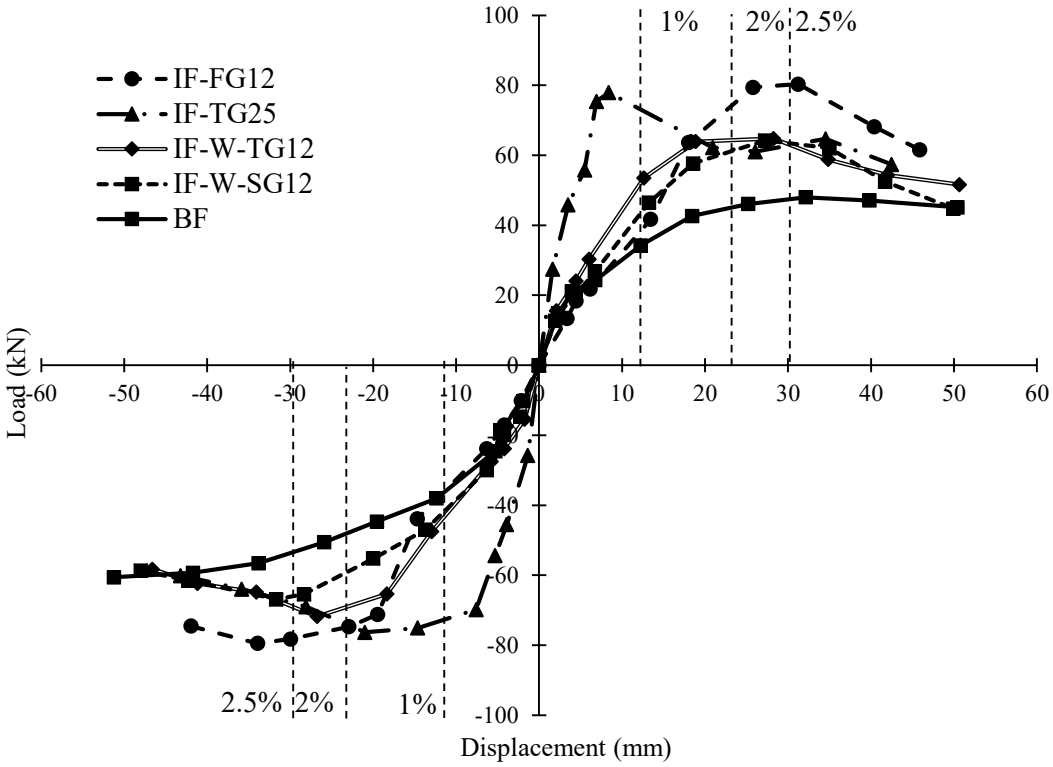

Figure 4.43 Load vs. Displacement Backbone Curves

For the 1% drift ratio, intended for post-disaster relief buildings, all specimens with gaps showed a notable decrease in strength when comparing specimens of similar geometry without gaps. When comparing specimen IF-FG12 and IF-TG25 to IFNG of Hu (2015) each showed an average reduction of 65% and 32% respectively in the 1% drift category. When the opening is present in the infill, specimens IF-W-TG12 and IF-W-SG12 showed an average reduction of 30% and 38% when compared to specimen IFW16 in the 1% category.

When comparing strength reductions in the 2% category, specimens IF-FG12 and IF-TG25

showed an average reduction of 13% and 22% in the 2% category when compared to specimen IFNG, respectively. Specimen IF-W-SG12 experienced a 7% average reduction when compared to specimen IFW16.The average strength of specimen IF-W-TG12 was the same as IFW16 in the 2% category.

In the 2.5% category specimen IF-FG12 and IF-TG25 showed a 3% and 22% average reductions respectively when compared to specimen IFNG. Specimen IF-W-SG12 showed 20% in the 2.5% category when compared to specimen IFSG12 of Hu (2015). Specimens IF-W-TG12 and IF-W-SG12 both saw a 1% reduction comparing specimen IFW16.

Combining the above and previous discussion on strength reduction due to interfacial gaps, this seems to suggest that the reduction factor is different depending on the limit state in consideration. The 0.5 reduction factor is shown to be conservative for ultimate limit state and drift level at 2% and 2.5% category, but for 1% drift category, the conservatism is not as significant.

4.4.6 EVALUATION OF MSJC 2013

This section is to evaluate the efficacy of method specified in MSJC 2013 for masonry infill stiffness and strength calculation. As mentioned in Chapter 2, the MSJC 2013 is the only design code in North America that provides methods for evaluating the stiffness and strength of masonry infills while accounting for the presence of an initial gap. Detailed calculations for the control specimen for both stiffness and strength are presented in Appendix A. The results are summarized in Table 4.16 where the calculated strength and

stiffness as proposed by MSJC 2013 along with the experimental ultimate strength and stiffness of specimen IF-TG25 and IFNG are shown. It is noted that the MSJC 2013 specifies that the smallest of ultimate strengths evaluated corresponding to three failure modes, i.e. corner crushing, sliding shear, and lateral displacement reaching 25 mm governs the design.

Table 4.16 MSJC 2013 Calculated Strength and Stiffness

		MSJC	0.5MSJC	IFNG	IF-TG25
Strength (kN)	Corner Crushing	51.8	25.9	98.0	61.5
	Sliding Shear	14.1	7.1*	-	-
	25 mm Displacement	384.6	192.3	-	-
Stiffness (kN/mm)		44.4	22.2	39.9	25.5

Governed strength is identified with "*"

In the case of strength design, the table shows that when corner crushing is considered, the MSJC 2013 grossly underestimates the infill strength by about 1.9 times (52.2 kN vs. 98.0 kN) for the control specimen (no gap). When the gap effect is considered with the 0.5 reduction, the underestimation is even more pronounced by about 2.4 times (26.1 kN vs. 61.5 kN). Further, it can be conceived that if the governing strength (sliding shear in this case) is used for design, the underestimation is close to 10 times. Noting that the experimental failure mode for both specimens was corner crushing, this suggests that MSJC 2013 is very conservative in the strength calculation and does not accurately predict the failure mode.

In the case of stiffness design, the MSJC 2013 calculated stiffness for the control specimen

is in a general agreement with the experimental stiffness (44.4 kN/mm vs. 39.9 kN/mm), indicating the MSJC equation for stiffness calculation is reasonably accurate. When a 50% reduction is applied for gap effect, the experimental stiffness is slightly higher than the calculated stiffness (25.5 kN/mm vs. 22.2 kN/mm). This indicates that the reduction obtained from the test is lower than the suggested 50%. This is in line with earlier discussion on the reduction factor in Section 4.4.1.

CHAPTER 5 SUMMARY AND CONCLUSION

5.1 SUMMARY

This research was conducted to investigate the effect of interfacial gaps on the in-plane cyclic behaviour of masonry infilled RC frames. Five specimens, including one bare frame, and four gapped infilled frame specimens were subject to quasi-static cyclic loading to failure. All masonry infilled frames shared the same dimensions at 980 mm high and 1350 mm with infills constructed with half-scale 200 mm blocks in a running bond. Two specimens had a window opening accounting for 20% of the infill area. Four gap scenarios were examined, a 12 mm gap surrounding the infill, a 25 mm gap between beam-infill interface, a 12 mm gap between the beam-infill interface, and a 6 mm gap between each column-infill interface. During testing, the general behaviour, cracking and failure pattern, and load-displacement hysteric response were recorded. The effect of gaps, the effect of window openings, strength, stiffness, ductility, and energy dissipation were presented and discussed. Results from a previous study conducted by a similar experimental program were also used for comparison of results obtained. The validity of CSA S304-14, MSJC 2013, and several other proposed analytical methods for infill design were compared with obtained experimental results.

5.2 CONCLUSION

The following conclusions are drawn from this research.

1. Compared to the bare frame, the presence of infills with or without gaps increased the initial stiffness and strength of infilled frames. The degree of increase in stiffness and strength was dependent on gap magnitude and location.

2. With respect to initial stiffness, when compared to an infill frame of similar geometry with no gaps, infilled frames with gaps showed a reduction in initial stiffness and this reduction was more pronounced for side gapped specimens than top gapped specimens. An increase in gap size at the beam-infill interface did not result in a marked increase in reduction. The reduction form 12 mm to 25 mm top gap remained approximately the same.

3. With respect to ultimate strength, infilled specimens with increasing gap size showed an increasing reduction in ultimate strength. When both openings and gaps are present, the reduction as a result of gap is not as significant. When considering the lateral drift levels defined by NBCC 2015, the most reduction due to gap occurred at the 1% drift level corresponding to post-disaster buildings. For the 2% and 2.5% drift levels corresponding to schools and all other buildings, reductions lessened.

4. Specimens with window openings showed an increasing reduction in ultimate strength as opening magnitude increased. Reductions due to infill opening in ultimate strength were best represented in the calculations proposed by Al-Chaar (2003) and Tasnimi and Mohebkhah (2011).

5. Specimens with window openings indicated a general trend in reduction in initial stiffness with increasing opening magnitude. The reductions in stiffness of specimens with openings are best represented by the equations proposed by Mohammadi and Nikfar (2013) and Al-Chaar et al. (2003).

6. An increase in ductility of the infilled frame specimens was observed in comparison to the ductility recommended by NBCC 2015 for unreinforced masonry. The ductility of the infilled frame specimens is comparable to that of a RC bare frame.

7. The energy dissipated from specimens with infills was greater than that of the energy dissipated by the bare frame specimens. Infilled specimens with gaps and no window openings dissipated more energy than specimens with gaps and window openings. The specimen with full gap dissipated the most energy overall.

8. The 0.5 reduction factor proposed by MSJC 2013 for the top gap effect proved to be overly conservative for strength reduction. Even gaps that are larger than the permitted 9.5 mm showed less than a 0.5 reduction in ultimate strength. initial stiffness. On the other hand, MSJC 2013 design stiffness agreed reasonably well with the experimental stiffness.

5.3 RECOMMENDATIONS FOR FUTURE RESEARCH

In summary, the results obtained from this study suggest that interfacial gaps of a certain magnitude, and openings can be accommodated in the design of masonry infilled frames.

Figures 4.35-4.38 can be viewed as a preliminary guide, however more specimens covering a wide range of gap magnitudes and locations are needed in order to assist numerical models for gap or opening reduction. For a long term objective, the infilled frame specimens subjected to dynamic loading should be tested to determine whether the findings from the static and quasi-static cyclic loading can be transferred to a dynamic loading situation.

REFRENCES

Abdul-Kadir, M.R. (1974). The structural behaviour of masonry infill panels in framed structures. Ph.D. Dissertation, University of Edinburgh, Edinburgh, England.

Al-Chaar, G. (2002). Evaluating strength and stiffness of unreinforced masonry infill structures. *Journal of Structural Engineering*, ASCE, 128(8):1055-1063.

Al-Chaar,G., Issa, M., and Sweeney, S. (2002). Behavior of masonry-infilled nonductile reinforced concrete frames. *Journal of Structural Engineering*, 128(8):1055-1063.

Al-Chaar, G., Lamb, G. E. and Issa, M. A. (2003) Effect of openings on structural performance of unreinforced masonry infilled frames. ACI, 211: 247-261.

Al-Nimry, H (2014) Quasi-Static Testing of RC Infilled Frames and Confined Stone-Concrete Bearing Walls, *Journal of Earthquake Engineering*, 18:1, 1-23

Asteris P. G., Antoniou S. T., Sophianopoulos D. S. Chrysostomou C. Z. (2011). Mathematical macromodeling of infilled frames: state of the art. *Journal of Structural Engineering*, 137 (12): 1508-1517

Asteris, P. G., Giannopoulos, I.P. and Chrysostomou, C.Z. (2012) Modelling of infilled frames with openings. *The Open Construction and Building Technology Journal*, 2012, 6 (1-M6): 81-91.

ATC-24 (1994) Guidelines for cyclic seismic testing of components of steel structures. *Applied Technology Council.* Redwood City, CA.

ASTM C143/C143M (2012). Standard test method for slump of hydraulic-cement concrete. ASTM International, West Conshohocken, PA.

ASTM C1314 (2016). Standard test methods for compressive strength of masonry prisms. ASTM International, West Conshohocken, PA.

ASTM C140/C140M (2016). Standard test methods for sampling and testing concrete masonry units and related units. ASTM International, West Conshohocken, PA.

ASTM C270 (2016). Standard specification for mortar for unit masonry. astm international, West Conshohocken, PA.

ASTM C39/C39M (2016). Standard test method for compressive strength of cylindrical concrete specimens. ASTM International, West Conshohocken, PA.

ASTM E8 (2008). Standard test methods for tension testing of metallic materials. ASTM International, West Conshohocken, PA.

Calvi M., Bolognini D. (2008) Seismic response of reinforced concrete frames infilled with weakly reinforced masonry panels. *Journal of Earthquake Engineering*, 5:2, 153-185.

CAN/CSA A165 (2004). CSA standards on concrete masonry units. Mississauga, ON, Canada: Canadian Standard Association. 127

CAN/CSA S304-14 Design of Masonry Structures. Mississauga, ON, Canada: Canadian Standards Association

Carrillo, J., Conzalez, G., Rubiano, A. (2014). Displacement ductility of seismic design of RC wall for low-rise housing. *Latin American Journal of Solids and Structures*, 11:725-737.

Dawe, J.L., and Seah, C.K. (1989). Behaviour of masonry infilled steel frames. *Canadian Journal of Civil Engineering*, 16(6): 865–876.

Drysdale, R.G., and Hamid, A.A. (2005). Masonry structures: behavior and design. Mississauga, Ontario: Canadian Masonry Design Centre.

Durrani, A.J., and Luo, Y.H. (1994). Seismic retrofit of flat-slab buildings with masonry infills. *Proceedings of the 5th US national conference on earthquake engineering*, 3:627–36

El-Dakhakhni, W. W. (2002). Experimental and analytical seismic evaluation of concrete masonry-infilled steel frames retrofitted using GFRP laminates. Ph.D. Dissertation, Drexel University.

El-Dakhakhni, W., Elgaaly, M. and Hamid, A. (2003). Three-strut model for concrete masonry-infilled steel frames. *Journal of Structural Engineering*, 129(2), 177-185.

Federal Emergency Management Agency (FEMA). (1997). NEHRP guidelines for the seismic rehabilitation of buildings, FEMA-273, Building Seismic Safety Council, Washington, D.C

Federal Emergency Management Agency (FEMA). (1998). Evaluation of earthquake damaged concrete and masonry wall buildings, FEMA-306, Building Seismic Safety Council, Washington, D.C

Federal Emergency Management Agency (FEMA). (2007) Interim testing protocols for determining the seismic performance characteristics of structural and non-structural components, FEMA-461, Building Seismic Safety Council, Washington, D.C.

Flanagan, R. D., & Bennett, R. M. (1999). In-plane behavior of structural clay tile infilled frames. *Journal of Structural Engineering*, ASCE, 125(6):590-599.

Harris I. (2013) Experimental and numerical testing of masonry infilled reinforced concrete frames for static and quasi static loads. Ph.D. dissertation. Budapest University of Technology and Economics. Budapest, Hungary.

Holmes M. (1961). Steel frames with brickwork and concrete infilling. *Proceedings of the Institution of Civil Engineers*, 19: 473-478. 128

Hu C. (2015) Experimental study of the effect of interfacial gaps on the in-plane behaviour of masonry infilled RC frames. MASc thesis, Dalhousie University, Halifax, Canada.

Ibarra L.F., Medina R.A., and Krawinkler H. (2005) Hysteric models that incorporate strength and stiffness. *Earthquake Engineering Structural Dynamics*, 34:1489–1511

Klinger, R.E. and Bertero, V.V. (1976) Infilled Frames in earthquake-resistant construction. EERC Report UBC/EERC-76/32, UC Berkley, Berkley, CA.

Liauw, T.C. and Kwan, K.H. (1983). Plastic theory of non-integral infilled frames. *Proceedings of the Institute of Civil Engineers*, 2(75): 379-396.

Liauw, T.C. and Kwan, K.H. (1984). Plastic theory of infilled frames with finite interface shear strength. *Proceedings of the Institute of Civil Engineers*, 75(4):707-723.

Liu, Y. and Soon, S. 2012. Experimental study of concrete masonry infills bounded by steel frames. *Canadian Journal of Civil Engineering*, 39: 180–190.

Mainstone, R. J. (1971). On the stiffness and strengths of infilled frames. *Proceedings of the Institute of Civil Engineers*, Suppl. (4):57–90.

Maleki, M., Hamid, A.A., El-Damatty, A.A. and Drysdale, R.G. (2007) Behavior of partially grouted reinforced concrete masonry panels under in-plane diagonal loading. *Proceedings of the 10th North American Masonry Conference*, pp. 1039-1050.

Masonry Standard Joint Committee (2013). Building code requirements for masonry structures. ACI 530/ASCE 5/TMS 402. American Concrete Institute, the American Society of Civil Engineers and the Masonry Society. USA.

Manesh, P.B. (2013). Experimental study of masonry-infilled steel frames subjected to combined axial and in-plane lateral loading. MASc thesis, Dalhousie University, Halifax, Canada.

Mehrabi, A. B., Shing, P. B., Schuller, M. P., and Noland, J. L. (1994) Performance of masonry infilled frames R/C Frames under in-plane lateral loads. Report CU/SR-94/6 Structural Engineering and Structural Mechanics Research Series. Department of Civil, Environmental and Architectural Engineering, University of Colorado at Boulder.

Mehrabi, A. B., Shing, P. B., Schuller, M. P., and Noland, J. L. (1996). Experimental evaluation of masonry-infilled RC frames. *Journal of Structural Engineering*, ASCE, 122(3):228-237.

Moghaddam, H., & Dowling, P. (1988). Earthquake resistant design of brick infilled frames. Brick and Block Masonry (8th IBMAC) London, Elsevier Applied Science, 2:774-784.

Mohammadi and Nikfar (2013) Strength and stiffness of masonry infilled frames with central openings, based on experimental results. Journal of Structural Engineering. 2013, 139(6): 974–984.

Mondal, G. and Jain, S. K. Lateral stiffness of masonry infilled reinforced concrete (RC) frames with central opening. Earthquake Spectra, 2008, 24 (3): 701-723.

Mosalam, K. H. (1996) Experimental and computational strategies for the seismic behaviour evaluation of frames with infill walls. Ph.D. dissertation, Cornell University, Ithaca, New York.

Mosalam, K. H., White, R. N., and Gergely, P. (1997). Static response of infilled frames using quasi-static experimentation. *Journal of Structural Engineering*, ASCE, 123(11)1462-1469.

Nazief, M.A. (2014). Finite element characterization of the behaviour of masonry infill shear walls with and without openings. Ph.D. dissertation, University of Alberta, Edmonton, Canada.

NBCC (2015). National building code of Canada. Institute for Research in Construction, NRCC, Ottawa, Ontario.

Ng'andu, B.M. (2006). Bracing steel frames with calcium silicate element walls. Ph.D. dissertation, Eindhoven University of Technology, the Netherlands.

Palmer H. S. (1900) Concrete wall for buildings. US.

Polyakov, S. V. (1956). Masonry in framed buildings (An investigation into the strength and stiffness of masonry infilling). Gosudarstvennoe izdatel'stvo Literatury po stroitel'stvu iarkhitekture, Moscow. (English translation by G. L. Cairns, National Lending Library for Science and Technology, Boston, Yorkshire, England, 1963).

Richardson. J. (1986) The influence of intial gaps on infilled frame behaviour. MASc thesis, University of New Brunswick, Fredericton, Canada

Riddington, J. R. (1984). The influence of initial gaps on infilled frame behavior. *Proceedings of the Institute of Civil Engineers*, 77(3):295-310.

Rosenblueth. E. (1980). Design of earthquake resistant structures. Pentech Press Limited: 195-222.

Stafford-Smith, B., and Carter, C. (1969). A method of analysis for infilled frames. *Proceedings of the Institution of Civil Engineers*, 44(1):31-48.

Stafford-Smith, B., and Coull, A. (1991). Tall building structures: analysis and design, Wiley-Interscience.

Salonikios, T., Kappos, A., Tegos, L., Penelis, G. (2000). Cyclic load behaviour of low-slenderness reinforced concrete walls: failure modes, strength and deformation analysis, and design implications. *ACI Structural Journal*, 97(1):132-142.

Soon, S. (2011). In-plane behavior and capacity of concrete masonry infills bounded by steel frames. MASc thesis, Dalhousie University, Halifax, Canada.

Tasnimi, A.A. and Mohebkhah, A. Investigation on the behavior of brick-infilled steel frames with openings, experimental and analytical approaches. Engineering Structures, 2011, 33 (3): 968–980.

Tawfik, A.S., Badr, M.R., Elzanaty, A. (2014). Behavior and ductility of high strength reinforced concrete frames. *HBRC Journal*, 10, 215–221.

Wood, R.H. (1978). Plasticity, composite action and collapse design of unreinforced shear wall panels in frames. *Proceedings of the Institution of Civil Engineers*, 65(2):381-411.

World house encyclopedia, Steel moment resisting frame with brick masonry partitions, digital image. < http://db.world-housing.net/building/95 >.

Yong, T.C. (1984). Shear strength of masonry infilled panel in steel frames. MSc thesis, University of New Brunswick, Fredericton, Canada.

APPENDIX A DESIGN STIFFNESS AND STRENGTH CALCULATIONS

Frame Properties:

E_f = 13203 MPa f'_c = 29.2 MPa I_b & I_c = 8.748×10^7 mm^4

h' =1195 mm l' = 1530 mm

Infill Properties:

E_m = 8500 MPa f'_m = 10 MPa t = 90 mm t_f = 34 mm t_e = 17 mm

h =980 mm l = 1350 mm

CSA S304-14

Specimen IF-TG25 was taken as the example for the sample calculation

Stiffness Calculation

The calculated diagonal strut width in addition to the effective stiffness. The calculation is computed as follows:

$$w = \sqrt{{\alpha_h}^2 + {\alpha_L}^2} = \sqrt{584^2 + 1350^2} = 1307\ mm$$

where,

$$\alpha_h = \frac{\pi}{2}\sqrt[4]{\frac{4E_f I_c h}{E_I t_e \sin 2\theta}}; \alpha_L = \pi\sqrt[4]{\frac{4E_f I_b l}{E_m t_e \sin 2\theta}}$$

$$\alpha_h = \frac{\pi}{2}\sqrt[4]{\frac{4(13203)(8.748 \times 107)(980)}{(8500)(34)\sin\big(2(0.628)\big)}} = 562.5\ mm$$

$$\alpha_L = \pi\sqrt[4]{\frac{4(13203)(8.748 \times 107)(1350)}{(8500)(34)\sin(2(0.628))}} = \ 609.4\ mm$$

where,

$$\theta = tan^{-1}\frac{h}{l} = \ tan^{-1}\frac{980}{1350} = 0.628\ rad$$

CSA S304.1 state the design strut width will be taken as the lesser of one-half the calculated diagonal strut width or one-quarter the length of the diagonal. The length of the diagonal is calculated as follows.

$$l_d = \sqrt{l^2 + h^2} = \sqrt{1350^2 + 980^2} = 1668\ mm$$

$$w_{eff} = lesser\ of\ \frac{w}{2}\ or\ \frac{l_d}{4}$$

$$\frac{l_d}{4} = \frac{1668}{4} = 417\ mm$$

$$\frac{w}{2} = \frac{1342}{2} = 671\ mm$$

417 mm < 671 mm, therefore the diagonal strut length is taken as 417 mm.

A S-Frame model was created with the geometric and material properties used during testing and the code defined diagonal strut geometry. A 100 kN load was placed at the top of the frame in the in-plane direction of loading. A linear static analysis was performed and a displacement of 1.53 mm was obtained.

The Stiffness was obtained as follows:

$$K = \frac{100}{1.53} = 65.3\ kN/mm$$

Strength Calculations

A. Diagonal Cracking Strength

$$P_{cr} = \phi_m(v_m b_w d_v + 0.25P_d)\gamma_g$$

$$P_{cr} = 1.0\big((0.89)(90)(1080) + 0.25(0)\big)(0.38) = 32.5\ kN$$

Self-weight of the infill is deemed negligible, therefore, $P_d = 0$. The resistance factor ϕ_{st} is taken as 1.0 in order to be compared with raw data.

where,

$$v_m = 0.16\left(2 - \frac{M_f}{V_f d_v}\right)\sqrt{f'_m} = 0.16(2 - 0.25)\sqrt{10} = 0.89$$

$$\frac{M_f}{V_f d_v} = 0.25$$

$$b_w = t = 90\ mm$$

$$d_v = 0.8l = 0.8(1350) = 1080\ mm$$

$$\gamma_g = \frac{t_e}{t} = 0.38$$

B. Sliding Shear Strength

$$V_r = 0.16\phi_{st}\sqrt{f'_m}A_{uc} + \phi_m \mu P_1$$

Where,

$$A_{uc} = 0.8lt_e = 0.8(1350)(34) = 36720\ mm^2$$

$$\mu = 1.0\ (masonry\ to\ masonry\ slidding\ sheare)$$

For specimen IF-FG12 μ was taken as 0.7 since the sliding shear took place along the frame-infill contact region.

$$P_1 = 0.9 \times 0.726V_r$$

C. Corner Crushing

For corner crushing strength calculations, the effective strut widths

$$l_d - w = 1668 - 417 = 1251mm$$

$$\frac{k(l_d - w)}{t} = \frac{0.9(1251)}{90}$$

$$P_r = \phi_m \chi (0.85 f'_m) b (2t_f - r)$$

Where χ is taken to be 0.5 as per CSA S304-14 cl. , k is taken as 0.9 as per CSA S304-14 Annex B, and b is taken as the diagonal strut width 417 mm.

$$r = \left(\frac{t}{2} - e\right) - \frac{1}{2}\sqrt{t^2 + 4te + 4e^2 - 16et_f}$$

Where, e = 0.1t = 0.1*90 = 9 mm

$$P_r = \frac{\pi^2 \phi_e (EI)_{eff}}{(kh)^2(1 + 0.5\beta_d)} = \frac{3.14^2(1.0)(6.54 \times 10^{10})}{(0.9 \times 1251)^2(1 + 0.5(0))} = 48.3$$

Where β_d is taken as 0 for temporary loading, and factor ϕ_m is taken as 1.0 in order to be compared with raw data.

$$(EI)_{eff} = 0.4 E_m I_o = 0.4(8500)(1.92 \times 10^7) = 6.54 \times 10^{10}$$

$$I_0 = \frac{(90^3 - (90 - 2 \times 17)^3)(417)}{12} = 1.92 \times 10^7 mm^4$$

$$e' = \frac{1}{1 - \left(\frac{P_r}{P_{cr}}\right)}$$

$$e = \frac{1}{1 - \left(\frac{48.3}{50.9}\right)}(9) = 9.97$$

An iteration process is conducted once the first e' is obtained, replacing the previous e and obtaining new results until e' and e converge. The final P_r and P_{cr} are 48.6kN and 50.9kN, respectively. The corner crushing strength is then obtained as follows:

$$P_{cr} = \frac{l}{l_d} P_r = \frac{1350}{1668}(48.3) = 39.1\ kN$$

MSJC 2013

Stiffness Calculation

Diagonal Strut width is calculated as follows:

$$w = \frac{0.3}{\lambda cos\theta} = \frac{0.3}{(0.00279)\cos(0.628)} = 132.8$$

Where,

$$\lambda = \sqrt[4]{\frac{E_m t(sin2\theta)}{4E_f Ih}} = \sqrt[4]{\frac{(8500)(34)(sin2(0.628))}{4(13203)(8.748 \times 10^7)(980)}} = 0.00279$$

The diagonal strut width was then reduced by 0.5 to account for the presence of gaps as recommended by MSJC 2013 cl B.3.1.2.1.

$$w \times 0.5 = 66.4\ mm$$

A linear analysis of the braced frame with a 100 kN in-plane lateral load and the reduced MSJC diagonal strut, produced a displacement of 4.51 mm.

$$K = \frac{100}{4.51} = 22.2\ kN/mm$$

Strength Calculation

MSJC 2013 provides three equations for the determination of infill strength. The three equations measure the corner crushing failure mode, sliding shear failure mode and 25 mm lateral displacement.

Corner Crushing

$$V_r = \frac{V_n}{1.5}$$

where,

$$V_n = \begin{cases} 3.8A_{nv}\sqrt{f'_m} \\ 300A_{nv} \\ \quad or \\ 56A_{nv} + 0.45N_u & \text{if not fully grouted} \\ 90A_{nv} + 0.45N_u & \text{if fully grouted} \end{cases}$$

And where,

$$A_{nv} = 0.8lt_e = 0.8(1350)(34) = 36720\ mm^2 = 56.9\ in^2$$

$$N_u = 0.726V_n$$

Thus,

$$V_n = \begin{cases} 3.8(56.9)(\sqrt{1450} = 8678\ lbs \\ 300(56.9) = 17074\ lbs \\ 56(56.9) + 0.45(0.726V_n) = \mathbf{4733\ lbs} \end{cases}$$

$$V_r = \frac{4733}{1.5} = 3156\ lbs = 14.1\ kN$$

25 mm Displacement

A braced frame analysis was conducted in S-Frame, utilizing the reduced diagonal strut width proposed by MSJC 2013 with the 0.5 reduction applied and a lateral load of 420 kN was required to move the infill specimen 25 mm. The axial force experienced by the diagonal strut was found to be 192.3 kN.